To the Graduate Council:

I am submitting herewith a thesis written by Michikage Matsui entitled "Nonisothermal Rheological Behavior of Polymer Melts." I recommend that it be accpeted in partial fulfillment of the requirements for the degree of Master of Science, with a major in Chemical Engineering.

Donald C. Bogue, Major Professor

We have read this thesis
and recommend its acceptance:

Accepted for the Council:

Vice Chancellor
Graduate Studies and Research

NONISOTHERMAL RHEOLOGICAL BEHAVIOR OF POLYMER MELTS

A Thesis

Presented for the

Master of Science

Degree

The University of Tennessee

Michikage Matsui

March 1976

1269752

ACKNOWLEDGEMENTS

The author wishes to express his appreciation to Dr. D. C. Bogue, his adviser and the conceptor of this research, who has always instructed the author with pertinent advice and encouraged him with great patience.

The author is indebted to Dr. H. F. Johnson for assisting him in many ways, and to the "Polymer Group" for providing financial assistance through the Polymer Consortium.

The author should like to express his thanks to Dr. J. L. White and Dr. J. E. Spruiell who gave him useful advice and comments.

The author also wishes to thank Mr. B. Thompson and his coworkers in the Mechanical Shop, and Mr. T. Long and his coworkers in the Electronics Shop.

The author in indebted to his Japanese employer, Teijin Ltd., which allowed the author the opportunity to study abroad and has supported him financially.

The author is also indebted to Ms. Carol Mason for her work in typing this thesis.

ABSTRACT

Most polymer processing operations involve melt flow under conditions of rapidly changing temperature. One the other hand, almost all basic work in rheology, both experimental and theoretical, has dealt with isothermal flow, with the temperature being held constant during any one measurement. The present work has dealt with nonisothermal response, both as a basic problem in rheology and as it is related to a polymer processing operation.

Generalized viscoelastic theory was formulated by combining the Boltzmann superposition concept with the time-temperature superposition principle and introducing a nonlinearity into the memory function. The generalized theory uses the concept of a weighted time scale to account for the speeding up or slowing down of the relaxation processes.

In the experimental part of the work an elongational deformation was imposed on a molten sample in a tensile testing apparatus, with the sample being surrounded by two reflecting heater walls which focussed radiant heat from nichrome wires onto a fiber-like sample. By applying a programmed voltage to the nichrome wires, a quick temperature change was imposed on the sample.

Certain preliminary runs were made under isothermal conditions. Then two kinds of nonisothermal experiments, involving changes of temperature during tensile pulling and after it, were carried out. In the latter (simple stress relaxation) experiments, the results were well explained by the weighted time history used in the theory. However, in

the former experiments (involving temperature changes during the pulling) the time scale of the accomodation to the temperature jump was smaller than expected from theory.

Finally, the generalized theory was applied to an actual processing operation (melt spinning). The theory was in good agreement with melt spinning data of J. R. Dees for high density polyethylene, although certain assumptions were necessary in estimating the material parameters.

For a better understanding of the above results, a more tractable problem was considered theoretcially: that of constant elongational flow with an imposed temperature change. An important result was that rapid cooling overpowers the effect of the viscoelastic response.

TABLE OF CONTENTS

CHAPTER		PAGE
I.	INTRODUCTION	1
II.	VISCOELASTIC THEORY FOR ISOTHERMAL AND NONISOTHERMAL HISTORIES	3
	Isothermal	3
	General Form and Shear Flows	3
	Elongational Flows	5
	Effect of Temperature	8
	Nonisothermal Rheological Response	9
	Prior Work	9
	Proposed Model	10
III.	EXPERIMENTAL EQUIPMENT AND PROCEDURES	15
	Materials	15
	Equipment	15
	Calibration and Preliminary Tests	18
	Measurement of Temperature	18
	Effect of Volume Changes	19
	Diameter Variations	19
IV.	ISOTHERMAL AND NONISOTHERMAL EXPERIMENTS AND ANALYSIS	25
	Determination of Parameters From Shear Experiments	25
	Shell TC3-30	25
	PS-670	29
	Temperature Change During Stress Relaxation	32
	Theoretical	32

CHAPTER PAGE

Experiments. 34
Temperature Change During Tensile Pulling. 38
Theoretical. 38
Isothermal Pulling 42
Nonisothermal Pulling. 46
V. ANALYSIS OF MELT SPINNING. 58
Background 58
Steady State Melt Spinning 60
Theoretical Considerations 62
General Relationships. 62
Consideration of Constitutive Theory 63
Analysis of Melt Spinning Data 71
Evaluation of Material Parameters. 72
Analysis of Dees' Melt Spinning Data 76
VI. THEORETICAL CONSIDERATION OF CONSTANT ELONGATIONAL FLOW WITH COOLING 89
Theoretical Analysis 89
Condition of Convergence 92
Condition of Divergence. 93
Critical Condition 94
Results and Discussion 96
VII. SUMMARY OF IMPORTANT RESULTS 102
REFERENCES 104
APPENDIX 109
VITA 112

LIST OF FIGURES

FIGURE		PAGE
1.	Sketch of Nonisothermal Test Apparatus.	17
2.	Simulation of Stresses due to Volume Change	20
3.	Diameter Variations along Sample Length at Various Stages of Pulling for Polystyrene TC3-30 at a Low Rate.	22
4.	Diameter Variations along Sample Length at Various Stages of Pulling for Polystyrene TC3-30 at a Medium Rate	23
5.	Diameter Variations along Sample Length at Various Stages of Pulling for Polystyrene TC3-30 at a High Rate	24
6.	Loss Modulus for Polystyrene TC3-30	26
7.	Steady Shear Properties of Polystyrene TC3-30, Reduced to 137°C.	28
8.	Loss Modulus for Polystyrene with Narrow Molecular Weight Distribution.	30
9.	Isothermal and Nonisothermal Stress Relaxation for Polystyrene TC3-30.	35
10.	Isothermal and Nonisothermal Stress Relaxation for Polystyrene PS-670.	36
11.	Superposition of Isothermal and Nonisothermal Stress Relaxation Data for Polystyrene TC3-30 (Reference Temperature 137°C).	39
12.	Superposition of Isothermal and Nonisothermal Stress Relaxation Data for Polystyrene PS-670 (Reference Temperature 135°C).	40

FIGURE PAGE

13. Comparison of Predicted and Experimental Tensile Stresses for Isothermal Tensile Pulling of Polystyrene TC3-30 at 137°C . . 43

14. Comparison of Predicted and Experimental Tensile Stresses for Isothermal Tensile Pulling of Polystyrene TC3-30 at 119°C . . 44

15. Isothermal and Nonisothermal (Heating) Data for Tensile Pulling of Polystyrene TC3-30 at a Low Rate 47

16. Isothermal and Nonisothermal (Heating) Data for Tensile Pulling of Polystyrene TC3-30 at a Medium Rate. 48

17. Isothermal and Nonisothermal (Heating) Data for Tensile Pulling of Polystyrene TC3-30 at a High Rate. 49

18. Isothermal and Nonisothermal (Cooling) Data for Tensile Pulling of Polystyrene TC3-30 at a Low Rate 50

19. Isothermal and Nonisothermal (Cooling) Data for Tensile Pulling of Polystyrene TC3-30 at a Medium Rate. 51

20. Isothermal and Nonisothermal (Heating) Data for Tensile Pulling of Polystyrene PS-670 at a Low Rate 52

21. Isothermal and Nonisothermal (Heating) Data for Tensile Pulling of Polystyrene PS-670 at a Medium Rate. 53

22. Isothermal and Nonisothermal (Heating) Data for Tensile Pulling of Polystyrene PS-670 at a High Rate. 54

23. Isothermal and Nonisothermal (Cooling) Data for Tensile Pulling of Polystyrene PS-670 at a Low Rate 55

24. Isothermal and Nonisothermal (Cooling) Data for Tensile Pulling of Polystyrene PS-670 at a Medium Rate. 56

FIGURE PAGE

25. Schematic Diagram of Melt Spinning. 65

26. Relaxation Spectrum for High Density Polyethylene Tenite 3340 . 74

27. Temperature Dependence of the Shift Factor for High Density Polyethylene Tenite 3340. 77

28. Shear Viscosity versus Shear Rate for High Density Polyethylene EMB 6050 78

29. Fiber Temperature along Spinline for High Density Polyethylene. 81

30. Tensile Stress and Apparent Elongational Viscosity in Melt Spinning for High Density Polyethylene for Dees' Run PE01 . . 82

31. Tensile Stress and Apparent Elongational Viscosity in Melt Spinning for High Density Polyethylene for Dees' Run PE02 . . 83

32. Tensile Stress and Apparent Elongational Viscosity in Melt Spinning for High Density Polyethylene for Dees' Run PE03 . . 84

33. Tensile Stress and Apparent Elongational Viscosity in Melt Spinning for High Density Polyethylene for Dees' Run PE06 . . 85

34. Tensile Stress and Apparent Elongational Viscosity in Melt Spinning for High Density Polyethylene for Dees' Run PE09 . . 86

35. Theoretical Calculation of Transient Elongational Viscosity under Constant Rate of Cooling at $\dot{E}_\tau(0) = 0.1$ 97

36. Theoretical Calculation of Transient Elongational Viscosity under Constant Rate of Cooling at $\dot{E}_\tau(0) = 2.0$ 98

CHAPTER I

INTRODUCTION

Temperature, of course, is an important variable in rheological studies and the well-known time-temperature superposition principle allows one to bring together data from experiments of very different time scales and temperatures. Where the experiments are isothermal ones (with temperature unvarying with time), there exists now quite general viscoelastic theory which embraces arbitrary deformations and wide ranges of rates and temperatures.

When it comes to analyzing practical problems in polymer processing, however, one is soon faced with the non-isothermal problem. Polymers are melted and extruded at elevated temperatures and then cooled, usually quite rapidly, to form useable glassy or crystalline (or oriented crystalline) solids. Depending on the deformations and temperatures, one can see flow instabilities or perhaps failure in the melt. Also, the orientation (or stress) that is trapped in the material by the rapid cooling just prior to solidification has an important effect on the resulting morphology and on the properties of the final product.

In the next section the existing literature on non-isothermal rheological response will be reviewed. There have been several suggestions for generalizing isothermal theory but there are not any accompanying experimental data. It was the objective of the present

work to develop a tractable non-isothermal theory and to test it with basic tensile experiments on well-characterized polymer samples (polystyrenes). The theory can then in principle be applied to polymer processing operations and, to make a start into that area, an analysis of melt spinning data for high density polyethylene was carried out.

CHAPTER II

VISCOELASTIC THEORY FOR ISOTHERMAL AND NONISOTHERMAL HISTORIES

A. ISOTHERMAL

General Form and Shear Flows

In experiments in which the temperature is held constant during the deformation (isothermal deformation), the theory for describing viscoelastic response is well-developed. Using the physical argument known as the Boltzmann superposition principle (as summarized, for example, in Ferry (28)), one writes

$$\sigma_{ij} = - p \, \delta_{ij} + \int_{-\infty}^{t} G \, (t - t') \, \dot{\gamma}_{ij} \, dt' \qquad \text{(II-1)}$$

where σ_{ij} is the stress, p is the pressure, G(t-t') is a time dependent elastic modulus, $\dot{\gamma}_{ij}$ is the deformation rate, t is the time, and t' is past time (the variable of integration). With an experimental form for G(t-t'), this equation can be thought of as a solution to the differential equation for the Maxwell element. Direct generalizations of the differential equations themselves have also been proposed, notably by Oldroyd (55). A special form involving one deformation-dependent time function has been proposed and applied by White and Metzner (75). While those differential models are not currently very popular, they offer advantages in certain kinds of convective-type problems, such as the analysis of melt spinning instabilites (Denn and

Marrucci (25); Fisher and Denn (29)). Generally, however, the theory and qualitative understanding has been built up around integral models of the form of Equation (II-1).

The generalization to arbitrary deformation was first done by Lodge (47, 48) and later, using general functional notation, by Green and Rivlin (31) and Coleman and Noll (20). Much of integral theory can be summarized by the equation (10)

$$\sigma_{ij} = - p \, \delta_{ij} + \int_{-\infty}^{t} [m_1(t-t')C_{ij}^{-1} - m_2(t-t')C_{ij}] \, dt' \qquad \text{(II-2)}$$

where $m_1(t-t')$ and $m_2(t-t')$ are deformation independent memory functions, C_{ij}^{-1} and C_{ij} are Finger and Cauchy tensors, respectively. Equation (II-2) is valid for either large or small strains but in the form shown it leads to a constant viscosity and is thus restricted to small deformation rates. The memory functions (for example m_1) may be expressed in terms of either discrete or continuous spectra

$$m_1 = \sum_n \frac{G_n}{\tau_n} \exp(-(t-t')/\tau_n) = \int_{-\infty}^{\infty} \frac{H(\tau)}{\tau} \exp(-(t-t')/\tau) \, d \ln \tau \qquad \text{(II-3)}$$

where G_n (or $H(\tau)$) are the elastic moduli (or spectrum) and τ_n (or τ) are the relaxation times. There is now large literature dealing with deformation-dependent (nonlinear) memory functions within the general framework of Equations (II-2) and (II-3) (5, 7, 8, 10, 12, 16, 34, 38, 46, 62, 65, 74, 79). As is well-known, high molecular weight materials exhibit a characteristic rubbery-like (entanglement) behavior which is closely associated with the nonlinear effects. An exhaustive review of

these effects have been made by Graessley (30) and one concludes from this review that we are still lacking a satisfactory picture of the basic phenomena involved.

In the present framework, then, one introduces nonlinear functions into Equation (II-3), using various empirical or intuitive arguments (6, 7). These are cast in terms of the invariants of the instantaneous strain rate (38), the strain itself (5, 69) or stress (65, 66). Steady shear and transient shear experiments of various kinds have been used. Recent studies of stress developments following the initiation of a steady shear have shown that the instantaneous rate models are not satisfactory and that one must use strain (or integrated strain rates), or stress, as the nonlinear variable (12, 16, 46).

Elongational Flows

Most of the basic rheological experiments used to develop Equations (II-2) and (II-3) (and the nonlinear counterpart of Equation (II-3)) have been done in shear. Recently, however, elongational flows have been widely studied both because they are good examples of non-viscometric flows and because of their obvious relationship to processing problems, such as melt spinning. A comprehensive review has been presented by Dealy (22). Other summaries are those of Cogswell (19) and Han and coworkers (35), who emphasized various processing implications.

One needs to clearly distinguish between experiments in which the elongational rate ($\dot{E} \equiv \frac{1}{L}\frac{dL}{dt}$, with L being the length of the sample or element) is constant and experiments where it is not. The case $\dot{E}$ = constant leads to an exponential increase in length and requires a

special apparatus, such as the roll-driven system developed by Meissner (51). Under this condition the tensile stress can be obtained by using a one time constant (simple Maxwell) form of Equations (II-2) and (II-3) with $m_2 = 0$.

$$\sigma_{11} = G \dot{E} \tau \left[\frac{2 - 2 \exp[-((1-2\dot{E}\tau)/\tau)t]}{1-2\dot{E}\tau} + \frac{1 - \exp[-((1+\dot{E}\tau)/\tau)t]}{1+\dot{E}\tau}\right] \tag{II-4}$$

If $\dot{E}\tau$ is smaller than 0.5, a steady state is eventually achieved, where Equation (II-4) reduces to the following form:

$$\sigma_{11} = \frac{3G\tau\dot{E}}{(1-2\dot{E}\tau)(1+\dot{E}\tau)} \tag{II-5}$$

At small $\dot{E}\tau$, Equation (II-5) leads to the Trouton viscosity relationship (i.e., that the elongational viscosity is three times the shear viscosity). If, however, $\dot{E}\tau$ is greater than (or equal to) 0.5, Equation (II-5) turns out to be an ever-increasing function to infinity in that the steady state is no longer built up, corresponding to a "blowing up" of the stress. Also, it should be noticed that if one puts nonlinear memory functions into Equation (II-3), the "blowing up" can be ameliorated or eliminated altogether with a sufficiently strong nonlinearity (13). Ide (39) and Cogswell (19) have summarized experiments where a steady state is achieved and the results seem to depend on the materials; for example, the elongational viscosity for low density polyethylene rises whereas that for high density polyethylene falls somewhat (as $\dot{E}$ is increased from the Trouton viscosity asymptote).

It is now understood, however, that a steady state does not always occur. Data presented by Meissner (51) and analyzed by Chang and Lodge (14) show that stress increases very rapidly with time (instead of approaching a steady value) if $\dot{E}$ is large. Further comments have been made by Takaki and Bogue (68). Physically it is clear that the molecules can not relax fast enough to accomodate the deformation imposed on them.

Most tensile experiments and practically all processing operations involve conditions varying $\dot{E}$. As summarized in the reviews (19, 22, 39), experiments have been done at constant force, constant stress, constant dL/dt (as in a tensile tester), and under conditions where all of these variables are changing (as in melt spinning). At the University of Tennessee constant force experiments have been carried out by Chen, et al. (17) and Takaki and Bogue (68); experiments at constant $\dot{E}$ by Ide (39); and melt spinning experiments by Acierno, et al. (2) and Chen, et al. (17). It is possible to analyze the former experiments rather accurately but not so successfully with the melt spinning flow, presumable due to the unknown influence of the flow in the die and die swell regions. In constant force experiments, performed with what is called a "weight dropping" apparatus, the principal result had to do with the relationship between failure (breaking) and the transient response of the materials; that is, failure occurs shortly after a rapid increase in the stress, again explainable in physical terms by imagining that the molecules are unable to accomodate themselves to the rapid deformation imposed.

Effect of Temperature

That time and temperature are closely related variables has been recognized for many years. Leaderman (45) first stated explicitly the now widely accepted time-temperature superposition principle, which allows one to normalize together experiments done at very different rates (or times) and temperatures. For example, the relaxation moduli at different temperatures can be superposed by shifting the times in logarithmic scale (i.e., ln t). Later Ferry (27) introduced a modulus shift ("vertical shift") for viscoelastic materials. While there is some understanding of the time-temperature superposition concept in terms of dilute solution theory, the principle seems to have wide applicability even in regimes, such as the entanglement regime, where we lack convincing molecular theory. In the idealized case of a single shift factor for all times scales, one must argue that the "ultimate" dissipative mechanism, resulting from molecular motions induced at various rates (time scales), must be the same mechanisms in all cases or at least very closely related mechanisms.

Markovitz (49) has recently reviewed the entire concept of superposition in a critical way and emphasizes the fact that there are a number of exceptions to the idea of "thermorheological simplicity" (i.e., that a constant time shift factor can be used over all time scales). He goes on to show that certain kinds of superpositions can be done anyway using less restrictive assumptions than that of a constant shift factor.

If one restricts his attention to a single regime of behavior, or invokes the assumption of thermorheological simplicity to cover several regimes of behavior, the essential ideas can be summarized by introducing

two shift factors, one for parameters bearing the units of time (such as τ) and one for parameters bearing the units of modulus (such as G). Using the subscript "o" to denote a reference state one writes

$$\frac{\tau(T)}{\tau_o} = \frac{a_T(T)}{a_{To}} \tag{II-6}$$

and

$$\frac{G(T)}{G_o} = \frac{\rho T}{\rho_o T_o} \tag{II-7}$$

The shift factor $a_T(T)$ is usually correlated with an equation due to Williams, Landel and Ferry (78), which is of the form

$$\log a_T(T) = \frac{-C_1(T-T_o)}{C_2+T-T_o} \tag{II-8}$$

The glass transition temperature T_g is a convenient reference state, although it has been found empirically that by selecting a reference temperature 50^oC or so above T_g, one can find "universal" constants for Equation (II-8), good for a wide variety of polymers (28).

B. NONISOTHERMAL RHEOLOGICAL RESPONSE

Prior Work

The problem of rheological response in the presence of a changing temperature (nonisothermal rheology) has barely been considered. In the framework of linear viscoelasticity for solid-like material (with a

reference state) Morland and Lee (53) first generalized the time-temperature superposition concept to allow for time-varying temperatures; they were able to explain expansion effects in cylindrical samples in a quantitative way. They introduced the idea of an equivalent past time increment (a weighted time) given by

$$(t-t')_{eq} = \int_{t'}^{t} a_T[T(t")]dt" \qquad \text{(II-9)}$$

Later Bernstein, Kearsley, and Zapas (5) introduced a general functional form, although without specific functions, for dealing with shifts and coined the phrase "clock function" to describe the speeding up or slowing down of the relaxation processes as the temperature is changed. Motivated by interest at the University of Tennessee in melt spinning, a similar form to that of Morland and Lee was suggested in an NSF proposal (76) and in a paper by Abbott and White (1). Finally, consideration of nonisothermal histories as a very general problem in continuum mechanics has been made by Crochet (21).

Proposed Model

In order to schematically generalize Equation (II-2) one may first consider the Boltzmann superposition principle:

$$\sigma_{ij} = -p\delta_{ij} + \int_{-\infty}^{t} G^{\dagger}(t-t') \frac{d\gamma_{ij}}{dt'} dt' \qquad \text{(II-10)}$$

where γ_{ij} is any relative strain tensor. The time-dependent modulus $G^{\dagger}(t-t')$ can generally be expressed by the following form because of the

time-temperature superposition using Equations (II-6) and (II-7):

$$G^{\dagger}(t-t') = G_o \frac{\rho T}{\rho_o T_o} \phi[\frac{t-t'}{\tau(T)}] = G_o \frac{\rho T}{\rho_o T_o} \phi[\frac{t-t'}{a_T(T)\tau_o}] \qquad \text{(II-11)}$$

where $\phi(\cdot)$ is an arbitrary function of time but with the requirement $\phi(0) = 1$ and $\phi(\infty) = 0$.

Let us consider an experiment in which temperature changes stepwise from T_1 to T_2 at time t_1. In other words, the time constant of the material changes from $\tau(T_1)$ to $\tau(T_2)$. This change can be translated into the change in time scale of the experiment by the time-temperature superposition as follows:

$$G^{\dagger}(t-t') = G_o \frac{\rho_2 T_2}{\rho_o T_o} \phi[\frac{t_1-t'}{a_T(T_1)\tau_o} + \frac{t-t_1}{a_T(T_2)\tau_o}], \quad t'<t_1<t \qquad \text{(II-12)}$$

This is a translational shift; that is, one involving no change in shape, of the relaxation modulus plotted against the logarithm of time at different uniform temperatures and leads to an equivalent relation between temperature and ln t. If the temperature change is continuous, Equation (II-12) leads to

$$G^{\dagger}(t-t') = G_o \frac{\rho(t)T(t)}{\rho_o T_o} \phi[\lim_{\Delta t \to 0} \sum_{K}^{n} \frac{t_K-t_{K-1}}{a_T(T_K)\tau_o}] \; ; \; t'=t_1 \text{ and } t=t_n$$

$$= G_o \frac{\rho(t)T(t)}{\rho_o T_o} \phi[\int_{t'}^{t} \frac{dt''}{a_T[T(t'')]\tau_o}]$$

$$= G(t) \phi[\int_{t'}^{t} \frac{dt''}{\tau[T(t'')]}] \qquad \text{(II-13)}$$

where

$$G(t) = G_o \rho(t) T(t) / (\rho_o T_o).$$

Substituting Equation (II-13) into Equation (II-10), one obtains

$$\sigma_{ij} = -p\delta_{ij} + \int_{-\infty}^{t} G(t) \phi \left[\int_{t'}^{t} \frac{dt''}{\tau[T(t'')]} \right] \frac{d\gamma_{ij}}{dt'} dt'. \qquad \text{(II-14)}$$

One can integrate Equation (II-14) by parts as follows:

$$\sigma_{ij} = -p\delta_{ij} + G(t) \phi \left[\int_{t'}^{t} \frac{dt''}{\tau[T(t'')]} \right] \gamma_{ij} \Big|_{-\infty}^{t} \quad (\to 0)$$

$$+ G(t) \int_{-\infty}^{t} \frac{1}{\tau[T(t')]} \dot{\phi} \left[\int_{t'}^{t} \frac{dt''}{\tau[T(t'')]} \right] \gamma_{ij} \, dt'. \qquad \text{(II-15)}$$

In Equation (II-15), $\phi(t)$ is generally assumed to have an exponentially decreasing form; that is, Equation (II-15) is then to be a solution to the differential equation for the simple Maxwell unit. Also, materials have a distribution of time constants. Therefore generalized Equation (II-2) (for the case $m_2 = 0$) leads to the following form:

$$\sigma_{ij} = -p\delta_{ij} + \sum_n G_n(t) \int_{-\infty}^{t} \frac{\exp\left[-\int_{t'}^{t} \frac{dt''}{\tau_n[T(t'')]}\right]}{\tau_n[T(t')]} C_{ij}^{-1}(t,t') dt' \qquad \text{(II-16)}$$

where

$$\tau_n[T(t)] = a_T[T(t)] \tau_n^o$$

and

$$G_n(t)/G_n^o = \rho(t)T(t)/(\rho_o T_o),$$

with τ_n^o and G_n^o designating the time constants and moduli at some reference temperature T_o at which $a_T = 1$, respectively. This equation incorporates the original concepts of Morland and Lee (53) and a generalization due to Abbott and White (1). Also it is within the framework of the theory of Bernstein, Kearsley, and Zapas. Most work to data has shown that practical experiments are often in the nonlinear range. The following nonlinear form is therefore proposed:

$$\sigma_{ij} = -p\delta_{ij} + \sum_n G_n(t) \int_{-\infty}^{t} \frac{\exp\left[-\int_{t'}^{t} \frac{dt''}{\tau_n^*[\Pi_d(t''),T(t'')]}\right]}{\tau_n^*[\Pi_d(t'),T(t')]} C_{ij}^{-1}(t,t')dt' \qquad \text{(II-17)}$$

where Π_d is the second invariant of the deformation rate tensor.

This equation has philosophical connections with a model suggested by Bogue (7) (later modified by Bogue and White (10)) and a more recent model by Carreau (12); that is, it involves an integral of the deformation rate (making it, therefore, more akin to models with a strain nonlinearity than to those with a rate nonlinearity). It is felt that Equation (II-17) is intuitively more reasonable than a statement in terms of strain itself; as presently written (see Chen and Bogue (16), for example), strain-type theories bring in nonlinearities with factors like $\dot{\gamma}t$ and $\dot{\gamma}t'$ rather than $\dot{\gamma}\tau$ (5, 69), with their being

no direct interaction between the relaxation function and the nonlinear function (i.e., the functions are factorable). While one could write down strain forms with those two effects "mixed together," it is not clear how one can do that without introducing new (and thus undetermined) functions.

Equation (II-17) does not prescribe the actual nonlinear function to be used. Probably many functions can be found, but one which has been used successfully in isothermal experiments is

$$\tau_n^*[\Pi_d(\cdot),T(\cdot)] = \frac{\tau_n^o a_T[T(\cdot)]}{1 + b\ \Pi_d^{1/2}(\cdot)\ a_T[T(\cdot)]\tau_n^o} \qquad \text{(II-18)}$$

where b is a dimensionless empirical parameter, usually 0.3 to 0.7 or so (10). Equation (II-17) combined with Equation (II-18) yield the results of the Bogue-White model in steady experiments, although the results in transient experiments will be somewhat different. (The integral in the argument of exp[ ] is slightly different, the form being similar to the Carreau model.)

CHAPTER III

EXPERIMENTAL EQUIPMENT AND PROCEDURES

A. MATERIALS

The materials investigated are two kinds of polystyrenes, the molecular weights of which are shown in Table I. Shell TC3-30 is a commercial material with a broad molecular distribution, while PS-670 is a special standard polystyrene with a narrow molecular distribution. These polystyrenes were extruded and formed into small cylindrical rods of about one millimeter diameter, to allow changing the sample temperature quickly.

B. EQUIPMENT

The experiments were carried out on an Instron tensile tester, with the sample being surrounded by two "clam shell" radiant heaters (Figure 1). The heater is basicly controlled by hot air circulated through a heating unit and the chamber. Also it has two shaped reflecting walls which focus radiant heat from thin nichrome wires onto the fiber-like sample. By applying (or removing) a voltage rapidly to the nichrome wires, one can quickly heat (or cool) the sample while it is being pulled.

TABLE I

MATERIALS USED IN THE PRESENT EXPERIMENTS

Polystyrene	M_n ($X10^3$)	M_w ($X10^3$)	M_w/M_n
Shell TC3-30*	61.2(59.0)	283(312)	5.30(5.29)
PS-670**	583.	670	1.15

*Manufactured by Shell Chemical Company.

**Manufactured by Pressure Chemical Corporation.

( ) Measured on GPC by Takaki (67)

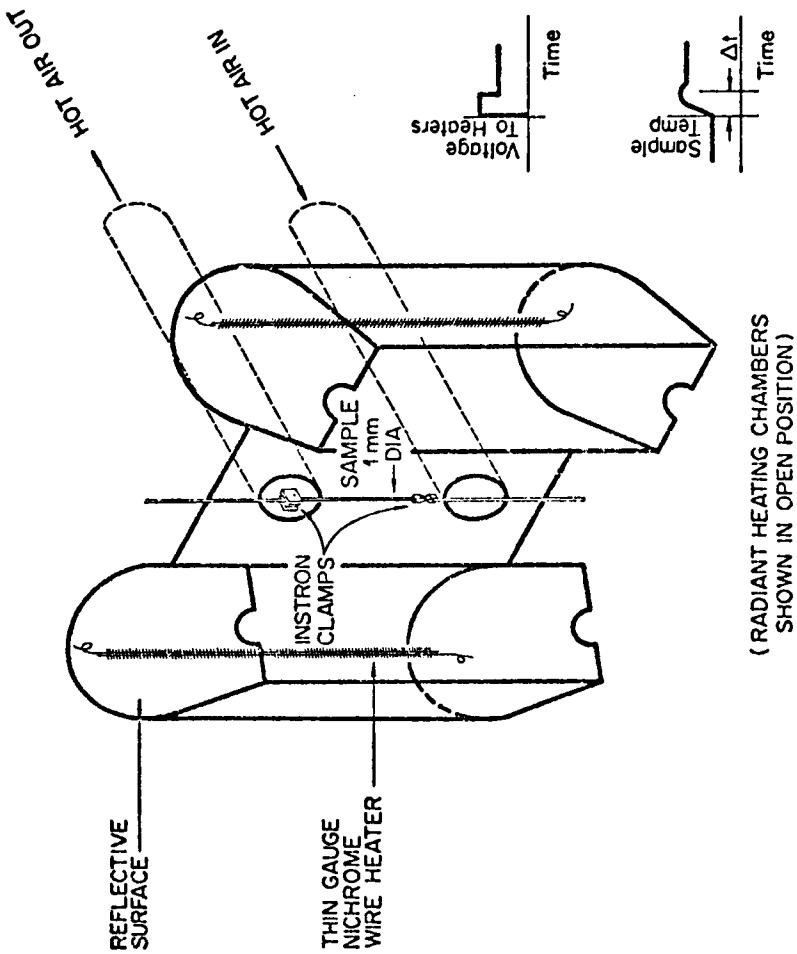

Figure 1. Sketch of Nonisothermal Test Apparatus.

C. CALIBRATION AND PRELIMINARY TESTS

Certain calibration and preliminary runs were made to determine the time lag in heating (or cooling) the sample, the effect of volume changes, and the magnitude of diameter variations along the length.

Measurement of Temperature

The temperature in the heater was measured by using a very thin thermocouple (about 0.1 mm) embedded in a dummy sample of the same diameter as the sample to be pulled. This allows one to experimentally obtain the time lag of the average temperature. The time lag can also be estimated by heat conduction theory. The estimated lag was about nine seconds (see Appendix). This value is not small enough for rapid changes in temperature. In order to produce a quick change of the sample temperature, programmed radiant heating was done. For heating, a certain high voltage (about 100 volts) was applied to the nichrome wires for a few seconds and then switched to a lower voltage (about 30 volts). For cooling, a high voltage was applied in advance, cut off for a few seconds, and then returned to a certain lower voltage. In both cases hot air at a constant temperature was being circulated. The temperature of the sample was changed from 119°C to 137°C (or vice versa). The time scale of the jump (Δt in Figure 1) was of order six seconds for the heating runs and 15 seconds for cooling runs (which were measured by the thermocouple coated by a dummy sample).

Effect of Volume Changes

In nonisothermal expansion one must take the thermal volume expansion (or contraction) into account because such changes affect the stresss. The effects were determined by first estimating the length change associated with a $20^{o}C$ jump of temperature; this length change was then imposed mechanically on an isothermal sample and the stress change measured. The estimated length change of polystyrene with a $20^{o}C$ jump was about 0.2 percent (see Appendix).

Figure 2 shows the tensile experiments with constant dL/dt in which the length changes were made by stopping the pulling, immediately contracting the sample by several precent, and starting the pulling again. From Figure 2, the stress change (decrease) due to the 0.2 percent length change was estimated as less than 0.6 percent, which is within the experimental error and may be neglected.

Diameter Variations

An important aspect of tensile experiments of this kind is the matter of diameter variation along the length of the sample. If the diameter variations are not uniform during the pulling, the analysis becomes extremely complicated. Recently Kamei and Onogi (41, 57) have done tensile experiments using polystyrene in the form of a rectangular sheet. They have reported that the sample tends to show a typical "thinning" when the strain goes beyond the yielding point; that is, the point where the load reaches a maximum value. In the present work, therefore, diameter variations along the length of the sample were measured by quickly opening the heating chamber and quenching

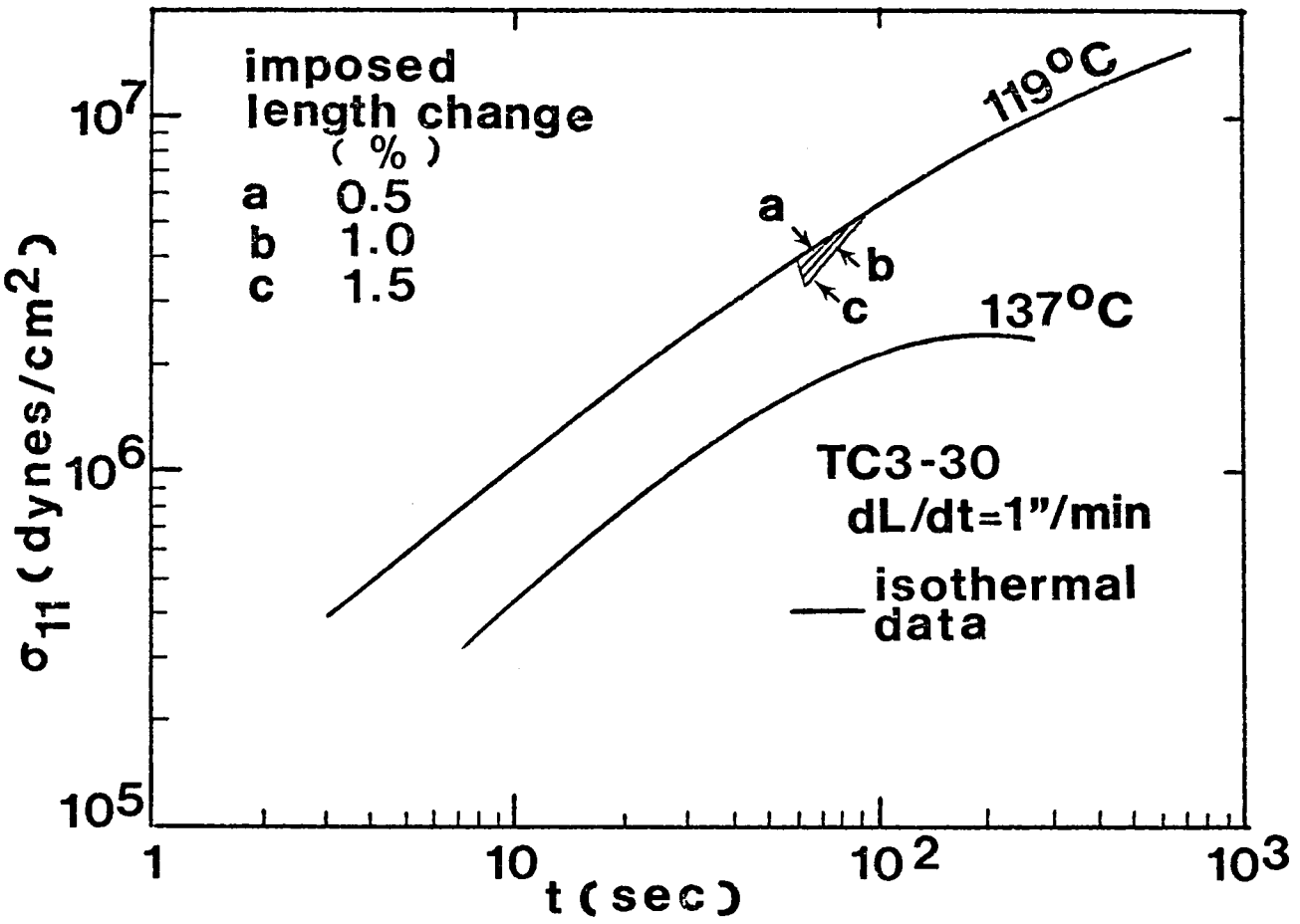

Figure 2. Simulation of Stresses due to Volume Change.

the samples at various stages of the pulling. Figures 3, 4, and 5 show the diameter distribution along the length. It is noticed that the elongational deformations remain fairly uniform up to large extensions although some irregular thinning takes place, especially at small elongation rates. This was suggested by prior viscoelastic theory (see White and Ide (74), for example) in that a material with small deformation rate asymptotically becomes Newtonian, for which case one has unstable behavior in stretching. Also there are some end effects, indirectly due to the clamps. It was felt, however, that except for a few randomly irregular samples, the diameter variations were within about 10 percent and could be neglected.

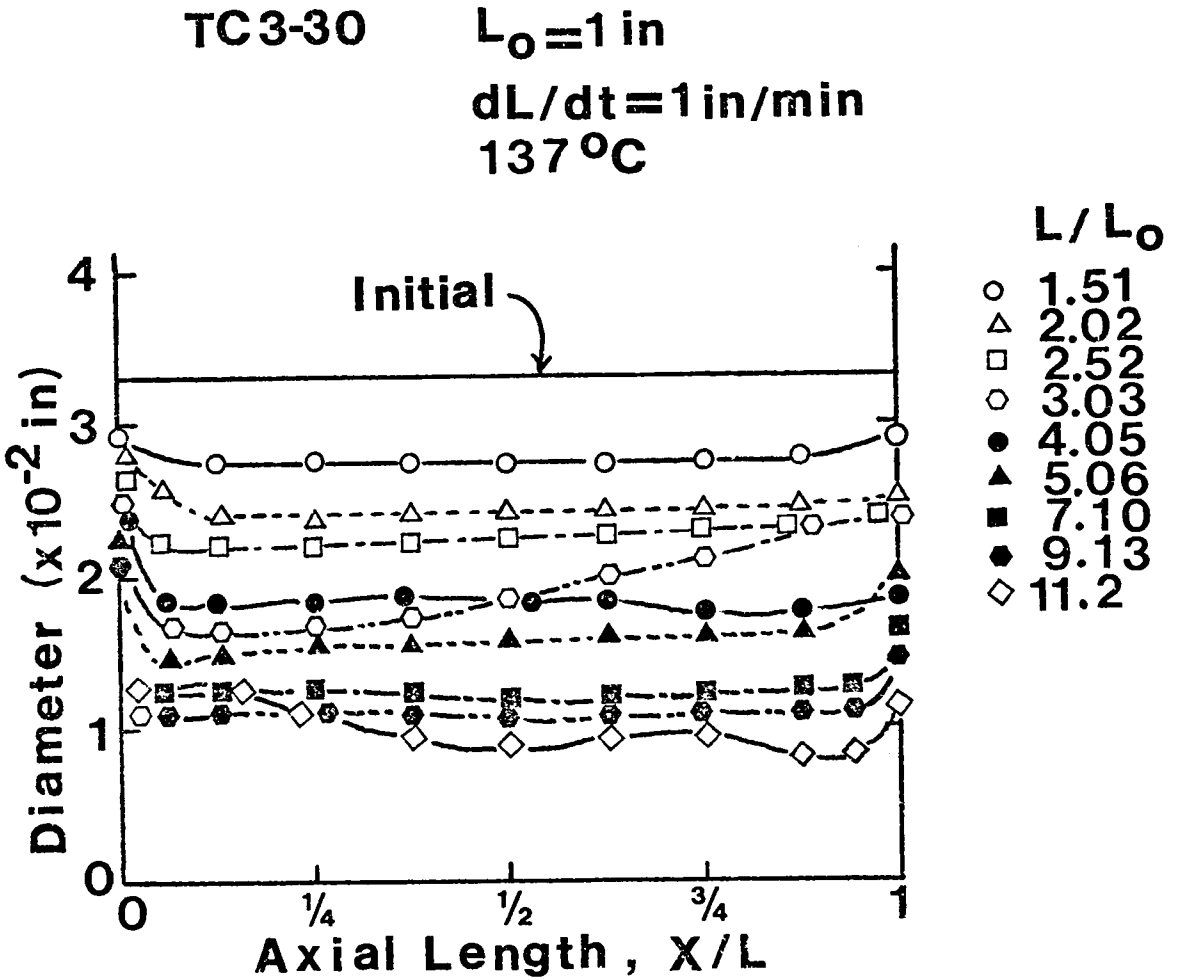

Figure 3. Diameter Variations along Sample Length at Various Stages of Pulling for Polystyrene TC3-30 at a Low Rate.

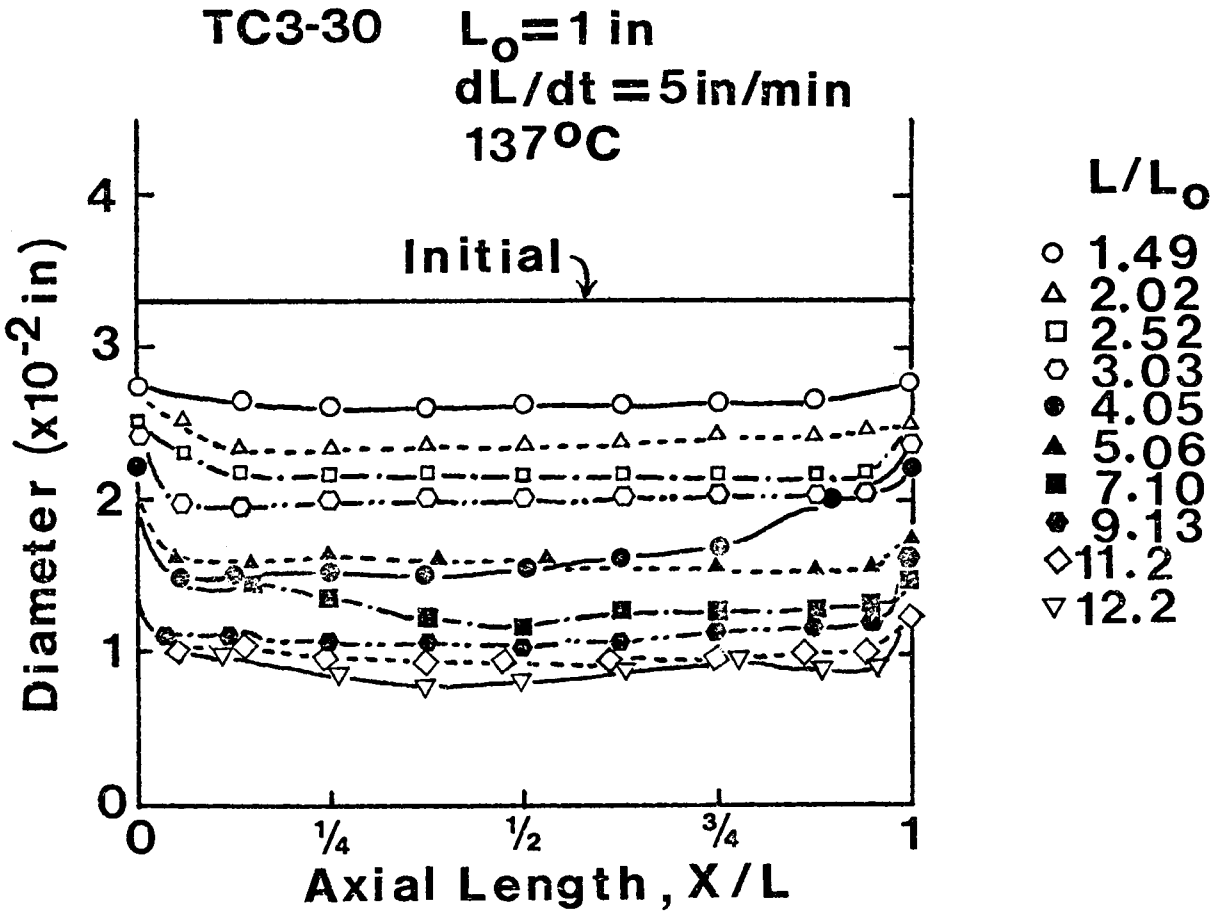

Figure 4. Diameter Variations along Sample Length at Various Stages of Pulling for Polystyrene TC3-30 at a Medium Rate.

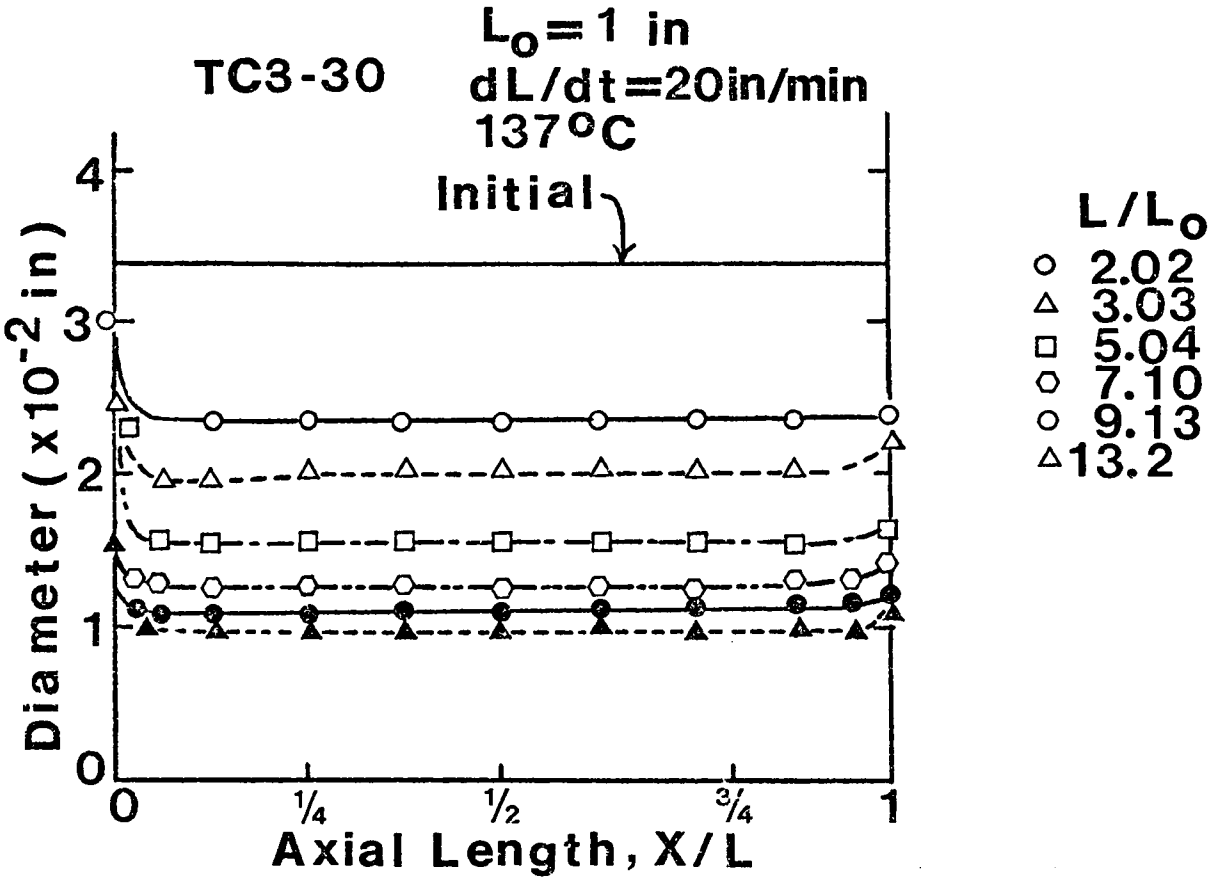

Figure 5. Diameter Variations along Sample Length at Various Stages of Pulling for Polystyrene TC3-30 at a High Rate.

CHAPTER IV

ISOTHERMAL AND NONISOTHERMAL EXPERIMENTS AND ANALYSIS

A. DETERMINATION OF PARAMETERS FROM SHEAR EXPERIMENTS

In order to analyze mechanical behavior, several material parameters, such as moculus, relaxation time, and the nonlinear parameter must be estimated in advance. Most of them were estimated from the shear rheogoniometer experiments reported by Takaki (67) and Masuda (50).

Shell TC3-30

Takaki studied viscometric flow and elongational behavior (involving failure) of polystyrene Shell TC3-30. His data for G" are shown in Figure 6. He evaluated the moduli and relaxation times from the molecular weight distribution using a quadratic blending law proposed by Masuda (50) combined with the corresponding constitutive theory by Bogue, et al. (9). The number of relaxation times was taken to be twenty five. In the present work, however, a rather simplified model was applied; that is, several moduli and relaxation times were determined in order to fit the G" data in Figure 6. These values at 137°C are summarized below:

$G_1 = 8.0 \times 10^6$ (dyne/cm^2) $\quad \tau_1 = 0.01$ (sec.)

$G_2 = 1.0 \times 10^6 \quad \tau_2 = 0.1$

$G_3 = 6.0 \times 10^5 \quad \tau_3 = 1.0$

$G_4 = 8.0 \times 10^5 \quad \tau_4 = 10$

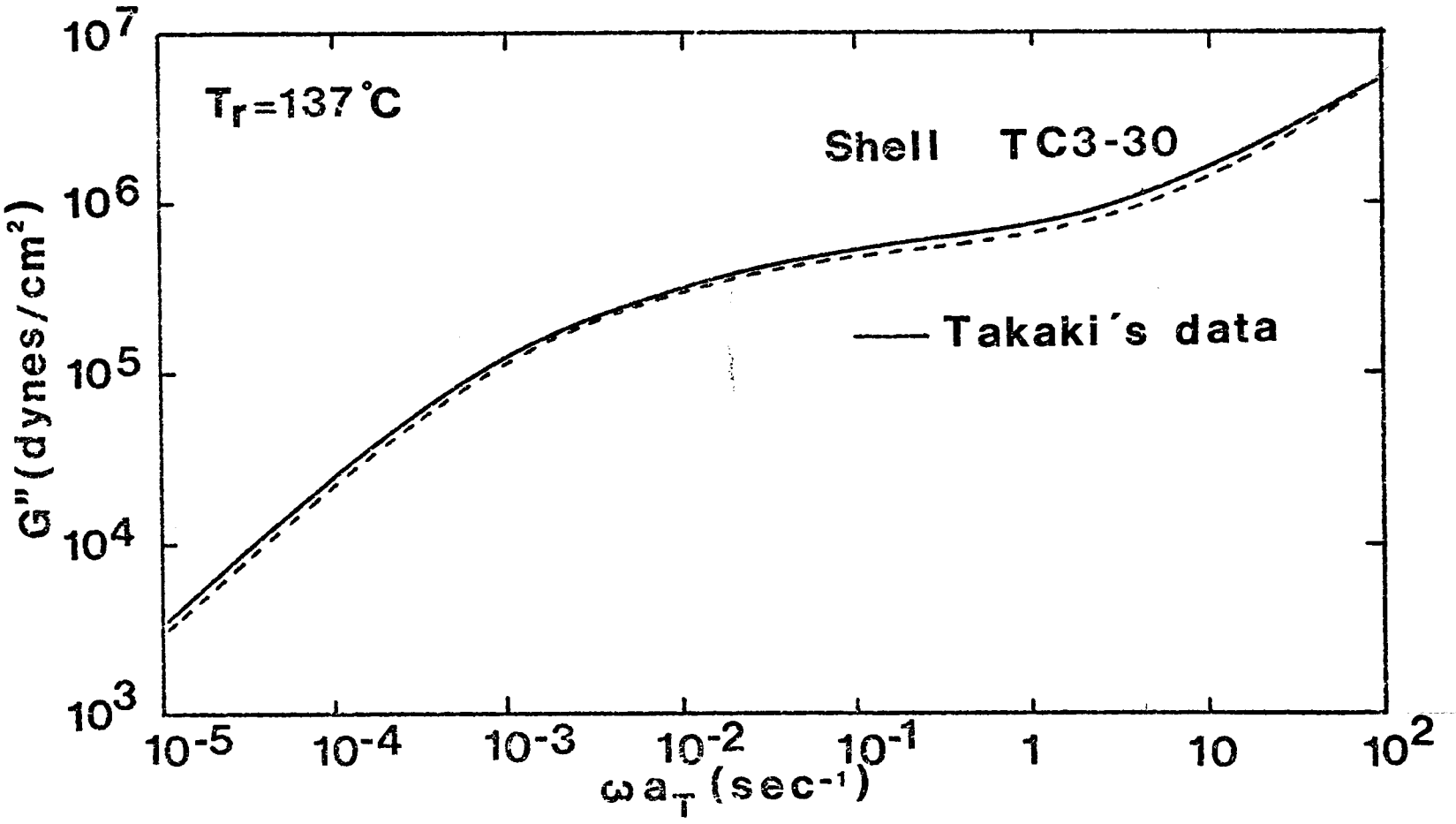

Figure 6. Loss Modulus for Polystyrene TC3-30.

$G_5 = 4.0 \times 10^5$ $\tau_5 = 100$

$G_6 = 1.6 \times 10^5$ $\tau_6 = 1000$

The G" curve was calculated by the following equation:

$$G''(\omega) = \sum_n G_n \frac{\omega \tau_n}{1 + \omega^2 \tau_n^2} \qquad \text{(IV-1)}$$

The result is shown by the dotted line in Figure 6. Also, those material parameters were tested by shear stress and normal stress data, using the well-known equations as follows (68):

$$\sigma_{12} = \sum_n G_n \frac{\dot{\gamma}\tau_n}{1 + b\dot{\gamma}\tau_n} \qquad \text{(IV-2)}$$

$$\sigma_{11} - \sigma_{22} = 2 \sum_n G_n \left[\frac{\dot{\gamma}\tau_n}{1 + b\dot{\gamma}\tau_n} \right]^2 \qquad \text{(IV-3)}$$

where $\dot{\gamma}$ denotes the shear rate, and b is equal to 0.5 which was suggested by Takaki (67). Figure 7 shows the above results. The solid lines are Takaki's data (67) and the dotted lines represent the theoretical evaluation by Equation (IV-2) and (IV-3). These theoretical results (based on the six moduli and time constants) agree well with the experimental data, and do not show any significant differences from Takaki's theoretical results. Therefore, these simplified material parameters can be reasonably introduced into the analysis for the elongational deformations.

The shift factors were evaluated from Takaki's work:

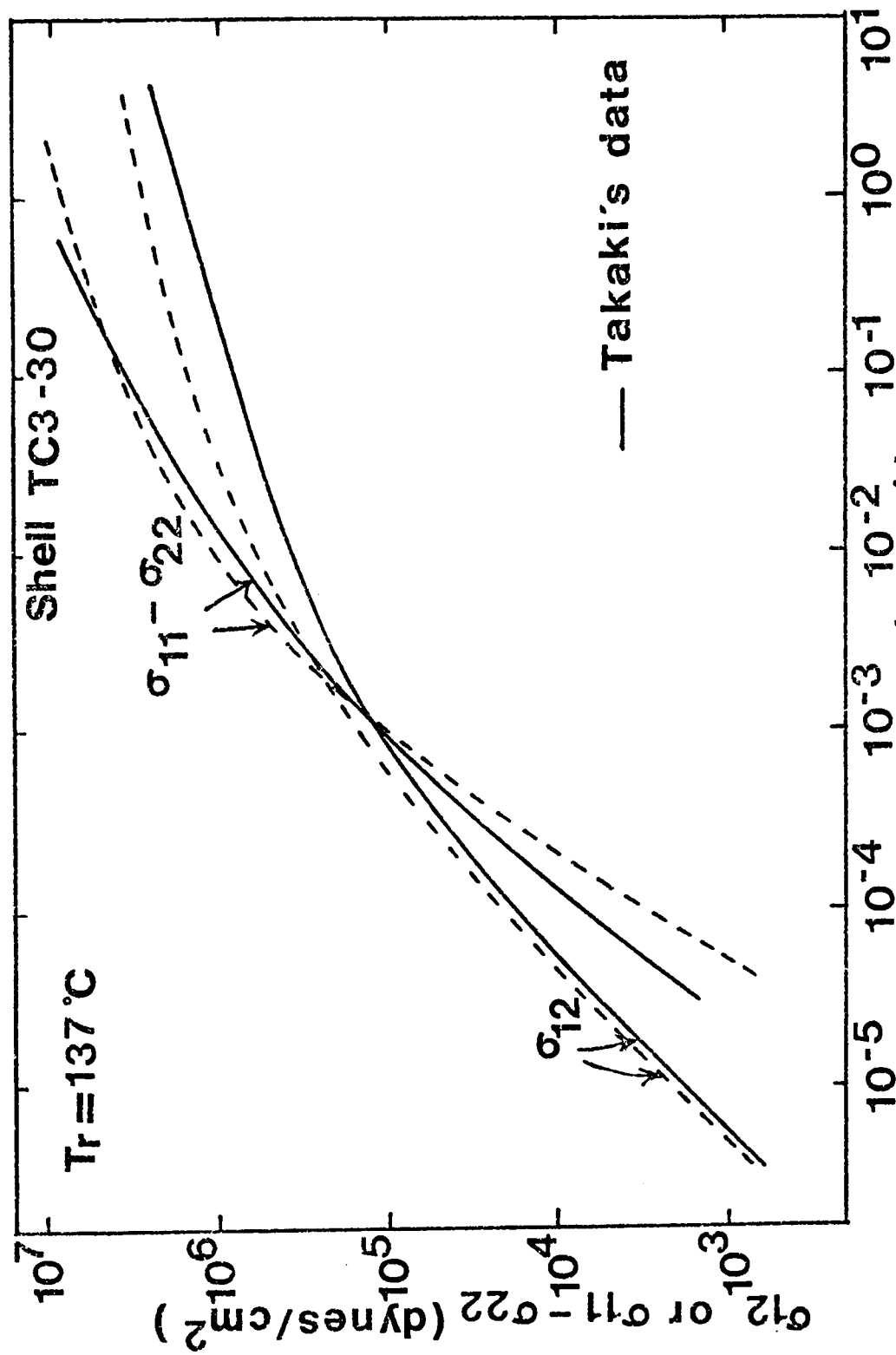

Figure 7. Steady Shear Properties of Polystyrene TC3-30, Reduced to 137°C.

a_T (160°C) = 0.033

a_T (137°C) = 1.0 (Reference)

a_T (119°C) = 60

PS-670

The material parameters for polystyrene PS-670, which has a high molecular weight and a narrow molecular weight distribution, have not been measured. However, one may determine these values from Masuda's work which deals with various kinds of polystyrene (50). Figure 8 shows a typical G" curve for a polystrene (L-44) with a narrow molecular weight distribution. A procedure similar to that used for the Shell TC3-30 was carried out to evaluate the moduli and relaxation times. The values obtained at 160°C are shown below:

$G_1 = 12 \times 10^6$ (dynes/cm^2)	$\tau_1 = 1.4 \times 10^{-4}$ (sec.)
$G_2 = 1.6 \times 10^6$	$\tau_2 = 1.4 \times 10^{-3}$
$G_3 = 0.6 \times 10^6$	$\tau_3 = 1.4 \times 10^{-2}$
$G_4 = 0.2 \times 10^6$	$\tau_4 = 1.4 \times 10^{-1}$
$G_5 = 0.3 \times 10^6$	$\tau_5 = 1.4 \times 10^{0}$
$G_6 = 0.4 \times 10^6$	$\tau_6 = 1.4 \times 10^{1}$
$G_7 = 0.5 \times 10^6$	$\tau_7 = 1.4 \times 10^{2}$
$G_8 = 0.7 \times 10^6$	$\tau_8 = 1.4 \times 10^{3}$

The dotted line in Figure 8 shows the curve obtained by substituting the above parameters into Equation (IV-1).

Since PS-670 has a different molecular weight from Masuda's (L-44),

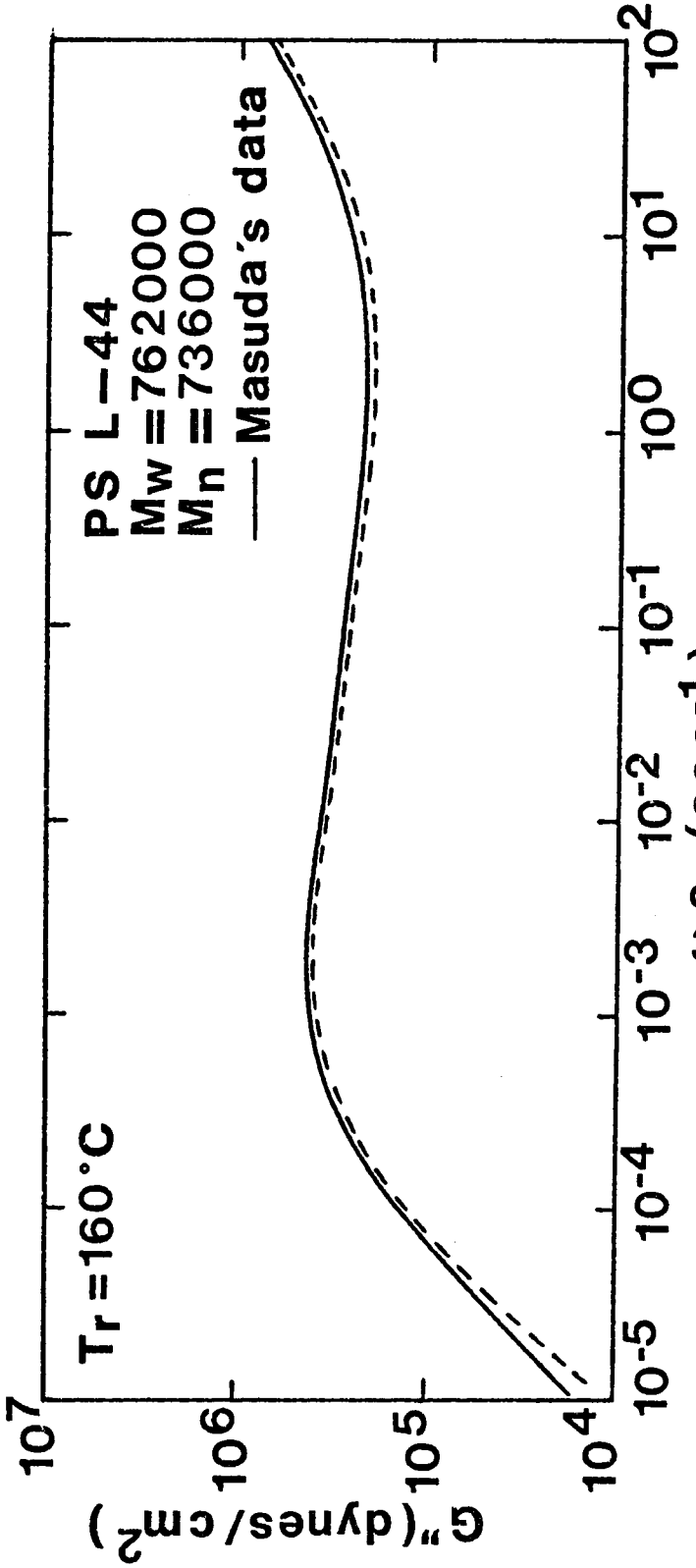

Figure 8. Loss Modulus for Polystyrene with Narrow Molecular Weight Distribution.

a certain adjustment is required for the relaxation times. As is well-known, the maximum relaxation time is proportional to the 3.5 power of molecular weight. Therefore, applying the factor

$$\left[\frac{M_w \text{ of PS-670}}{M_w \text{ of PS L-44}}\right]^{3.5} = 0.643$$

to the above relaxation times, one may estimate the relaxation times distribution for polystyrene PS-670 at 160°C as follows:

$G_1 = 12 \times 10^6$ (dynes/cm^2)	$\tau_1 = 0.9 \times 10^{-4}$ (sec.)
$G_2 = 1.6 \times 10^6$	$\tau_2 = 0.9 \times 10^{-3}$
$G_3 = 0.6 \times 10^6$	$\tau_3 = 0.9 \times 10^{-2}$
$G_4 = 0.2 \times 10^6$	$\tau_4 = 0.9 \times 10^{-1}$
$G_5 = 0.3 \times 10^6$	$\tau_5 = 0.9 \times 10^{0}$
$G_6 = 0.4 \times 10^6$	$\tau_6 = 0.9 \times 10^{1}$
$G_7 = 0.5 \times 10^6$	$\tau_7 = 0.9 \times 10^{2}$
$G_8 = 0.7 \times 10^6$	$\tau_8 = 0.9 \times 10^{3}$

The shift factors were calculated from Masuda's data (50).

a_T (160°C) = 1	(Reference)
a_T (135°C) = 112	
a_T (119°C) ≈ 10^4	

The b value was set equal to 0.4.

B. TEMPERATURE CHANGE DURING STRESS RELAXATION

Theoretical

The general solution of Equations (II-17) and (II-18) for nonisothermal stress relaxation is given by the following form:

$$\sigma_{11} = \sum_n G_n(t) \exp\left[-\int_0^t \frac{dt''}{\tau_n(t'')}\right]\left[\frac{\lambda^{(2-\sqrt{3}b)} - 1}{1 - \frac{\sqrt{3}}{2} b} - \frac{\lambda^{-(1+\sqrt{3}b)} - 1}{1 + \sqrt{3}b}\right] \tag{IV-4}$$

where $\tau_n(t'') = a_T[T(t'')]\tau_o$ and $\lambda = L/L_o \equiv 1 + \varepsilon$. In the case $b = 0$ and $T(t)$ = constant (i.e., isothermal linear viscoelastic case), Equation (IV-4) reduces to the familiar form

$$\sigma_{11} = (\lambda^2 - \lambda^{-1}) \sum_n G_n \exp(-t/\tau_n). \tag{IV-4a}$$

From the above equation the relaxation modulus has usually been defined by the equation

$$G(t) = \frac{\sigma_{11}}{\lambda^2 - \lambda^{-1}} = \sum_n G_n(T) \exp(-t/\tau_n[T]). \tag{IV-4b}$$

On the other hand, Equation (IV-4) involves the nonlinearity effect of the b parameter; that is, the tensile stress σ_{11} becomes nonlinear in the strain $(\lambda^2 - \lambda^{-1})$ for large elongation. However, one may define a reduced relaxation modulus by the equation

$$\tilde{G}(t) = \frac{\sigma_{11}}{\Lambda} = \sum_n G_n(t) \exp\left(-\int_0^t \frac{dt''}{\tau_n(t'')}\right) \tag{IV-5}$$

where

$$\Lambda = \frac{\lambda^{A} - 1}{(A/2)} - \frac{\lambda^{-B} - 1}{B}$$

$$A = 2 - \sqrt{3}\, b, \quad B = 1 + \sqrt{3}\, b.$$

If one introduces the weighted time

$$\xi = \int_0^t \frac{dt''}{a_T[T(t'')]} \tag{IV-6}$$

the reduced relaxation modulus can be rearranged to

$$\tilde{G}(\xi) = \sum_n G_n(\xi) \exp(-\xi/\tau_n^0). \tag{IV-7}$$

This result is important because it shows that in nonisothermal relaxation experiments the relaxation moduli can be superposed on a isothermal reference in terms of the weighted time. This idea was first proposed by Morland and Lee (53). For example, in the case of a stepwise temperature change of the type

$$T = \begin{cases} T_1 & (0 < t < t_1) \\ T_2 & (t > t_1) \end{cases}$$

the weighted time is given by

$$\xi = \begin{cases} \dfrac{t}{a_T[T_1]} & (t < t_1) \\ \dfrac{t}{a_T[T_1]} + \dfrac{t - t_1}{a_T[T_2]} & (t > t_1) \end{cases}$$

Experiments

The first experiments consisted of changes of temperature during stress relaxation; i.e., an initial "instantaneous" pull, followed by a stress relaxation of the now stationary sample; the temperature jump is imposed at various points during the relaxation period. The data are shown in Figures 9 and 10. The open circles, triangles, and squares are nonisothermal experimental data in which the temperature was held at 119°C up to the points shown by the arrows, at which time it was changed abruptly to 137°C (or 135°C for PS-670). The isothermal data are also plotted by closed symbols. The solid lines are theoretical lines, the upper and lower ones being the isothermal asymptotes (relaxation at 137°C (or 135°C) and 119°C) and the line interpolating between them being the nonisothermal prediction by Equation (IV-5) for a step change of temperature. The theory fits the data fairly well for Shell TC3-30, while it does poorly for PS-670. Probably this is due to our incomplete knowledge of the material parameters which were estimated from Masuda's work (50).

The dotted lines show a phenomenological test on the nonisothermal constitutive theory (Equation (IV-5)) without predetermining the material parameters such as G_n and τ_n. In Figure 9, for example, one can draw the optimum line (shown by the dotted line number 1) through the data for the isothermal stress relaxation at 137°C. One calls this

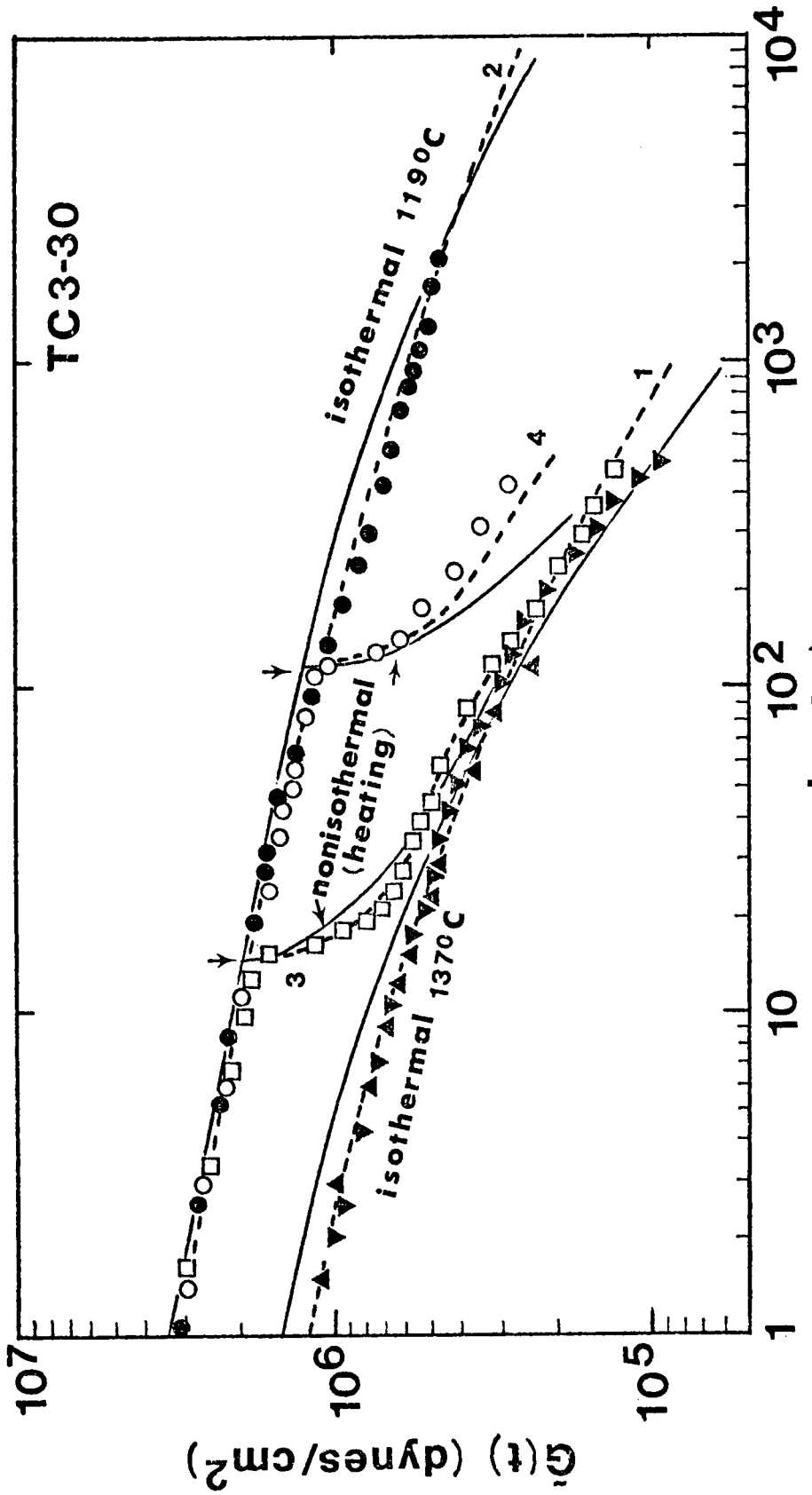

Figure 9. Isothermal and Nonisothermal Stress Relaxation for Polystyrene TC3-30.

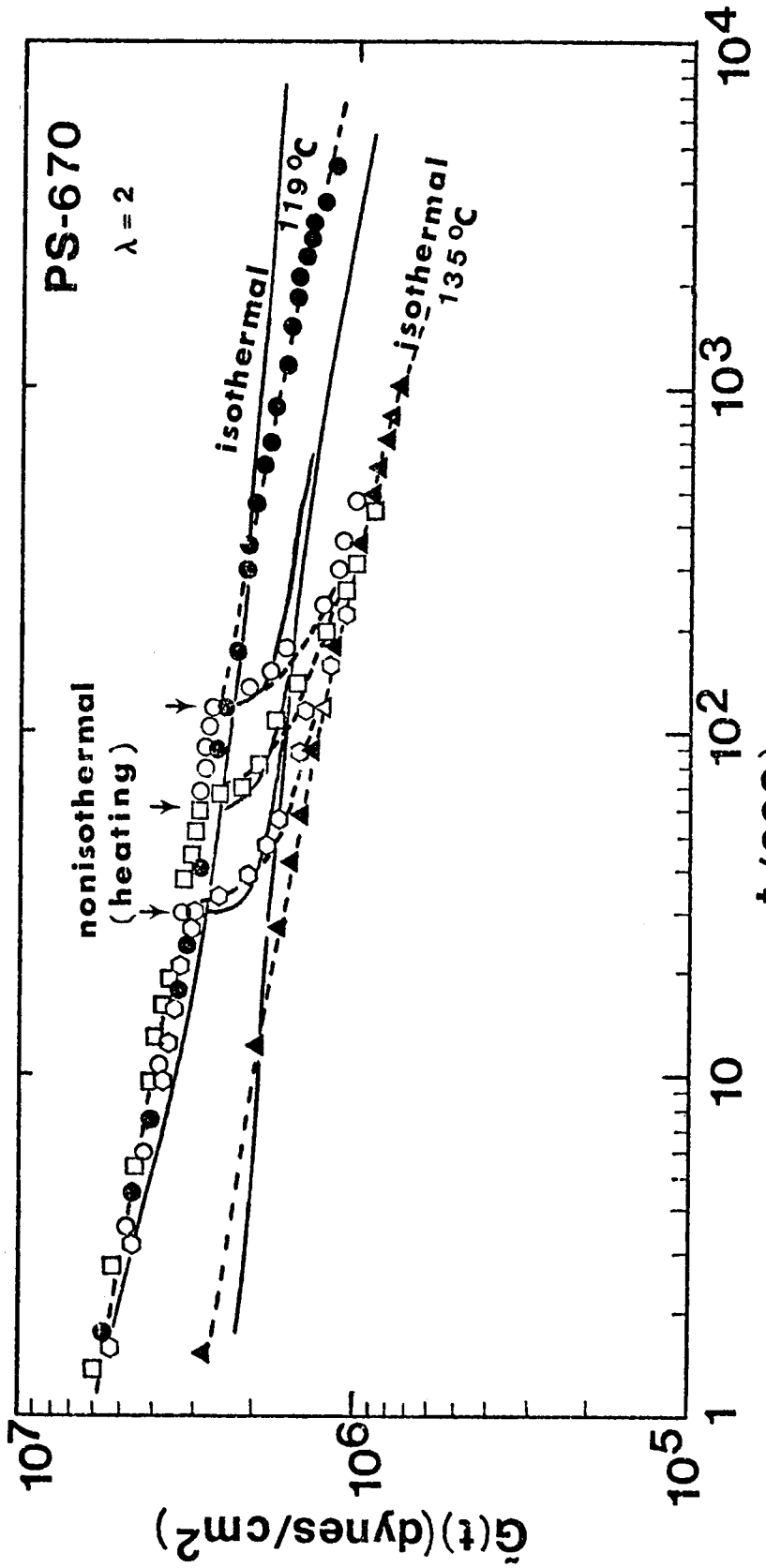

Figure 10. Isothermal and Nonisothermal Stress Relaxation for Polystyrene PS-670.

dotted line (the relaxation modulus) $\tilde{G}(t)$ at 137°C, without specifying its mathematical form. For the isothermal data at 119°C, the relaxation modulus should be identical to the shifted $\tilde{G}(t)$ as follows:

$$\tilde{G}\left[\frac{a_T[137^oC]}{a_T[119^oC]}\, t\right]$$

This is a simple time-temperature superposition and works well as shown by the dotted line number 2. The ratio $a_T[137^oC]/a_T[119^oC]$ is determined by the shift between two isothermal levels and its value is 1/60. For the nonisothermal (heating) cases, Equation (IV-5) leads to the following form of the relaxation modulus:

$$\tilde{G}\left[\frac{a_T[137^oC]}{a_T[119^oC]}\, t_c + (t-t_c)\right], \quad t > t_c$$

where t_c is the time of temperature change. This partially translational shift is shown by the dotted lines (numbers 3 and 4) interpolated between isothermal lines. These dotted lines show better agreement with experimental data than the prediction (solid lines) in which the material parameters were evaluated from shear flow. This suggests the difficulties of exact determination of the material parameters. Particularly for PS-670 there seems to be some inaccuracy in estimating the relaxation times. However, the important fact in these nonisothermal relaxation experiments is that the time scale of the experimental stress change from one isothermal stage to another is longer than that of the imposed temperature change (which is about six seconds).

Another important aspect of the nonisothermal constitutive theory in the relaxation experiments is whether or not one can deal with the nonisothermal relaxation modulus in terms of a generalized time-temperature superposition as proposed by Equations (IV-6) and (IV-7). These superpositions are shown in Figures 11 and 12, in which the relaxation moduli are plotted against the weighted time from Equation (IV-6). The shift factors used were calculated from two isothermal levels of the relaxation experiments as

$$a_T[137^oC] = 1,\ a_T[119^oC] = 60 \text{ for TC3-30}$$
$$a_T[135^oC] = 1,\ a_T[119^oC] = 50 \text{ for PS-670.}$$

The values of the shift factor obtained above for PS-670 were different by a factor of two from those estimated in the previous section. The results in Figures 11 and 12 show that superposition works well although some data are not exactly fitted in the nonisothermal case. Therefore, the essential idea of the nonisothermal constitutive theory seems to be satisfied.

C. TEMPERATURE CHANGE DURING TENSILE PULLING

Another type of experiment was done by imposing abrupt changes of temperature during tensile pulling with a constant rate of total elongation (i.e., dL/dt = constant, with $\dot{E}$ decreasing in time).

Theoretical

Before discussing the experimental results, it is convenient to

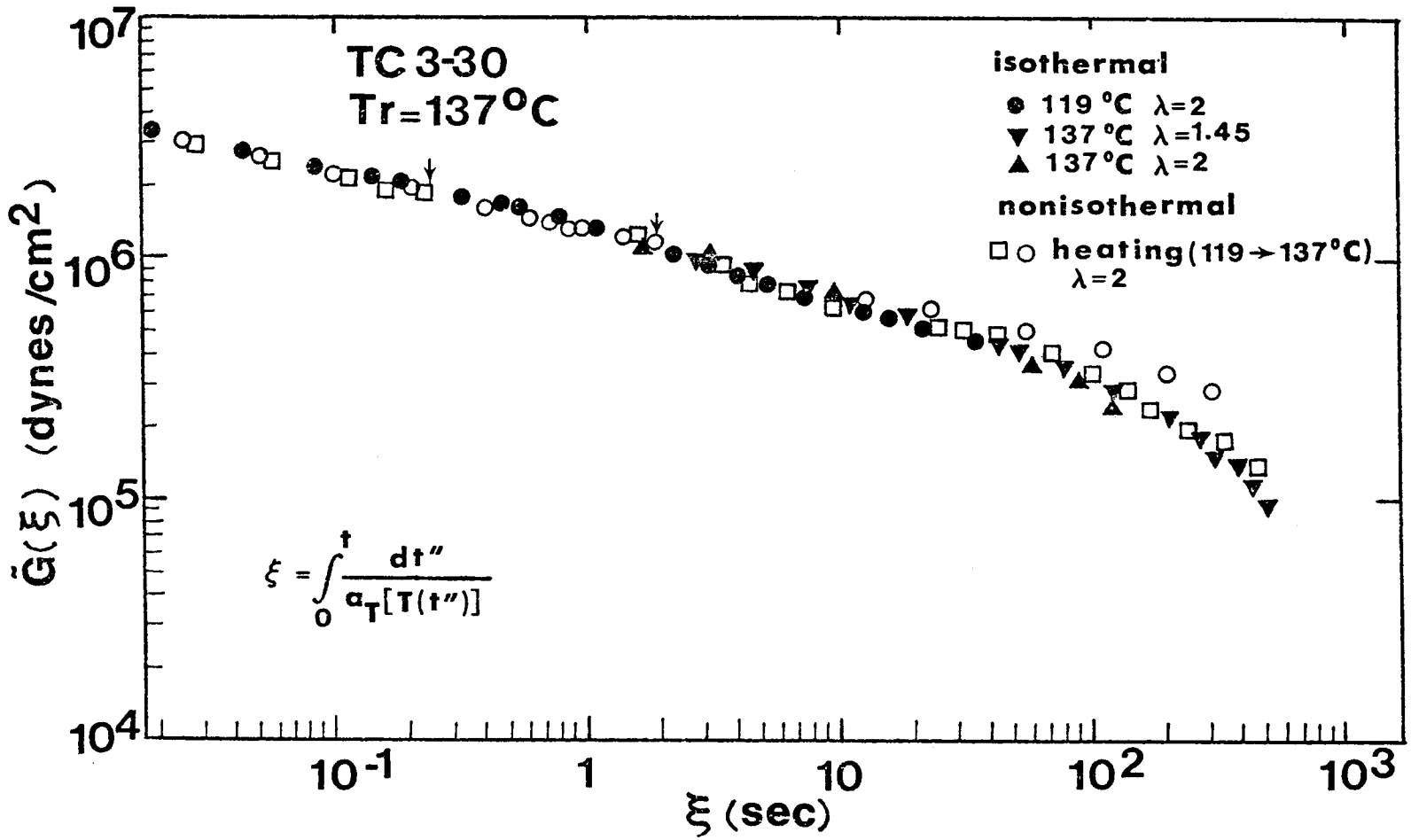

Figure 11. Superposition of Isothermal and Nonisothermal Stress Relaxation Data for Polystyrene TC3-30 (Reference Temperature 137°C).

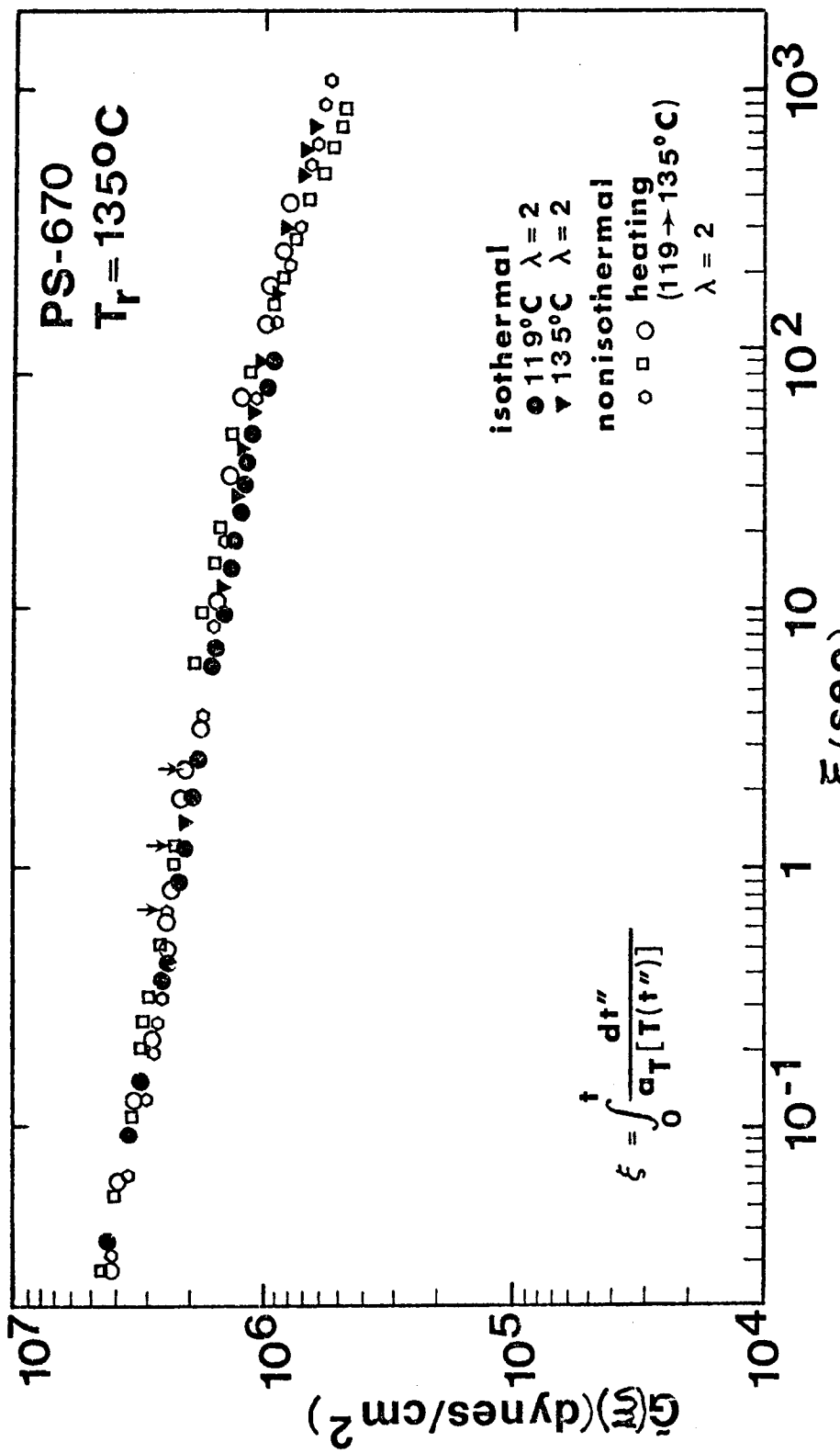

Figure 12. Superposition of Isothermal and Nonisothermal Stress Relaxation Data for Polystyrene PS-670 (Reference Temperature 135°C).

have a theoretical derivation starting with Equation (II-17). As dL/dt is constant the Finger deformation tensors can be determined as below:

$$C_{11}^{-1} = \left(\frac{1 + \dot{E}_o t}{1 + \dot{E}_o t'} \right)^2 ; \quad C_{22}^{-1} = \frac{1 + \dot{E}_o t'}{1 + \dot{E}_o t} \quad ; \quad t' \geq 0$$

$$C_{11}^{-1} = (1 + \dot{E}_o t)^2 ; \quad C_{22}^{-1} = (1 + \dot{E}_o t)^{-1} ; \quad t' < 0 \qquad \text{(IV-8)}$$

$$\Pi_d = \frac{\sqrt{3}\,\dot{E}_o}{1 + \dot{E}_o t'} \quad \text{for } t' \geq 0; \; \Pi_d = 0 \text{ for } t' < 0 \qquad \text{(IV-9)}$$

where

$$\dot{E}_o = \left(\frac{1}{L} \frac{dL}{dt} \right)_{t=0} \text{ (initial elongation rate).}$$

Equation (II-17) can be integrated by parts under the boundary condition $\sigma_{22} = 0$ as follows:

$$\sigma_{11} = -\sum_n G_n(t) \int_{-\infty}^{t} \exp \left[-\int_{t'}^{t} \frac{dt''}{\tau_n^*[T(t''),\Pi(t'')]} \right] (\dot{C}_{11}^{-1} - \dot{C}_{22}^{-1}) dt' \qquad \text{(IV-10)}$$

Substituting Equation (IV-8) into Equation (II-18) one obtains

$$\int_{t'}^{t} \frac{dt''}{\tau_n^*[T(t''),\Pi(t'')]} = \int_{t'}^{t} \frac{dt''}{\tau_n^o a_T[T(t'')]} + \sqrt{3}\, b \ln\left(\frac{1 + \dot{E}_o t}{1 + \dot{E}_o t'} \right). \qquad \text{(IV-11)}$$

Then Equation (IV-10) leads to the following form:

$$\sigma_{11} = \frac{\dot{E}_o}{1+\dot{E}_o t} \sum_n G_n(t) \int_0^t \exp\left(-\int_{t'}^t \frac{dt''}{\tau_n^o a_T[T(t'')]}\right)\left(\frac{1+\dot{E}_o t'}{1+\dot{E}_o t}\right)^{\sqrt{3}\, b} \left[1+ 2\left(\frac{1+\dot{E}_o t}{1+\dot{E}_o t'}\right)^3\right] dt' \qquad \text{(IV-12)}$$

Since Equation (IV-12) cannot be integrated analytically, a numerical integration was carried out on the IBM 360 computer, while the $G_n(t)$ were regarded as constant within the range of the experimental temperature changes. The material parameters evaluated in Chapter IV-A were used in the calculations. Equation (IV-12) already involves the nonlinear effect which decreases the value of the memory function with a large deformation. There are several ways for introducing the nonlinearity. Some will be discussed later.

Isothermal Pulling

Before the nonisothermal experiments were done, isothermal tensile experiments with constant (dL/dt) were carried out in order to understand the basic behavior. The initial length of the samples was one inch. Three different rates of pulling were applied:

(1) $\frac{dL}{dt}$ = i in./min. $(\dot{E}_o = 0.0167)$

(2) $\frac{dL}{dt}$ = 5 in./min. $(\dot{E}_o = 0.0833)$

(3) $\frac{dL}{dt}$ = 20 in./min. $(\dot{E}_o = 0.333)$

Typical data for polystyrene TC3-30 are shown in Figures 13 and 14.

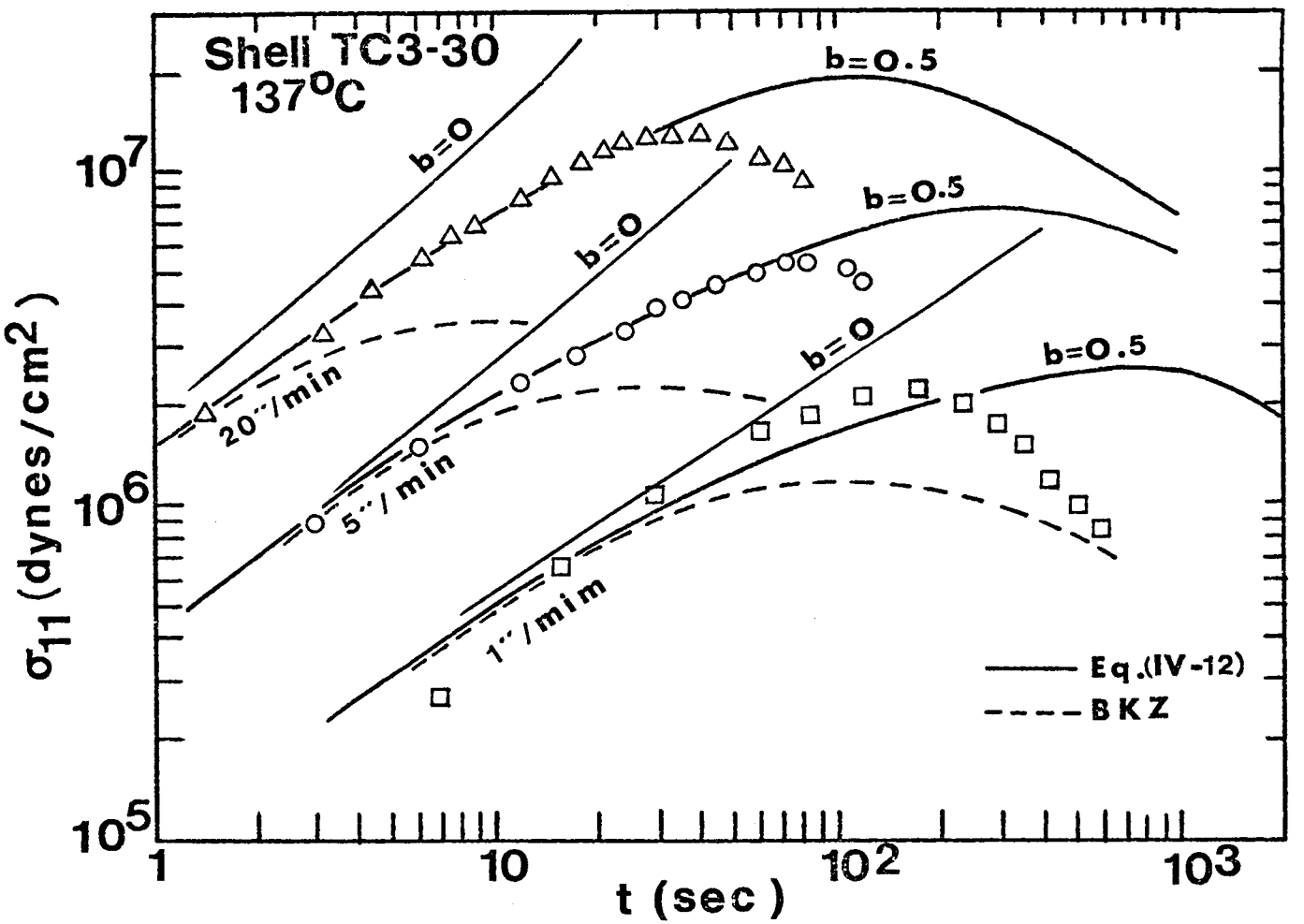

Figure 13. Comparison of Predicted and Experimental Tensile Stresses for Isothermal Tensile Pulling of Polystyrene TC3-30 at 137°C.

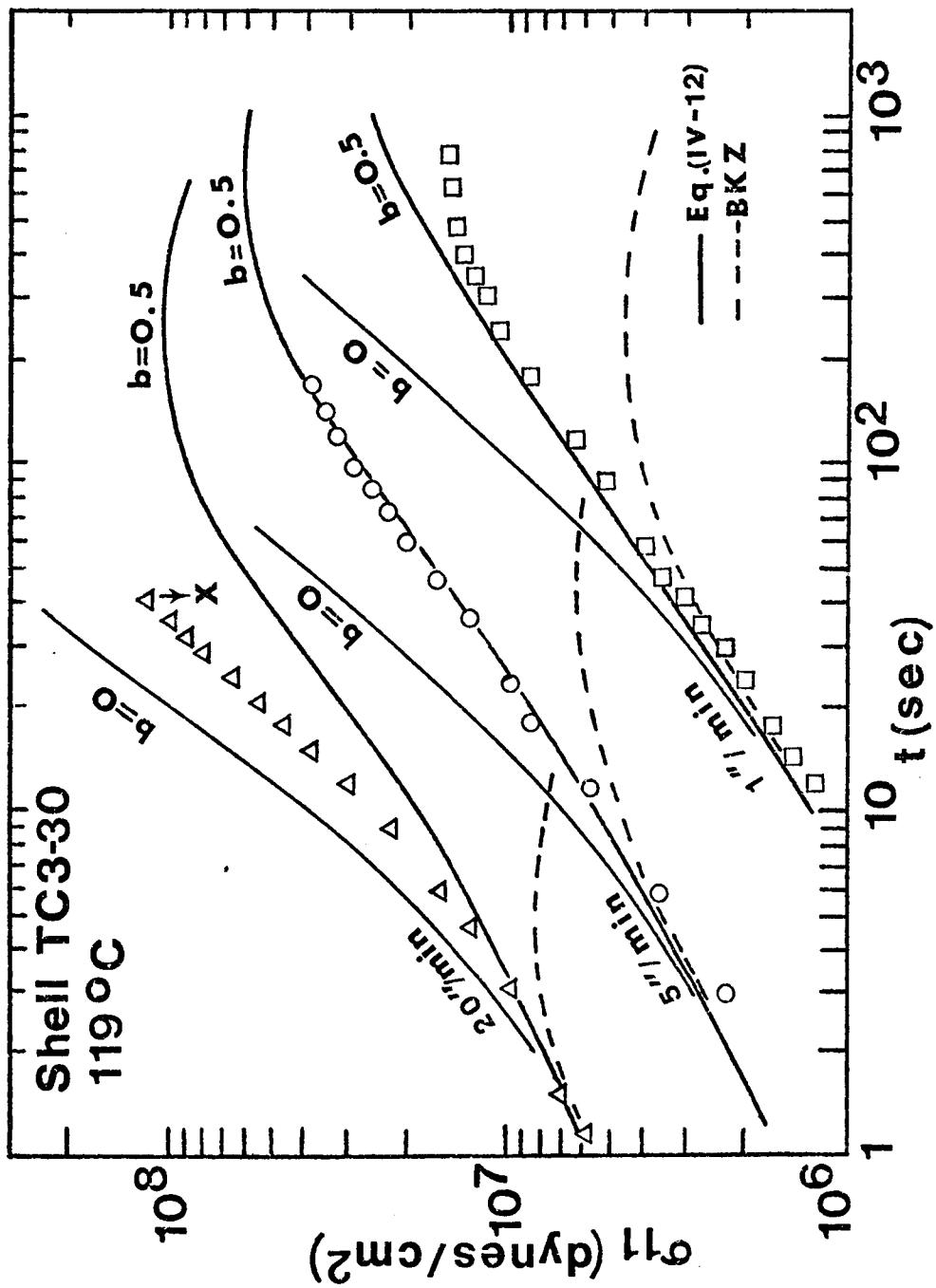

Figure 14. Comparison of Predicted and Experimental Tensile Stresses for Isothermal Tensile Pulling of Polystyrene TC3-30 at 119°C.

The stress curve shows an initial increase due to the mainly elastic deformation, followed by a falling off due both to decreasing $\dot{E}(t)$ and to relaxation. Unlike experiments with constant $\dot{E}(t)$ (39, 51), the stress falls off at the final stage because $\dot{E}(t)$ is decreasing. The data show a maximum in the stress (or a break before the stress reaches the maximum).

Three kinds of theoretical curves are shown for comparison. The solid lines with b = 0 represent the linear viscoelastic theory, which is calculated by Equation (IV-12) setting the nonlinear parameter b equal to zero. The predicted stress by this theory is higher than the experimental data at the larger elongations. This suggests that one must introduce some kind of nonlinearity into the theory of elongational flows in a manner similar to that for shear flows. The solid lines with b = 0.5 represent the present nonlinear viscoelastic theory by Equation (IV-12) setting the b value equal to 0.5, which was assigned in the previous section. The theory shows fairly good agreement with the experimental data, but the maximum points in the stress data appear earlier than predicted. This trend is partly because the longer relaxation times disappear more rapidly at large deformations than the theory predicts; also partly because of the experimental difficulty of achieving a uniform elongation. The dotted lines represent the theory from the first approximation of the BKZ model (5); that is,

$$\sigma_{ij} = -p\delta_{ij} + \int_{-\infty}^{t} [m_1 C_{ij}^{-1} - m_2 C_{ij}]dt' \qquad \text{(IV-13)}$$

where

$$m_1 = 2\frac{\partial U}{\partial I_{C^{-1}}} \; ; \quad m_2 = 2\frac{\partial U}{\partial II_{C^{-1}}}$$

$$U = \sum_n \frac{G_n}{\tau_n} \exp\left(-\frac{t-t'}{\tau_n}\right) \frac{9}{4} \ln\left[1 + \frac{1}{9}\left[I_{C^{-1}} + II_{C^{-1}} - 6\right]\right]$$

and $I_{C^{-1}}$ and $II_{C^{-1}}$ are the first and second invariants of the Finger tensor, respectively. The BKZ model brings in the nonlinearity as a function of the strain invariants, while the present theory brings in an integral of the second invariant of the strain rate tensor. The predicted stress from Equation (IV-13) is much lower than the experimental data at the larger elongation. At least for the particular U-function used here, the BKZ model (Equation IV-13) seems too strong. The Carreau model (12) was not tested because of many unknown parameters. With the present uncertainty about appropriate nonlinear models for even the isothermal case, further consideration of the nonisothermal case is probably not fruitful at the present time.

Nonisothermal Pulling

The nonisothermal experiments consisted of imposing changes of temperature during the tensile pulling as mentioned in the last section. The temperature changes were imposed in a way similar to those in the relaxation experiments: heating within six seconds and cooling within 15 seconds. The theoretical prediction was calculated by numerically integrating Equation (IV-12). The experimental data for polystyrenes Shell TC3-30 and PS-670 are shown in Figures 15 through 24. There seems to be a consistent trend to the effect that the

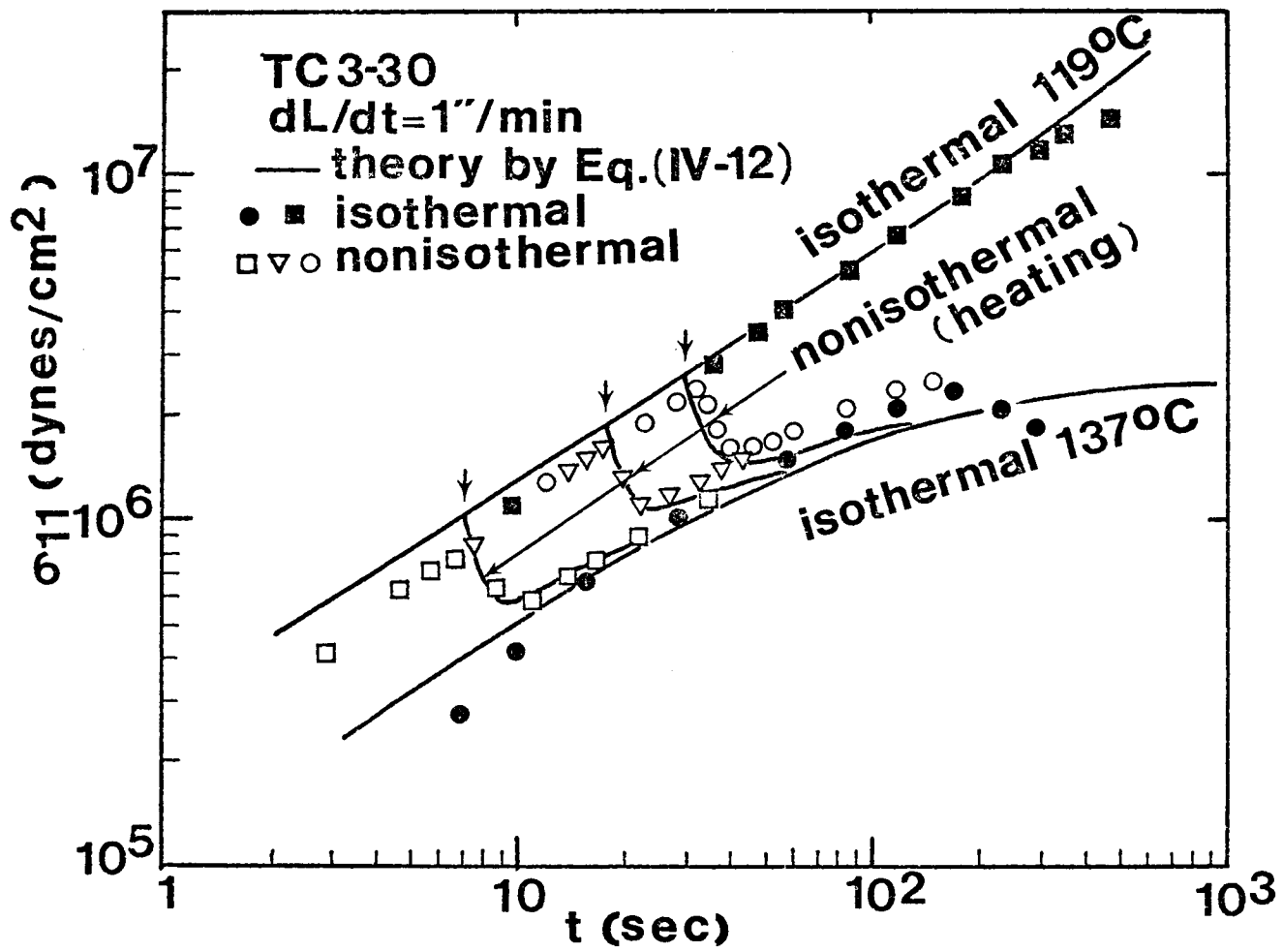

Figure 15. Isothermal and Nonisothermal (Heating) Data for Tensile Pulling of Polystyrene TC3-30 at a Low Rate.

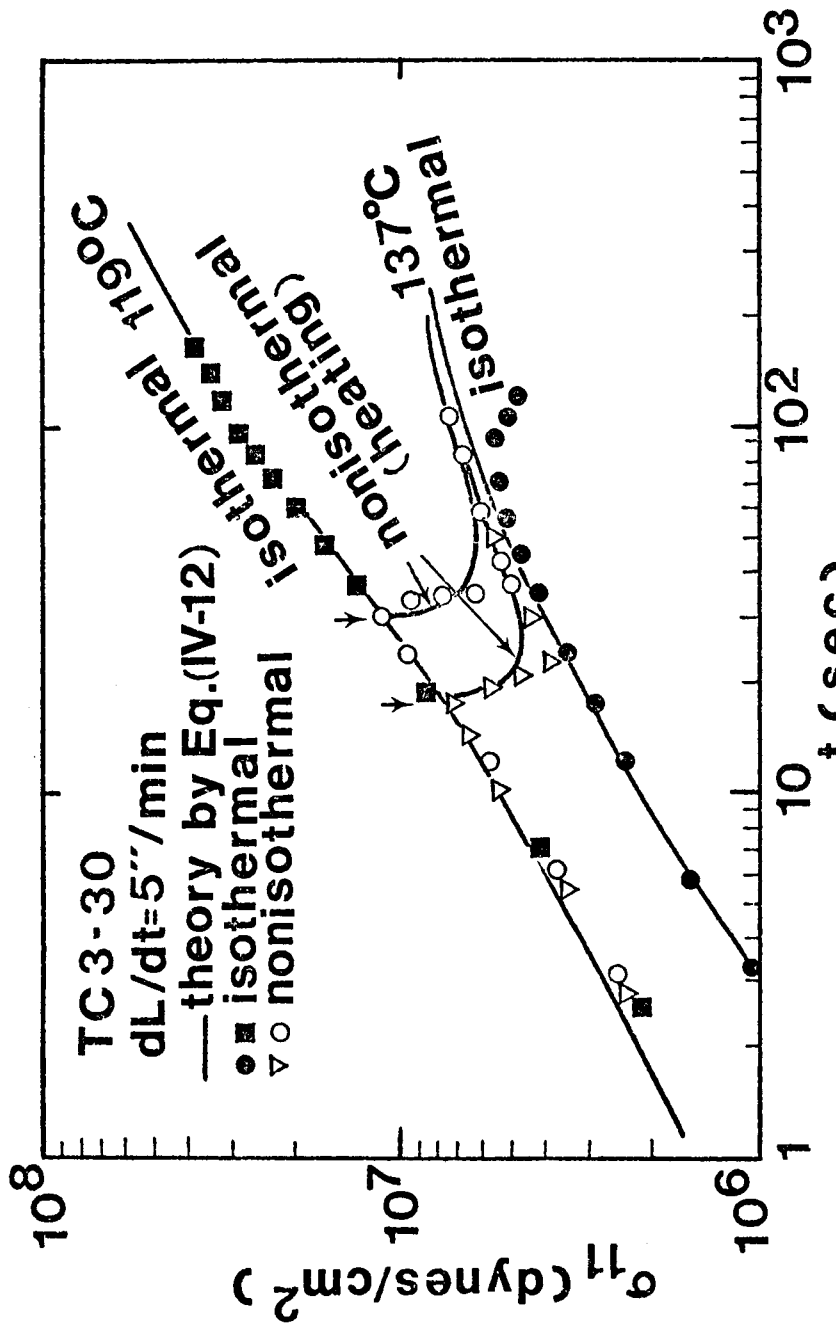

Figure 16. Isothermal and Nonisothermal (Heating) Data for Tensile Pulling of Polystyrene TC3-30 at a Medium Rate.

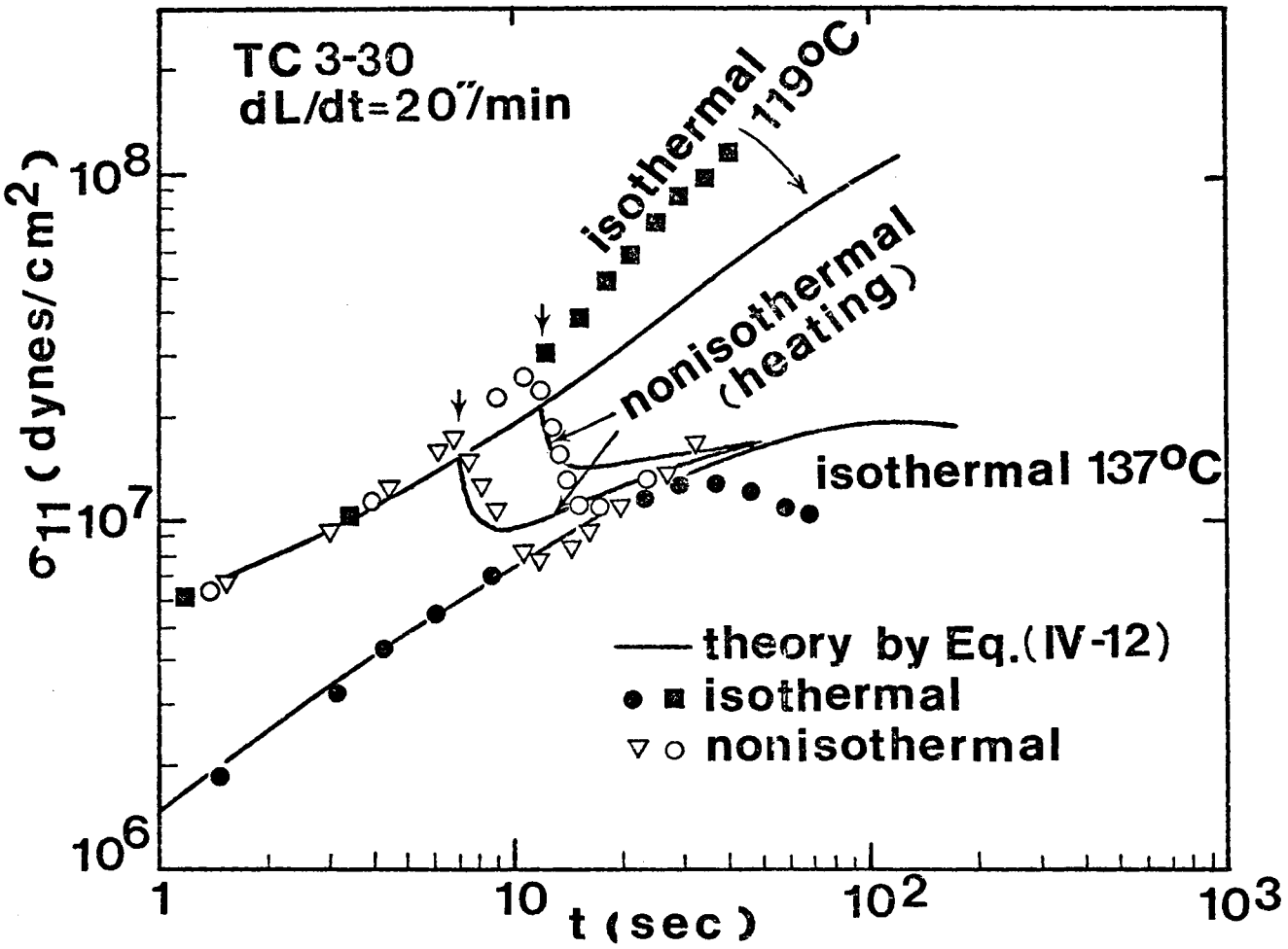

Figure 17. Isothermal and Nonisothermal (Heating) Data for Tensile Pulling of Polystyrene TC3-30 at a High Rate.

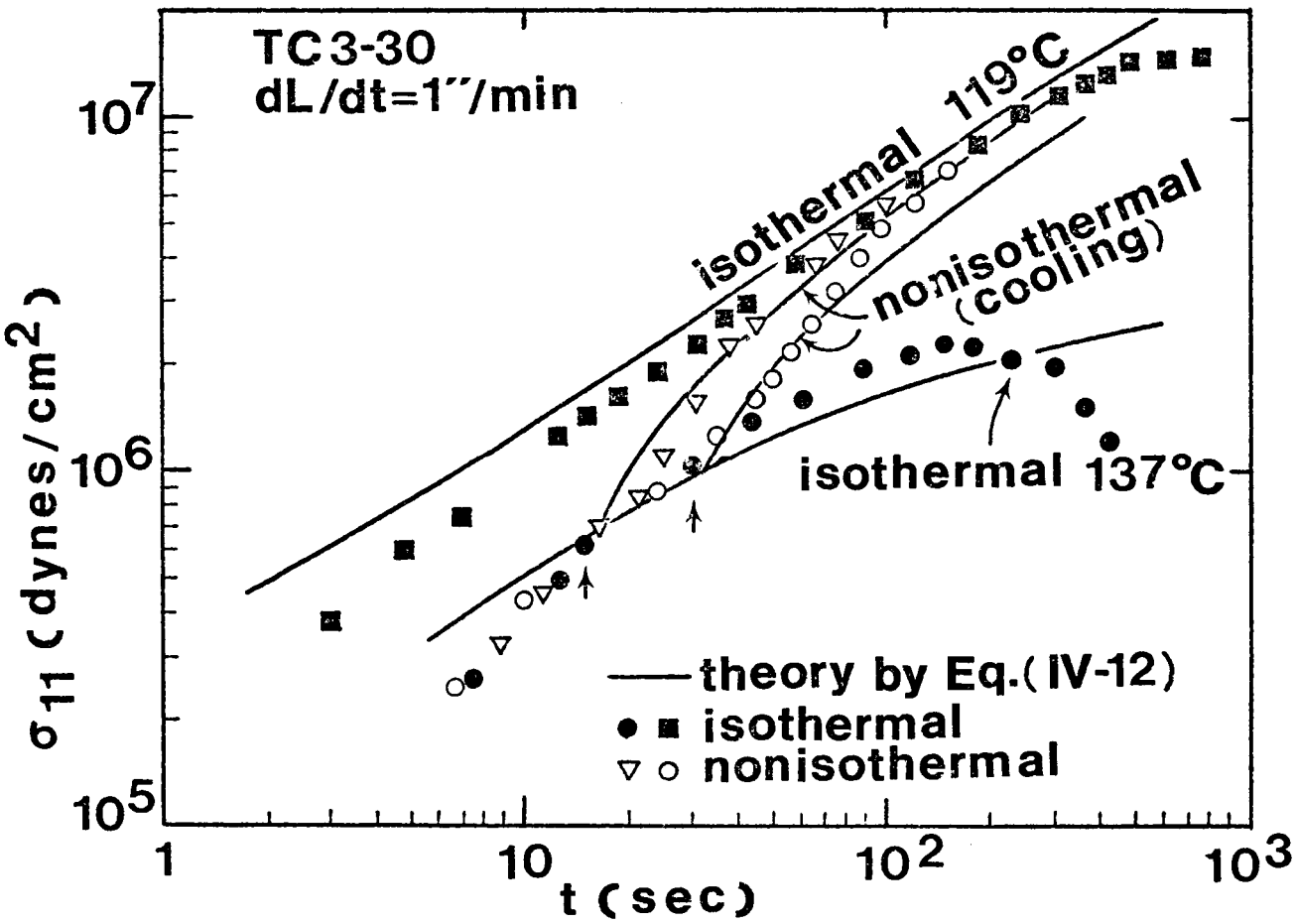

Figure 18. Isothermal and Nonisothermal (Cooling) Data for Tensile Pulling of Polystyrene TC3-30 at a Low Rate.

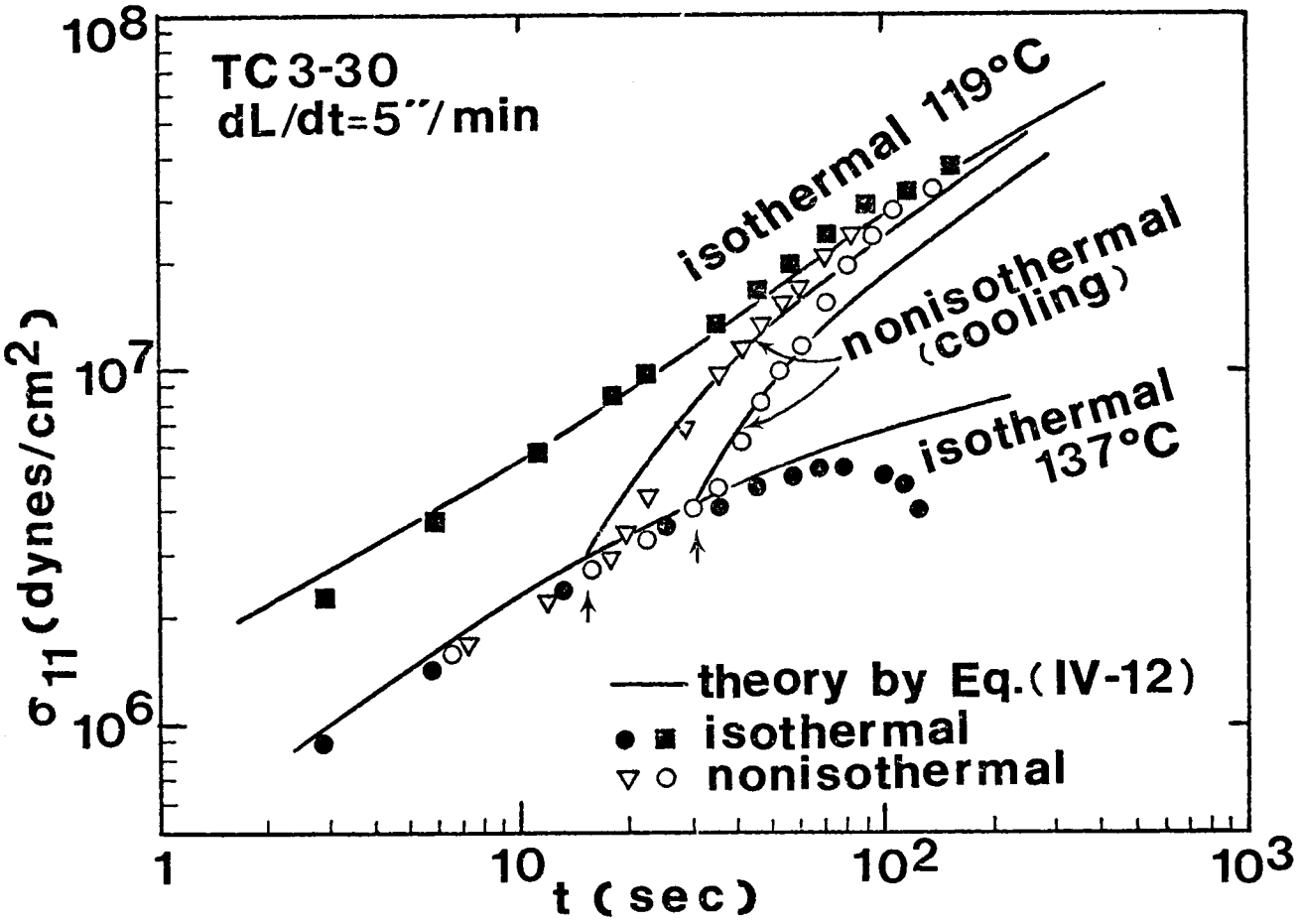

Figure 19. Isothermal and Nonisothermal (Cooling) Data for Tensile Pulling of Polystyrene TC3-30 at a Medium Rate.

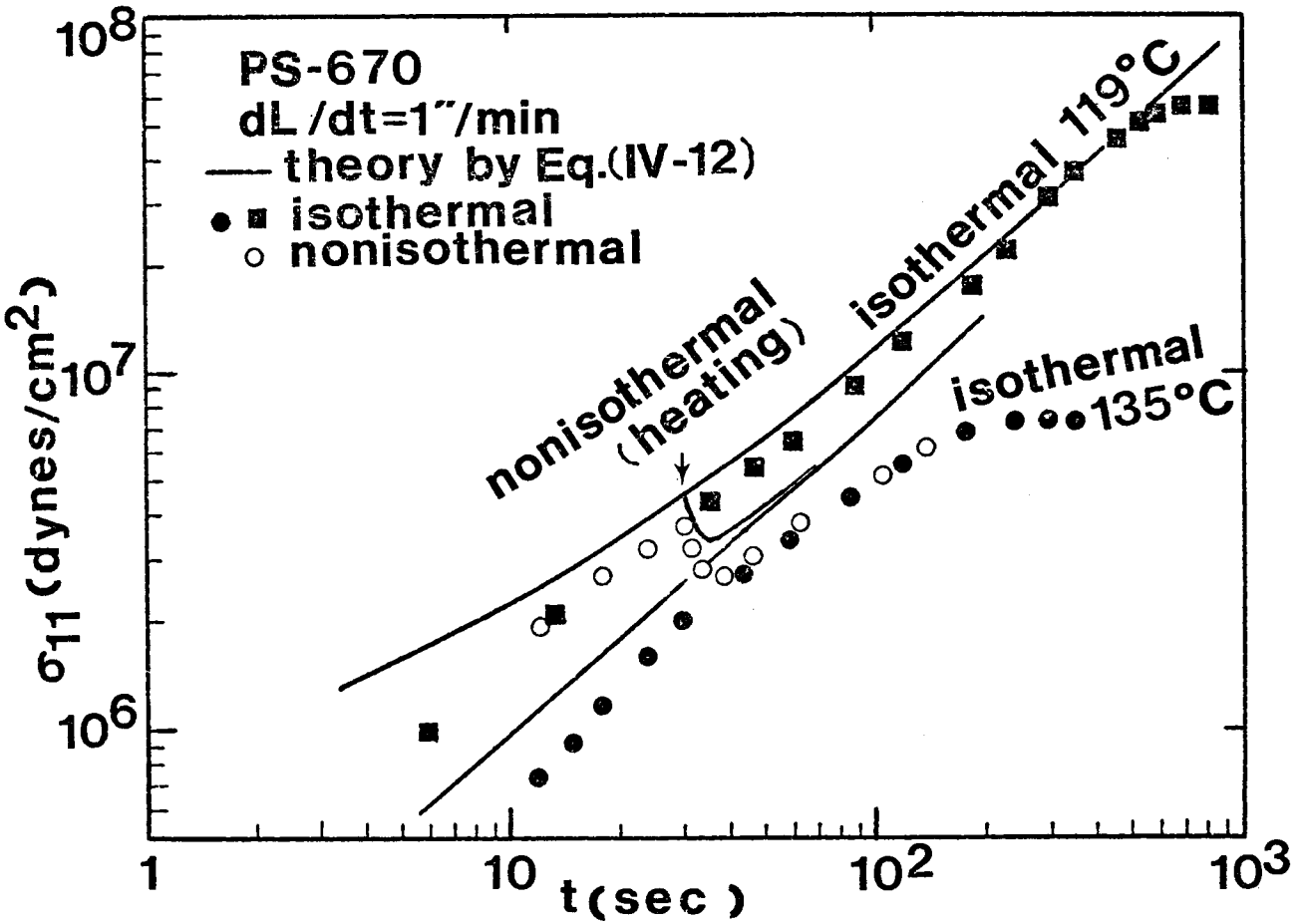

Figure 20. Isothermal and Nonisothermal (Heating) Data for Tensile Pulling of Polystyrene PS-670 at a Low Rate.

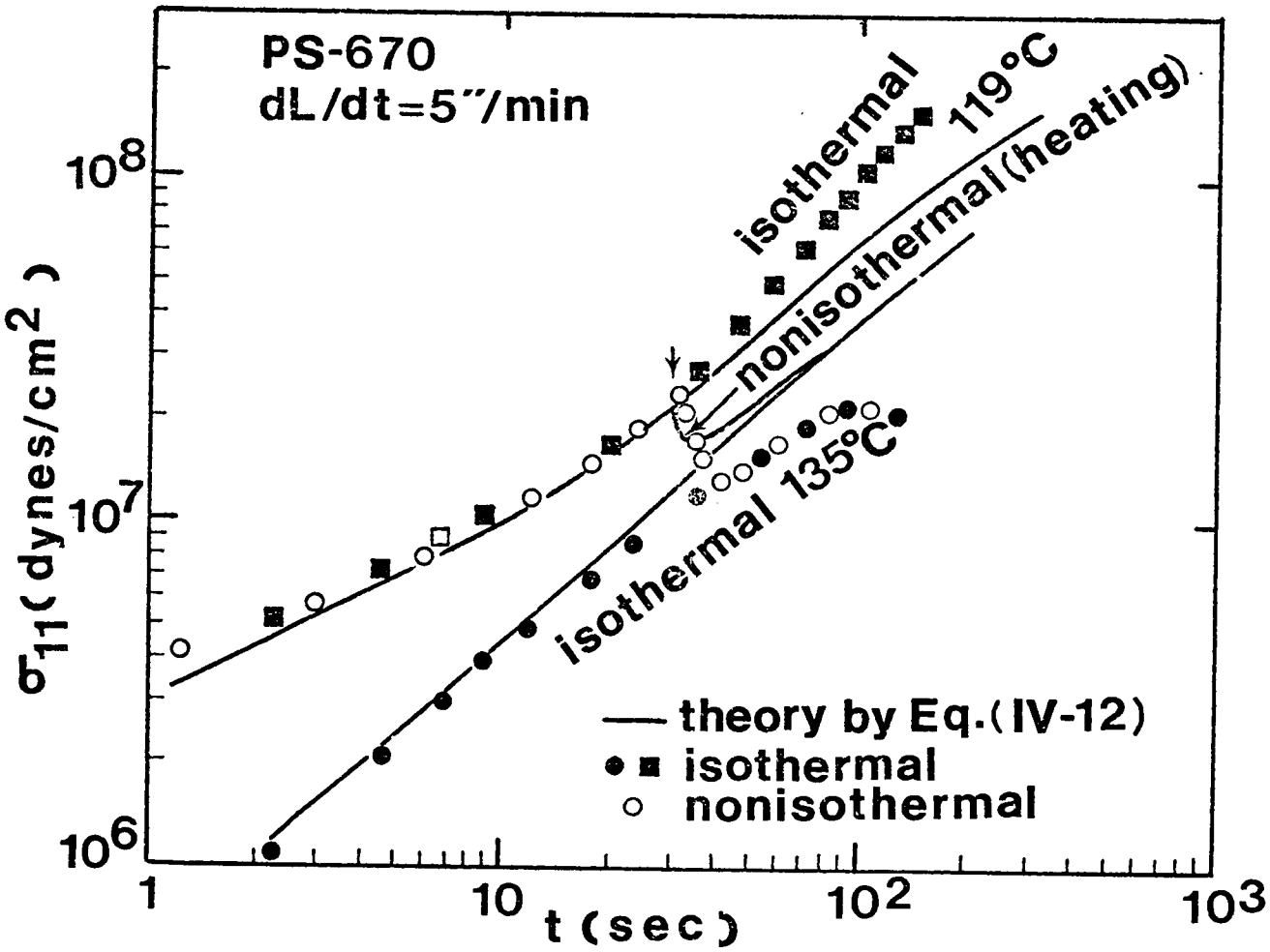

Figure 21. Isothermal and Nonisothermal (Heating) Data for Tensile Pulling of Polystyrene PS-670 at a Medium Rate.

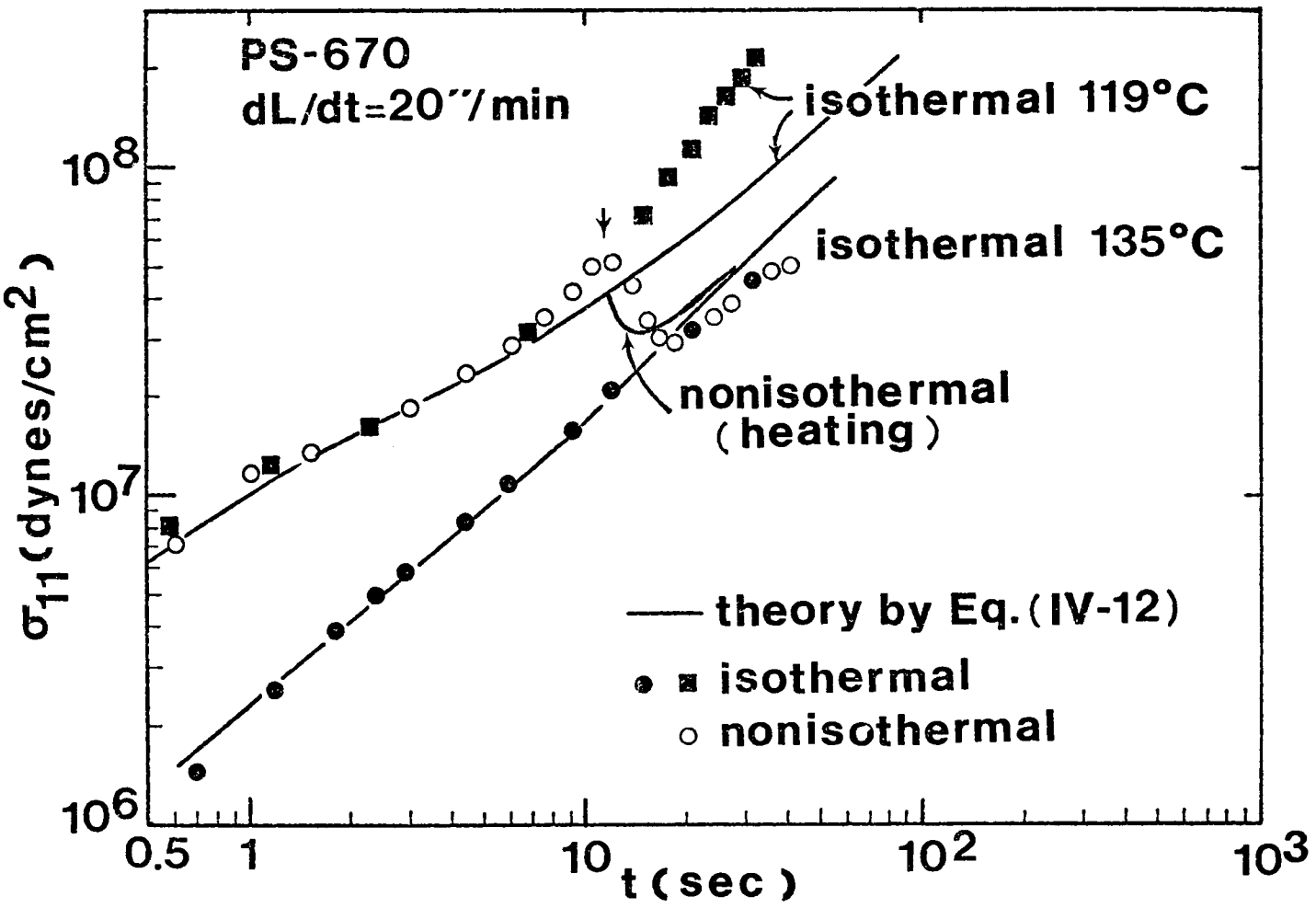

Figure 22. Isothermal and Nonisothermal (Heating) Data for Tensile Pulling of Polystyrene PS-670 at a High Rate.

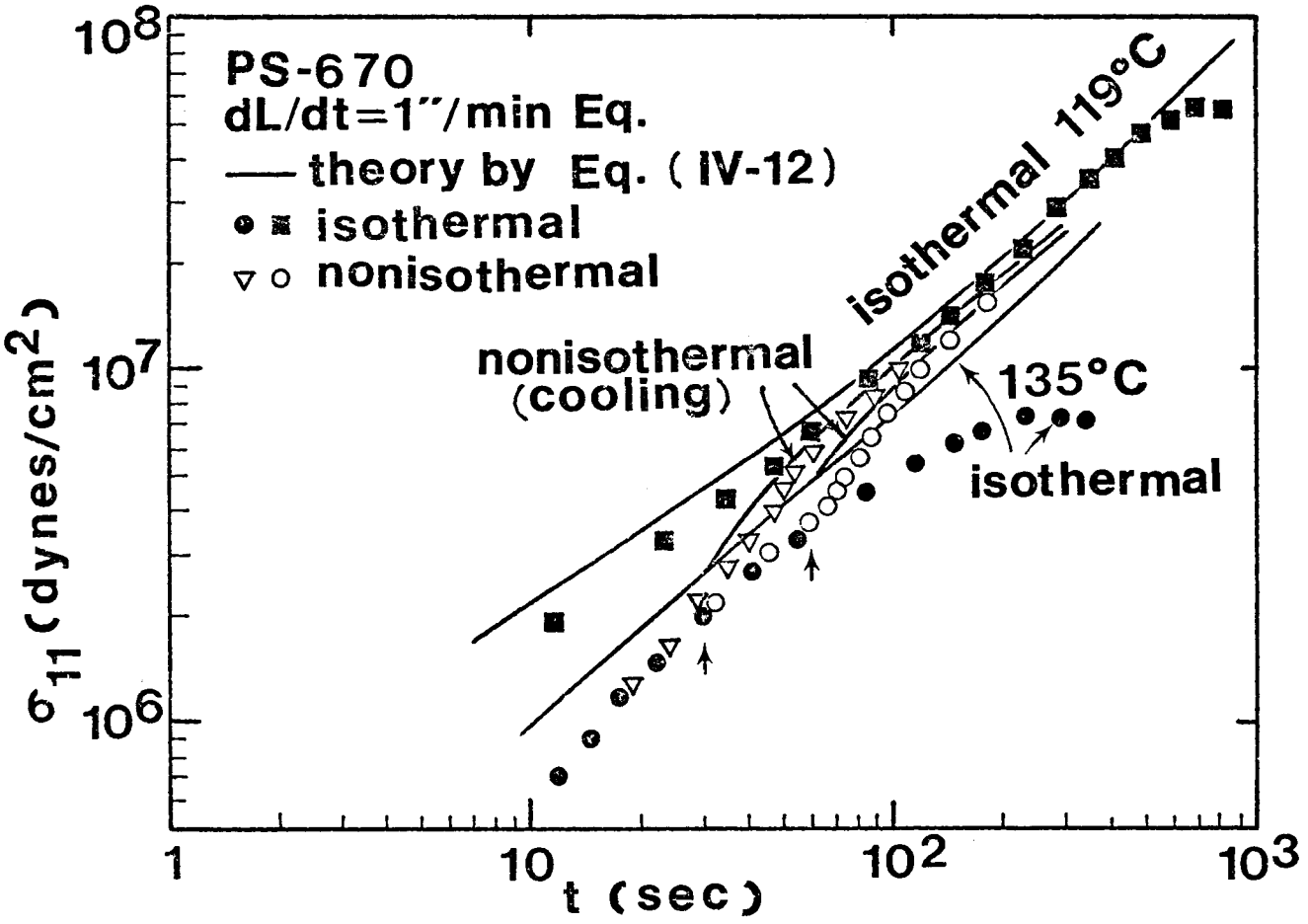

Figure 23. Isothermal and Nonisothermal (Cooling) Data for Tensile Pulling of Polystyrene PS-670 at a Low Rate.

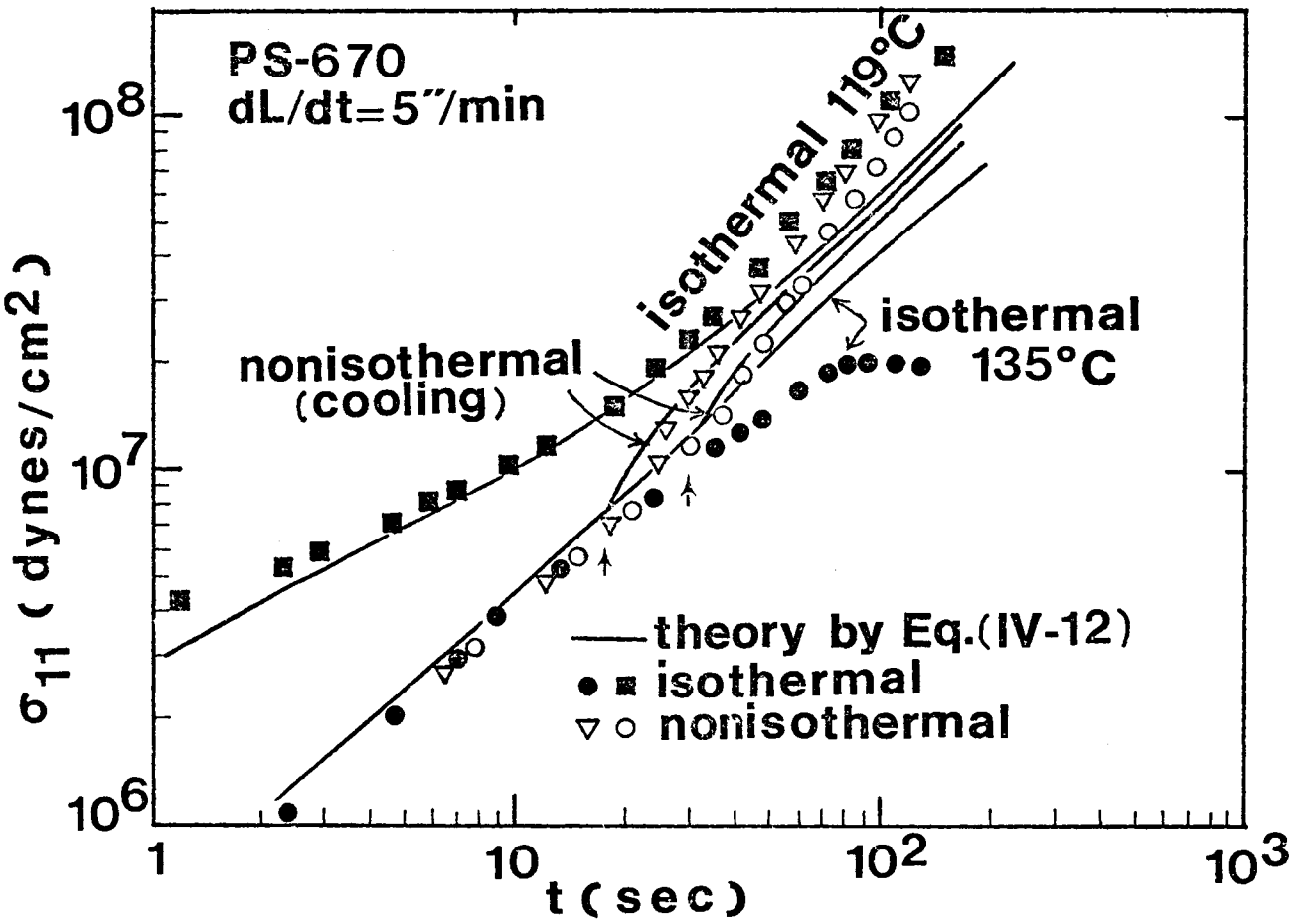

Figure 24. Isothermal and Nonisothermal (Cooling) Data for Tensile Pulling of Polystyrene PS-670 at a Medium Rate.

accommodation to the new temperature is more rapid (being often of the time scale of the imposed temperature change itself especially in the heating) than expected from theory or intuitive understanding of these materials with very large time constants. As mentioned in the previous section, this tendency was not seen in the nonisothermal stress relaxation, where the accomodation to the new temperature was of the time scale predicted by the theory (Equation (IV-5)). One may conclude that elongational motion during the temperature change has a strong influence (particularly on longer relaxation times); that is, the motion helps the molecules to accomodate themselves rapidly to the new temperature. It is clear that the form of the nonlinear function will be an important consideration in the theoretical treatment.

CHAPTER V

ANALYSIS OF MELT SPINNING

A. BACKGROUND

The understanding of flow problems in polymer processing operations is, of course, one of the major motivations for developing a theory of nonisothermal rheology. Most processing operations involve moving and shaping the polymer as a melt and then cooling it rapidly to a solid state. Theory for nonisothermal rheological response would help us understand the melt flow region itself (where flow instabilities or failure can occur) and the region just prior to crystallization (which seems to have a profound effect on the resulting morphology). Example processes are the production of fibers and films by melt extrusion, injection molding, blow molding, etc. To the extent that models are available, it has been assumed that the rheology can be handled with a Newtonian or a power law viscous model, into which is put a temperature-dependent viscosity or K-factor. Examples are the analyses of injection molding and filling presented by Ballman, Shusman, and Toor (3), Kamal and Kenig (40), and White, et al. (71, 72), and others (4, 11, 37, 58, 60). Melt spinning has been studied in the most detail and the implications in this area will not be considered.

The dynamics of melt spinning have been considered both as a steady state problem and as a transient problem leading to instabilities. Early reviews were made by Ziabicki (80, 81) and a recent comprehensive one has been presented by White and Ide (74). The most general

statement of the problem involes all of the following: rheological and surface tension relationships; force, energy, and material balances; and suitable boundary conditions. To a considerable extent, however, the rheological/surface tension part of the problem can be broken off from the rest of it and one can consider the matter of whether a molten filament in extension will pull out uniformly, thin down and flow out viscously, or break into waves or drops. This is the problem of "spinnability." The three competing forces of elasticity, viscosity and surface tension, related to the pulling conditions by suitable dimensionless groups, give rise to the various flow responses just noted. The analyses and the accompanying experimental studies are limited to isothermal conditions, however.

The more general problem of spinline dynamics, which includes also equations for the heat transfer, the force balance, the material balance and suitable boundary conditions, was first dealt with by Ziabicki and Kedzierska (82). The unstable part of the general problem largely centers on the phenomenon known as "draw resonance," in which diameter variations appear and grow in a periodic fashion. Mathematical analyses started with the work of Kase, Matsuo, and Yoshimoto (43) and Pearson and Matovich (59) and have been developed by a number of recent researchers, especially Pearson and coworkers (61) and Denn and coworkers (25, 29). Extensive experimental contributions have been made by Han and coworkers (35, 36). The phenomenon of draw resonance does not itself require either nonlinear viscous or elastic responses or nonisothermal conditions and occurs even in Newtonian fluids under isothermal

conditions. However, these various complications have been introduced and have a marked influence on the criteria for defining stable, unstable and unattainable regions of behavior. Nonlinear viscous and elastic effects have been dealt with by Denn and coworkers (29), who used a generalized differential Maxwell model (the White-Metzner model) in which the time parameter is expressed with a power law type of relationship.

Kase and Matsuo (42), Ziabicki and Kedzierska (82), and others have dealt with the nonisothermal aspects of both the steady spinline problem and the draw resonance problem by introducing a viscous relationship of the form

$$\sigma_{11} = \eta_{el}(T) \frac{dv_x}{dx}$$

where $\eta_{el}(T)$ is a point elongation viscosity, strongly dependent on temperature. Rheologically speaking, this equation seems too simple and one supposes that elastic responses should be included also. The argument has been made that because the temperature changes are so fast, they overpower the effects of a changing deformation history (74, 80); while one can perhaps accept this argument intuitively, the mathematical basis for it is vague.

The combined effect of transient thermal conditions and transient deformation conditions has not yet been considered.

B. STEADY STATE MELT SPINNING

In the previous section, an overall view of the problem of

melt spinning, both steady and unsteady, was made. One of the objectives of such analyses is, of course, to relate operating conditions to the properties of the as-spun fiber, and ultimately to the properties of the final fiber. In recent years detailed studies of the crystalline morphology in fibers, particularly polyolefin fibers, has been made using several experimental methods, including small angle and wide angle X-ray diffraction, optical microscopy, and electron microscopy. This work is reviewed by Clark (18) in the technical literature and in a very colorful article by Uhlmann and Kolbeck (70) in the popular literature. An essential feature is the appearance of the so-called "shish kebab" structure, or at least a highly ordered row structure, as the melt is elongated. This contrasts with spherulitic crystallites if the melt is stagnant.

The most comprehensive work of structure devemopment in melt spinning is that of Dees and Spruiell (24), who carried on research started by Katayama, Amano, and Nakamura (44), in which direct on-line observations of the development of the crystalline morphology is made by X-ray diffraction and other measurements. This work on polyethylene is closely related to recent work of White, Dharod, and Clark (78) and others at the University of Tennessee on both polyolefins and nylon and has been summarized in detail by Spruiell and White (63, 64). In the case of the polyethylenes, there seems to be a regular progression to increased c-axis orientation as the elongational deformation is made more stringent. White and coworkers believe that stress is the key variable to characterize the state of the melt as crystallization takes place.

From such studies it is clear that we must create models which

tie together the rheological and morphological problems. Elaborating on the models of Kase and Matsuo and Ziabicki and coworkers, as discussed on the previous pages, the basic balances and associated constitutive relations would involve the following: (1) a continuity (mass) balance, (2) a force balance including terms for gravity, drag, surface tension, inertial and rheological forces, (3) an energy balance combined with correlations for the heat transfer coefficient, (4) a crystal structure and rate equation which would describe, probably in vector form, the development of the crystalline structure as it grows out of the oriented melt. No tractable form for (4) which catches the essential ideas of the crystalline morphology is yet available. In his pioneering work, Ziabicki (80, 81) used a simple first-order model for the crystallization rate, although it was clearly understood that the actual crystallization processes are much more complicated than that. Crystallization rates are strongly dependent on the molecular orientation (or stress) and can be orders of magnitude larger than the rates for stagnant materials (Nakamura, et al., (54)). It is thus essential that we have a good understanding of the rheological response in the melt, not only as it affects the force balance but also as it relates to the model for the crystal structure.

C. THEORETICAL CONSIDERATIONS

General Relationships

As summarized in prior work (50), the dynamics of melt spinning (in the steady state) can be described by the following equations:

Material balance:

$$\rho v A = W \ (= \text{constant}) \tag{V-1}$$

Force balance:

$$\sigma_{11} A = F_{ext} + \int_x^{x_L} \rho g A \, dx - W(v_L - v) - \int_x^{x_L} f_{aero} \, dx - \int_x^{x_L} f_{surf} \, dx \tag{V-2}$$

Energy (heat) balance

$$W \frac{dT}{dx} = - \frac{h}{c_p} (T - T_a) \tag{V-3}$$

where ρ denotes the density of polymer; x, the distance from the spinneret; v, the velocity; W, the throughput; σ_{11}, the rheological tensile stress; A, the fiber cross sectional area; F_{ext}, the external force on a take-up device; g, gravity constant; f_{aero}, the air drag on a filament; f_{surf}, the surface tension; T, the fiber temperature; T_a, the ambient temperature; h, the heat transfer coefficient; and the subscript L, the take-up position. The effect of the heat of crystallization which would come into Equation (V-3) is omitted because in the present work the behavior before the crystallization point only will be considered. These equations have been discussed in some detail in prior work (42, 80).

Consideration of Constitutive Theory

The important problem at present is how to describe the rheological

tensile stress σ_{11}. As mentioned before, the following simple form has mostly been applied:

$$\sigma_{11} = \eta_{el}(T) \frac{dv}{dx} \qquad (V\text{-}4)$$

This simple viscous model has often been applied to practical melt spinning successfully (32, 42). However, the lack of a viscoelastic term makes such a model not satisfactory in the general cases. Therefore a more general form seems to be required for a thorough understanding of melt spinning.

In short, it is proposed to introduce a nonisothermal constitutive equation of the type shown in Equation (II-17). Also, to determine the deformation tensors, one must describe the kinematics of the flow. However, it seems extremely difficult to completely describe the intricacy of the die flow, the spinning flow, and of the transient flow between them. Some assumptions or modeling of the flow should be made. A schematic diagram of the deformation is shown in Figure 25, where t' denotes a past time of transit; x', the corresponding distance from the spinneret; t, the present time; x, the corresponding distance. The velocity distribution along the spinline was assumed as in the form of a uniform elongation. Since the volume element is moving and deforming, the translational (or rigid) motion of the element must be mathematically eliminated.

This can be done by first fixing in a volume element a coordinate system, the origin of which moves with the element along the streamline as shown by three arrows (1, 2, and 3), and then embedding

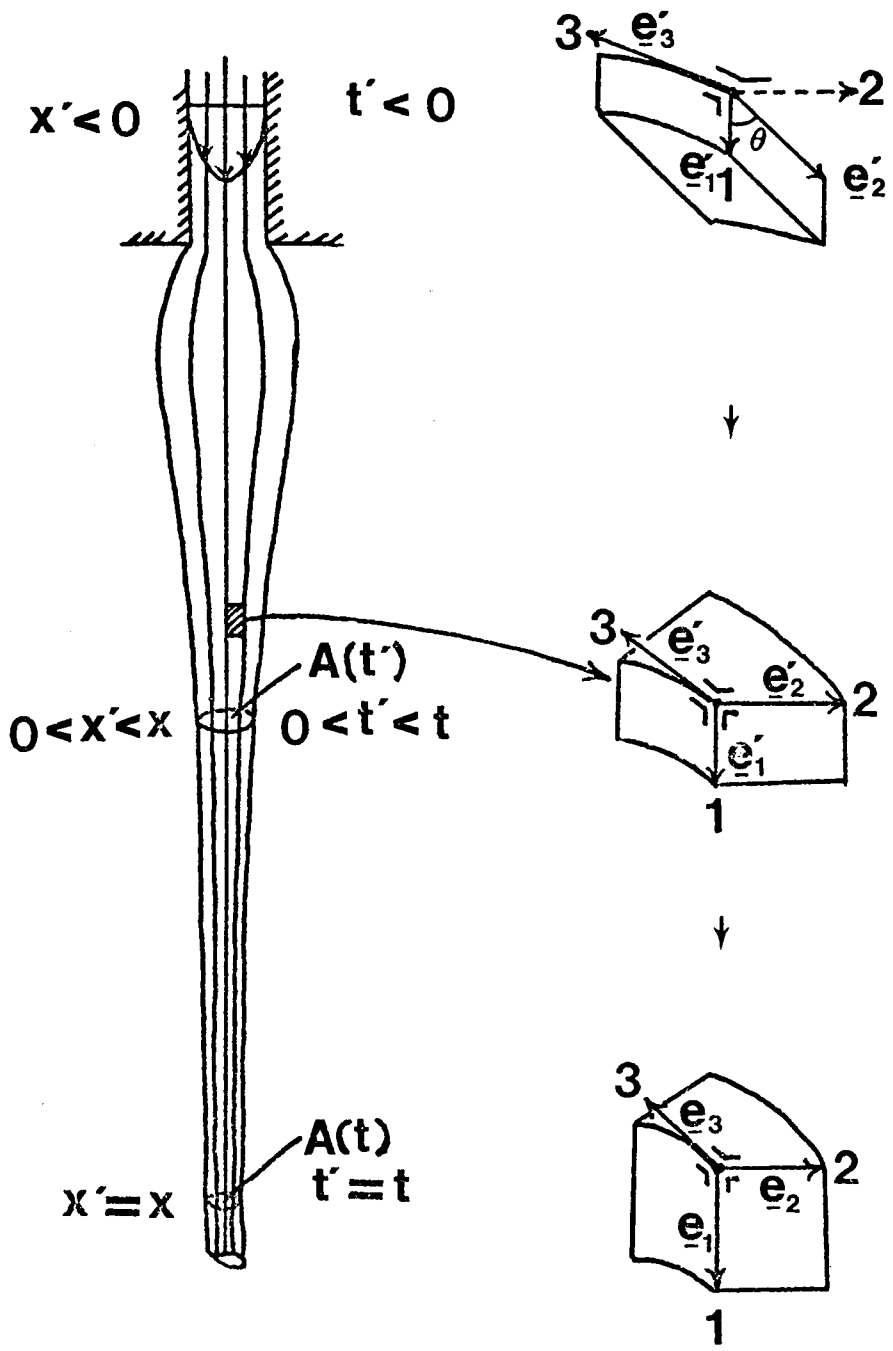

Figure 25. Schematic Diagram of Melt Spinning.

three base vectors $\underline{e}_1$, $\underline{e}_2$, and $\underline{e}_3$ (or $\underline{e}_1'$, $\underline{e}_2'$, and $\underline{e}_3'$) in the element. The axis 1 indicates the spinline dirention; 2, the radial direction; 3, the circular direction. Also, if the volume element is small enough, one can regard the coordinate system [1,2,3] as Cartesian. The base vectors $\underline{e}_i$ are of the present time and $\underline{e}_i'$ are of a past time. The embedded vectors $\underline{e}_i'$ deform in accordance with the elongation in the spinline and the shear in the die. Thus, the $\underline{e}_i'$ directly show the relative deformation of the material coordinates. The idea of this treatment is essentially similar to the convective differential model suggested by Oldroyd (55) and White and Metzner (75). In other words, the coordinated system [1,2,3] is, so to speak, a locally translating coordinate system. The magnitude of the vectors $\underline{e}_i$ is based on the present time, from which one looks into the past; that is, at the present time ($t = t'$) each base vector $\underline{e}_i$ has the magnitude of unity. At a certain past time ($t' > 0$) $|\underline{e}_1'|$ is smaller than $|\underline{e}_2'|$ or $|\underline{e}_3'|$ because of the elongation, while $|\underline{e}_2'| = |\underline{e}_3'|$. In the spinneret ($t' < 0$) the direction of $\underline{e}_2'$ becomes skew to $\underline{e}_1'$ because of the shear flow, while $\underline{e}_1' \perp \underline{e}_3'$ and $\underline{e}_2' \perp \underline{e}_3'$, also $|\underline{e}_1'|$ and $|\underline{e}_2'| \sin\theta$ are constant.

Rigorously speaking the real deformation is not as simple as modeled by the vectors ($\underline{e}_i$). The elongation along the spinline is not exactly uniform. The flow pattern around the die exit becomes more complicated than illustrated in Figure 25. While the rigorous description of the deformation tensors must be expressed in the fixed coordinate system or general convected coordinate system, one does not see any way of doing it wihtout knowing the complete kinematics of melt spinning. However, one can imagine that the volume element is subjected

to shear (in the die) and then to uniform elongation (in the spinline) in the locally translating coordinate system [1,2,3].

Let x^1, x^2, and x^3 be the material coordinates at the present time and x'^1, x'^2, and x'^3 be those at a past time with respect to the coordinate system [1,2,3]. The relationships between x^i and x'^i are summarized below:

$$\begin{cases} x'^1 = x^1 \, |\underline{e}_1'| \, / \, |\underline{e}_1| = x'/\lambda \\ x'^2 = x^2 \, |\underline{e}_2'| \, / \, |\underline{e}_2| = \sqrt{\lambda}\, x^2 \qquad 0 < t' < t \text{ (on the spinline)} \\ x_3' = x^3 \, |\underline{e}_3'| \, / \, |\underline{e}_3| = \sqrt{\lambda}\, x^3 \end{cases} \tag{V-5}$$

$$\begin{cases} x'^1 = x^1 \, |\underline{e}_1'| \, / \, |\underline{e}_1| + x'^2 \, (|\underline{e}_2'| \, / \, |\underline{e}_2|) \cos\theta \\ \quad = x^1/\lambda_o + x'^2 \cot\theta \\ x'^2 = x^2 \, |\underline{e}_2'|_{t'=0} \, / \, |\underline{e}_2| = \sqrt{\lambda_o}\, x^2 \qquad t' < 0 \text{ (in the die)} \\ x'^3 = x^3 \, |\underline{e}_3'|_{t'=0} \, / \, |\underline{e}_3| = \sqrt{\lambda_o}\, x^3 \end{cases} \tag{V-6}$$

where

$$\lambda = \left[\frac{A(t')}{A(t)}\right]^2 = \left[\frac{v(t)}{v(t')}\right]^2$$

$$\lambda_o = \left[\frac{A(0)}{A(t)}\right]^2 = \left[\frac{v(t)}{v(0)}\right]^2 \tag{V-7}$$

$$\cot \theta = \left| \frac{dv}{dr} \cdot t' \right| \qquad \text{(V-8)}$$

The Finger tensors are directly calculated using the following equation:

$$C_{ij}^{-1} = \delta^{\alpha\beta} \frac{\partial x^i}{\partial x'^{\alpha}} \frac{\partial x^i}{\partial x'^{\beta}} \qquad \text{(V-9)}$$

$$C_{ij}^{-1} = \begin{vmatrix} 1 & 0 & 0 \\ 0 & 1 & 0 \\ 0 & 0 & 1 \end{vmatrix} \qquad (t'=t) \qquad \text{(V-10)}$$

$$C_{ij}^{-1} = \begin{vmatrix} \lambda^2 & 0 & 0 \\ 0 & \lambda^{-1} & 0 \\ 0 & 0 & \lambda^{-1} \end{vmatrix} \qquad (t'> 0) \qquad \text{(V-11)}$$

$$C_{ij}^{-1} = \begin{vmatrix} \lambda_o^2 (1+\cot^2\theta) & -\lambda_o^{-1/2} \cot \theta & 0 \\ -\lambda_o^{-1/2} \cot \theta & \lambda_o^{-1} & 0 \\ 0 & 0 & \lambda_o^{-1} \end{vmatrix} \qquad (t'< 0) \qquad \text{(V-12)}$$

This analysis is similar in principle to that done by Chen et al. for isothermal spinning (17), except that the effect of the flow in the die has been taken into account.

The velocity distribution in the spinneret may approximately be assumed in terms of the well-known parabolic form. Then one obtains

$$\cot\theta = \frac{4\bar{v}r(-t')}{R^2} = \frac{4v(0)r(-t')}{R^2} \qquad \text{(V-13)}$$

where $\bar{v}$ denotes the mean velocity; r, the radial distance; R, the radius of the die. Also the assumption is made that the parabolic velocity distribution instantaneously changes to a uniform elongation at the spinneret exit. The momentum decrease ($p\pi R^2\bar{v}^2/3$) is also neglected. Introducing the above strain tensors, one can arrange the constitutive Equation (II-17) into the following form for t>0.

$$\bar{\sigma}_{11} = -p + \sum_n G_n \int_{-\infty}^{0} \left[\int_0^R \frac{\exp\left[-\int_{t'}^{t} \frac{dt''}{\tau_n^*}\right]}{\tau_n^*} \lambda_o^2 \left(1 + \frac{16\bar{v}^2 t'^2 r^2}{R^4}\right) \frac{2\pi r dr}{\pi R^2}\right.$$

$$\left. + \int_0^t \frac{\exp\left[-\int_{t'}^{t} \frac{dt''}{\tau_n^*}\right]}{\tau_n^*} \lambda^2\right] dt' \qquad \text{(V-14)}$$

$$\sigma_{22} = -p + \sum_n G_n \left[\int_{-\infty}^{0} \frac{\exp\left[-\int_{t'}^{t} \frac{dt''}{\tau_n^*}\right]}{\tau_n^*} \lambda_o^{-1} dt' + \int_0^t \frac{\exp\left[-\int_{t'}^{t} \frac{dt''}{\tau_n^*}\right]}{\tau_n^*} \lambda^{-1} dt'\right] \qquad \text{(V-15)}$$

where

$$\tau_n^* = \frac{a_T[T(\cdot)]\tau_n^o}{1 + b\ \Pi_d\ a_T[T(\cdot)]\tau_n^o} \qquad \text{(V-16)}$$

$$\Pi_d = \begin{cases} \sqrt{3}\left|\frac{dv}{dx}\right| & (t' \geq 0) \\ \dot{\gamma} \equiv \frac{4\bar{v}r}{R^2} & (t' < 0) \end{cases} \qquad \text{(V-17)}$$

Since Equations (V-14) and (V-15) describe the stresses outisde the spinneret, σ_{22} may be set equal to zero. Also, using the following relationships

$$dt' = v(x')\,dx' \tag{V-18}$$

the final results can be written as follows:

$$\bar{\sigma}_{11} = \sum_n G_n \int_0^x \left(\frac{1}{\tau_n(x')v(x')} + \frac{\sqrt{3}\,b}{v(x')}\left|\frac{dv}{dx'}\right|\right) \exp\left[-\int_{x'}^x \frac{dx''}{\tau_n(x'')v(x'')}\right]$$

$$\left[\left(\frac{v(x)}{v(x')}\right)^A - \left(\frac{v(x)}{v(x')}\right)^{-B}\right] dx'$$

$$+ \sum_n G_n \left[\left(\frac{v(x)}{v(0)}\right)^A - \left(\frac{v(x)}{v(0)}\right)^{-B}\right] \exp\left[-\int_0^x \frac{dx''}{\tau_n(x'')v(x'')}\right]$$

$$+ \sum_n G_n F_n \left(\frac{v(x)}{v(0)}\right)^A \exp\left[-\int_0^x \frac{dx''}{\tau_n(x'')v(x'')}\right] \tag{V-19}$$

where

$$A = 2 - \sqrt{3}\,b, \quad B = 1 + \sqrt{3}\,b$$

$$\tau_n(x'') = a_T[T(x'')]\tau_n^0$$

$$F_n = \int_0^1 \frac{4\xi^2 d\xi}{(K_n^{-1} + b\xi)^2} \tag{V-20}$$

$$K_n = \frac{4\bar{v}\tau_n(0)}{R} \equiv \dot{\gamma}_w\,\tau_n(0)$$

Equation (V-19) seems to give a better intuitive understanding of the mechanism of melt spinning than the previous equation; that is, the first term represents the stress development due to the deformation history along the spinline and the second and third terms represent the effect due to those inside the die. In particular, the third term comes from the normal stress caused by the shear flow in the die.

The significance of Equation (V-19) is that one need not introduce an elongational viscosity as an unknown parameter using Equation (V-4); rather, the elongational viscosity can be determined at each point as the result of the deformation combined with characteristic material parameters such as G_n, τ_n, $a_T[T]$, and b. Strictly speaking it should be called "apparent (or transient or time dependent) point elongational viscosity," defined by the equation

$$\eta_{el} = \frac{\bar{\sigma}_{11}}{(dv/dx)} \cdot \qquad \text{(V-21)}$$

One should bear in mind that η_{el} in Equation (V-21) is a transient quantity which depends not only on temperature but also on deformation histories, while η_{el} in the viscous model Equation (V-4) is a material parameter depending only on temperature. The latter must be determined empirically by setting it equal to three times the shear viscosity.

D. ANALYSIS OF MELT SPINNING DATA

As discussed in the last section, the matter of modeling combined rheological and morphological changes during melt spinning involves

several interacting constitutive relations and balances. The rheological part of the problem involves describing the state of the flow in terms of the strain history, or the recoverable strain, or stress, all of these quantities being related, of course. To begin such studies, Dees' melt spinning data for high density polyethylenes (23) will now be considered and compared with the prediction of Equation (V-19).

Evaluation of Material Parameters

Although most rheological quantities involved in Equations (V-1), (V-2), and (V-3) were measured along the spinline in Dees' experiments, complete rheological characterization of his polyehtylenes has not yet been completed. Therefore certain assumptions are necessary to estimate suitable memory functions for the theory. Essentially the estimation is made using rheological data for similar materials. In order to make this treatment clear, the prior measurement for these polyethylenes are summarized in Table II.

It was first assumed that Dees' two polyethylenes have approximately the same rheological properties because of the same melt index. Most of the material parameters were evaluated from Tenite 3340 which was well characterized in a wide range by Chen (15). The relaxation spectrum of Tenite 3340 is shown in Figure 26. From this data, one may estimate the relaxation spectrum of Dees' polyethylenes having different melt indices by consideration of the following general principles:

1. The zero shear viscosity is approximately proportional to the reciprocal melt index.

TABLE II

PRIOR WORK ON DEES' HIGH DENSITY POLYETHYLENE AND REFERENCE HIGH DENSITY POLYETHYLENE

	Dees' Polyethylenes		Reference Polyethylene
	Texas Eastman	Phillips	Tennessee Eastman
	Tenite 3310	EMB 6050	Tenite 3340
Melt Index	5.0	5.0	2.6
Shear Data	——	White and Roman	Chen and Bogue
		Shear stress	Shear viscosity
		Viscosity	Normal stress
			Relaxation spectra
			Shift factor

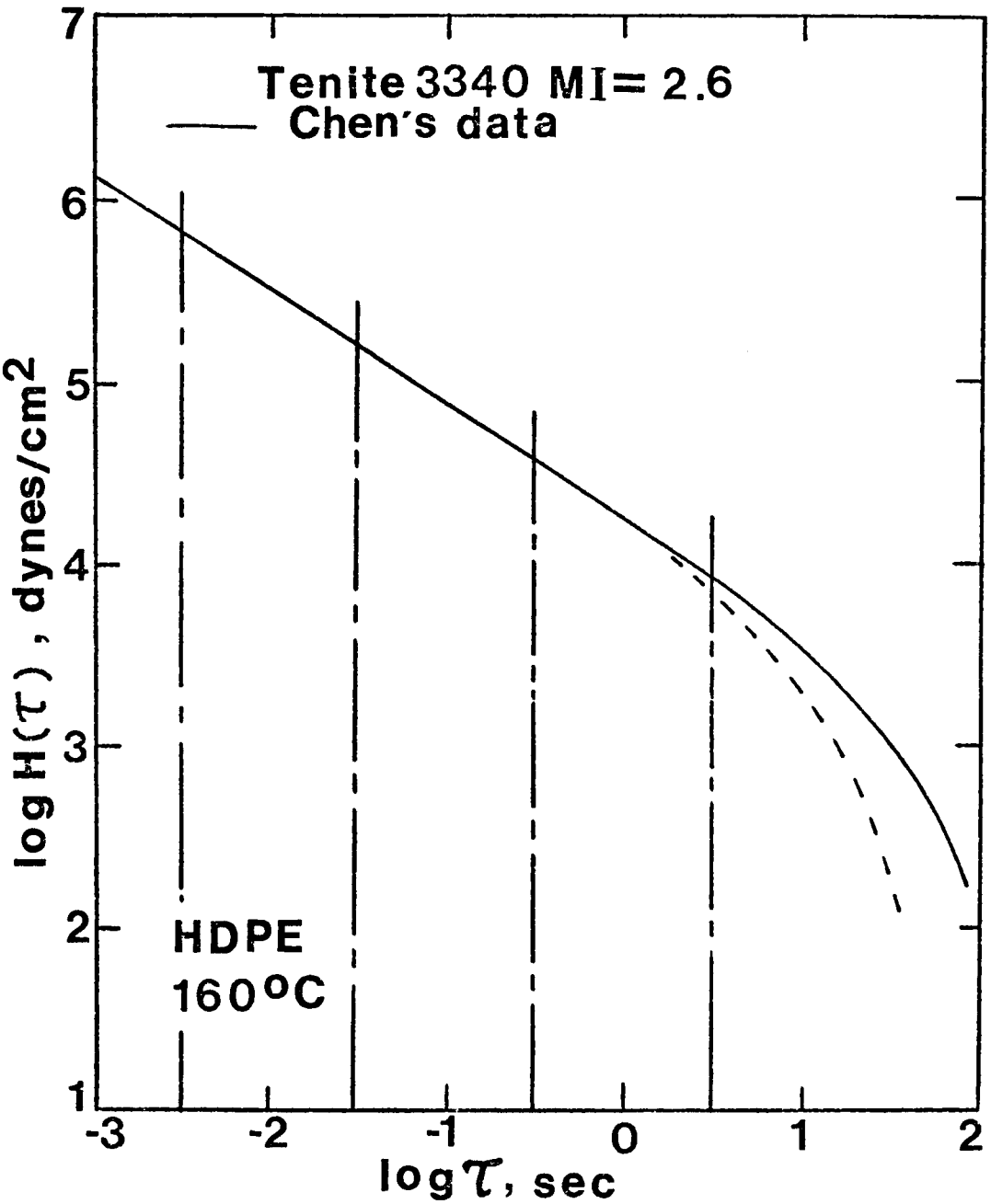

Figure 26. Relaxation Spectrum for High Density Polyethylene Tenite 3340.

$$\eta_{sh}^{o} \propto MI^{-1}$$

2. The zero shear vicosity is determined by integrating the relaxation spectrum over all relaxation times.

$$\eta_{sh}^{o} = \int_{-\infty}^{\infty} \tau\, H(\tau)\, d \ln \tau$$

3. The zero shear viscosity and maximum relaxtion times are proportional to the 3.5 power of molecular weight.

$$\eta_{sh}^{o} \propto M_w^{3.5} \propto \tau_{max}$$

According to the above relationships the spectrum of Dees' polyethylenes seems to have approximately the same shape as Tenite 3340 except that the maximum relaxation time is nearly half of that for Tenite 3340. This is shown by the dotted line in Figure 26. Since this approach is not very accurate, one may substitute it with a discrete spectrum shown by four spikes in Figure 26. Those values at 160°C are

$G_1 = 1.51 \times 10^6$ (dynes/cm^2)	$\tau_1 = 0.003$ (sec.)
$G_2 = 3.60 \times 10^5$	$\tau_2 = 0.03$
$G_3 = 8.58 \times 10^4$	$\tau_3 = 0.3$
$G_4 = 2.04 \times 10^4$	$\tau_4 = 3$

The shift factor and b value taken from Chen's data (Tenite 3340) (15)

shown in Figure 27 are approximated by

$$a_T[T] = \exp [-0.016\ (T-160)]$$

$$b = 0.5 \qquad \text{(V-20)}$$

Before applying the above material parameters to melt spinning, they were tested on the shear viscosity data of White and Roman (77). The theoretical viscosity was computed using the following equation

$$\eta_{sh} = \sum_n G_n \frac{\tau_n}{1 + b\dot{\gamma}\tau_n} \qquad \text{(V-21)}$$

The comparison is shown in Figure 28. The theoretical curve agrees with the experimental data quite well. Therefore the four moduli G_n, the corresponding relaxation times τ_n, the shift factor a_T, and the b value estimated above seem to describe the rheological behavior reasonably well and will now be applied in the melt spinning analysis.

Analysis of Dees' Melt Spinning Data

From Dees' data (23) five cases were selected for comparison with the theory of Equation (V-19). As mentioned befroe, two high density polyethylenes were involved. Spinning runs 1, 2, and 3 were made using Texas Eastman Tenite 3310 and runs 6 and 9, Phillips EMB-6050. The spinning conditions are listed in Table III.

To compute the theoretical stress and elongational viscosity, the velocity and temperature changes along the spinline were taken from

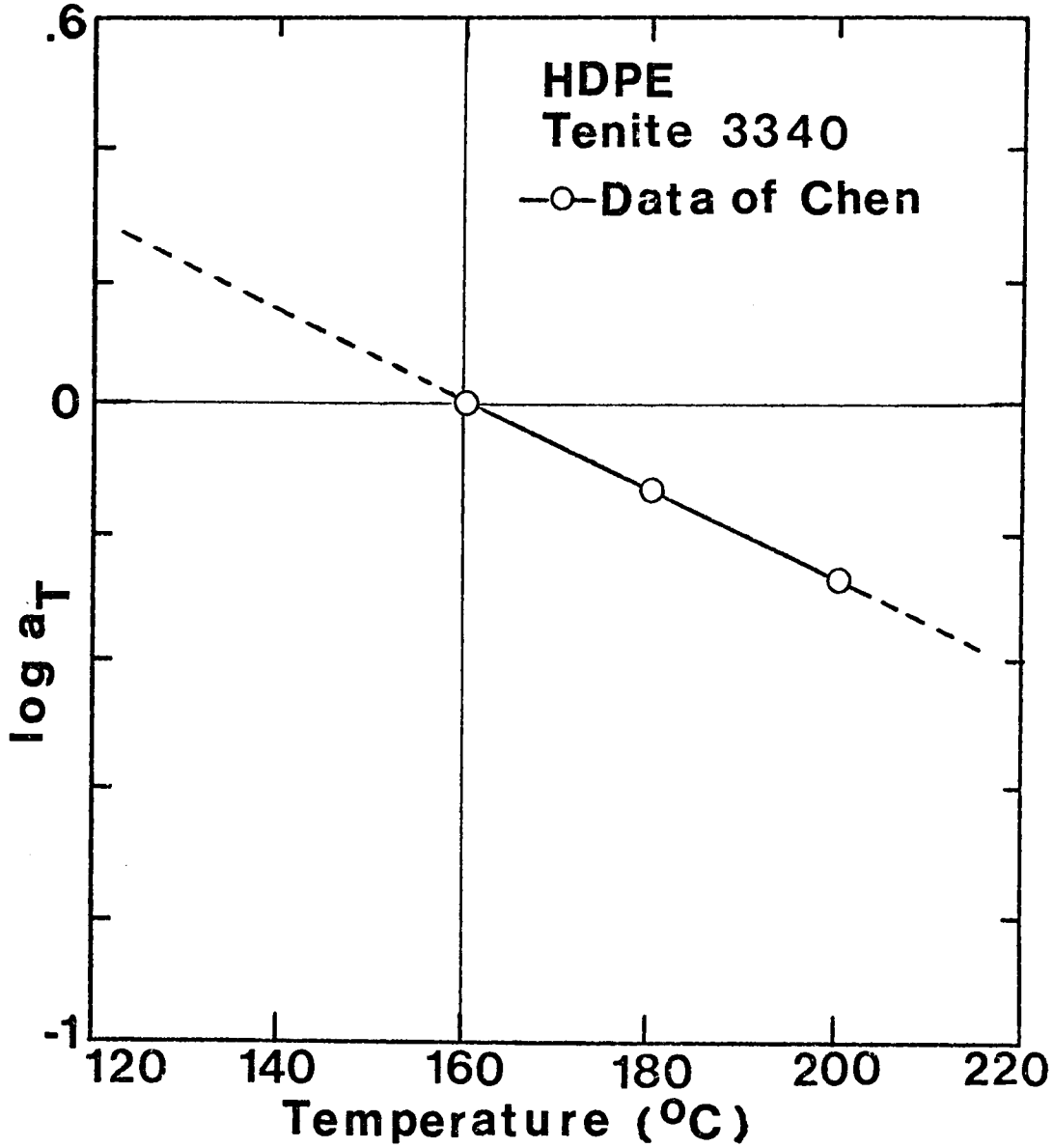

Figure 27. Temperature Dependence of the Shift Factor for High Density Polyethylene Tenite 3340.

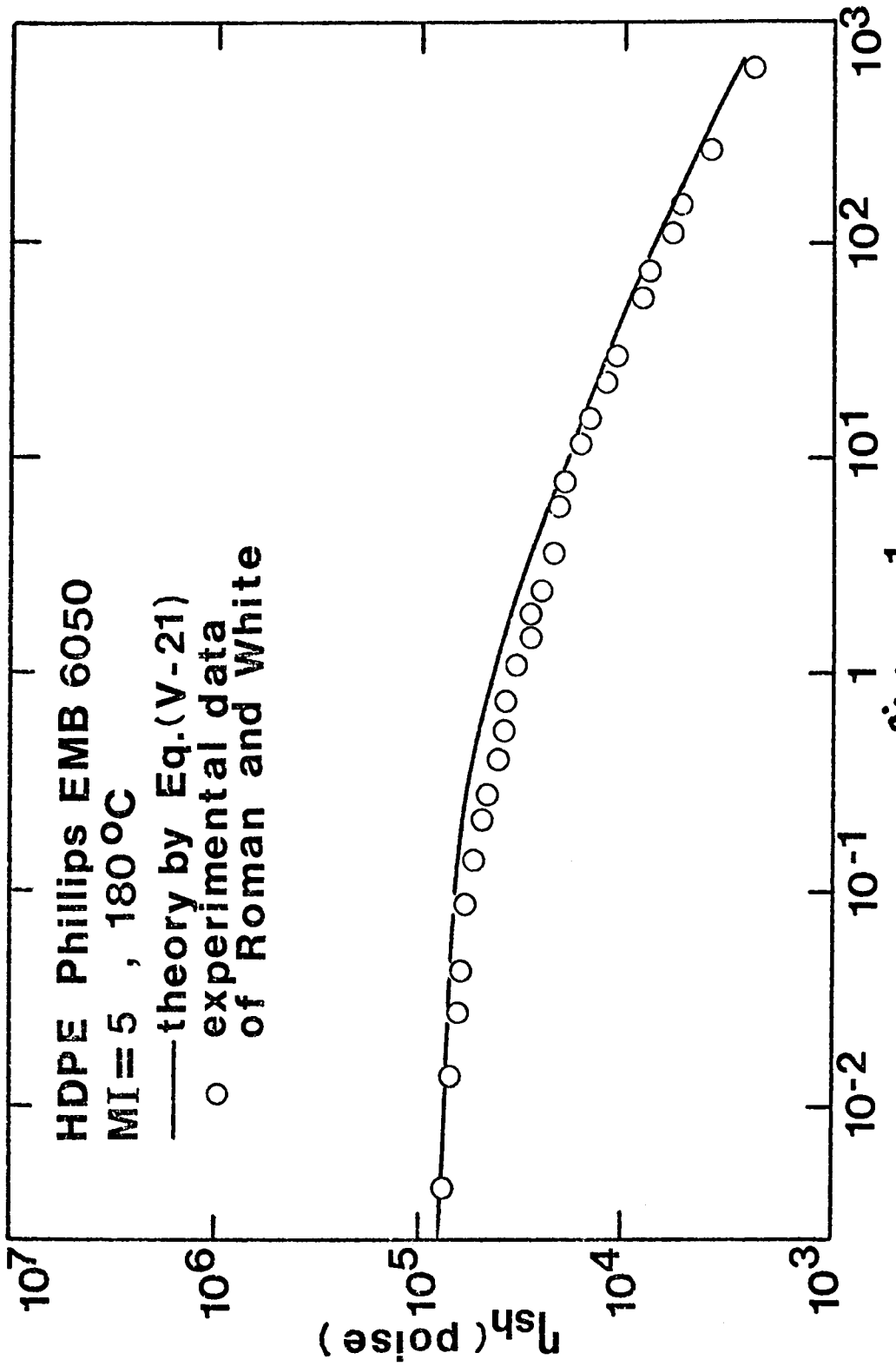

Figure 28. Shear Viscosity versus Shear Rate for High Density Polyethylene EMB 6050.

TABLE III

SUMMARY OF DEES' EXPERIMENTAL MELT SPINNING RUNS

Run Number	Throughput (g/min)	Takeup Velocity (m/min)	Spinning Temperature (^{o}C)
PE01	1.93	100	210
PE02	1.93	200	210
PE03	1.94	50	210
PE06	1.91	400	210
PE09	0.705	200	210

Dees' data. He obtained the velocity change by first measuring the diameter along the spinline and then converting it to velocity with Equation (V-1) (the material balance). Also he approximated the velocity change with axial position by using the following empirical equation:

$$v = A \exp [B(x/D)^E] + F \qquad (V\text{-}22)$$

where A, B, D, E are empirical constants depending on each run (23).

Also he measured the temperature change along the splinline, as shown in Figure 29. There are experimental difficulties in his temperature measurements due to the inaccuracy of the contact thermocouple method in the upper part of the splinline where the measured temperatures were higher than the temperature in the die. Therefore adjustments were made in Figure 29 by drawing lines which intercept the axis with the die temperature (210^oC) as shown by two straight lines

$T = 210 - 1.33\ x$ (PEO 1, PEO 2, PEO 3, PEO 6)

$T - 210 - 3.7\ x$ (PEO 9)

Combining these velocity and temperature changes with the material parameter (G_n, τ_n, a_T, b) evaluated in the previous section, the predicted stress and elongational viscosity were computed using an IBM computer and compared with those which Dees obtained experimentally with Equation (V-2) (force balance). Figures 30 through 34 show the comparison.

The comparison was made only in the amorphous range (from the

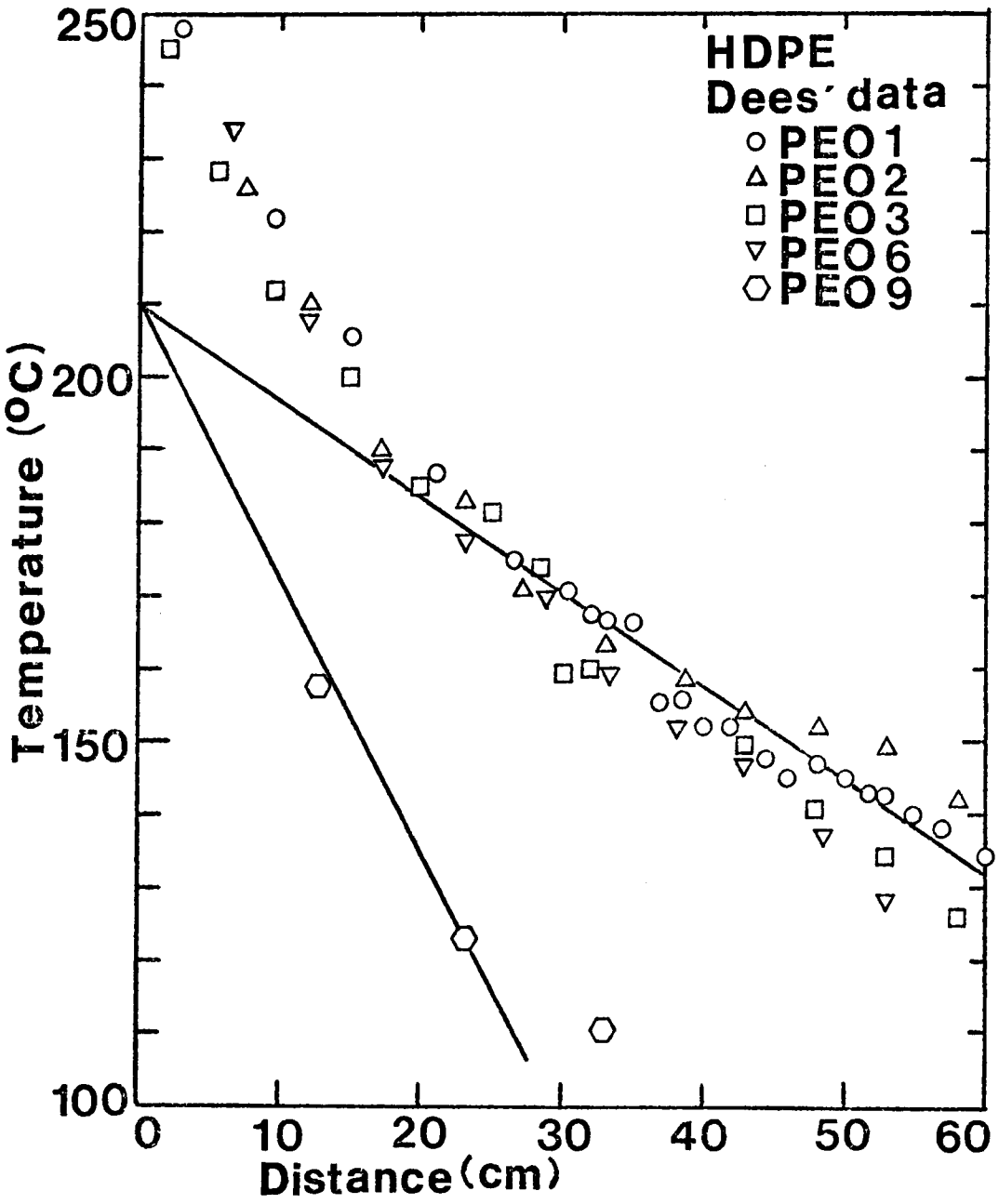

Figure 29. Fiber Temperature along Spinline for High Density Polyethylene.

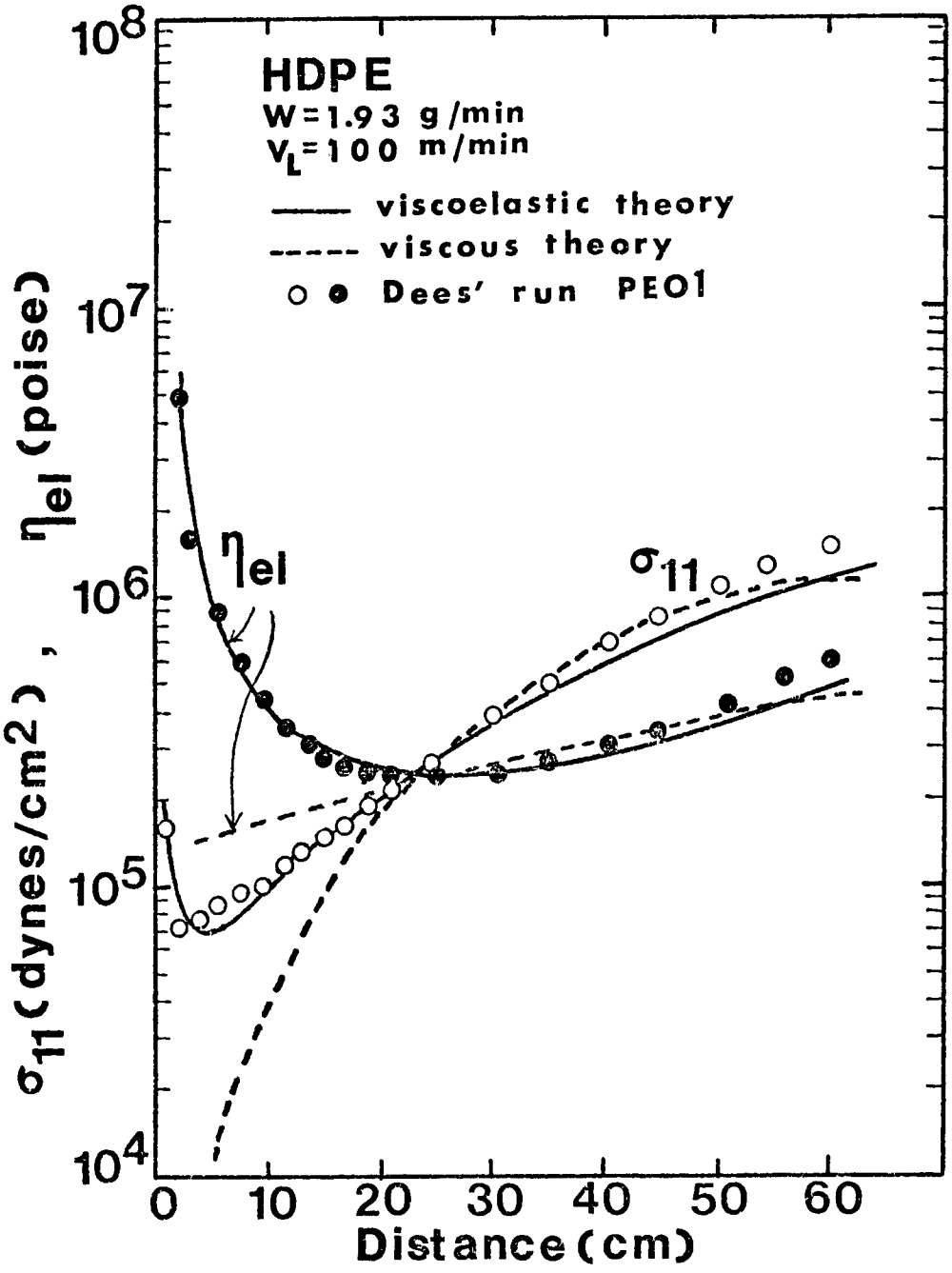

Figure 30. Tensile Stress and Apparent Elongational Viscosity in Melt Spinning for High Density Polyethylene for Dees' Run PE01.

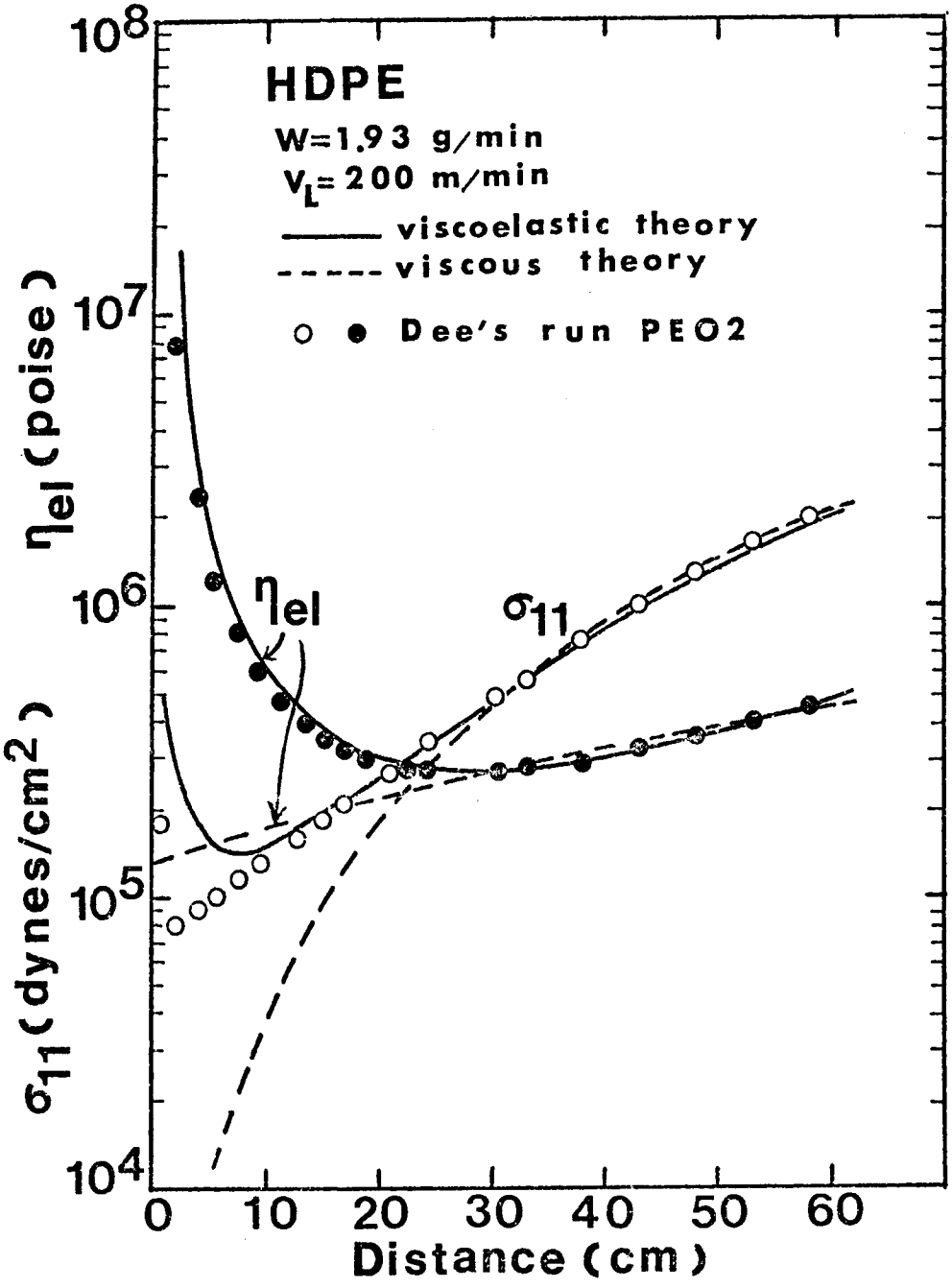

Figure 31. Tensile Stress and Apparent Elongational Viscosity in Melt Spinning for High Density Polyethylene for Dees' Run PEO2.

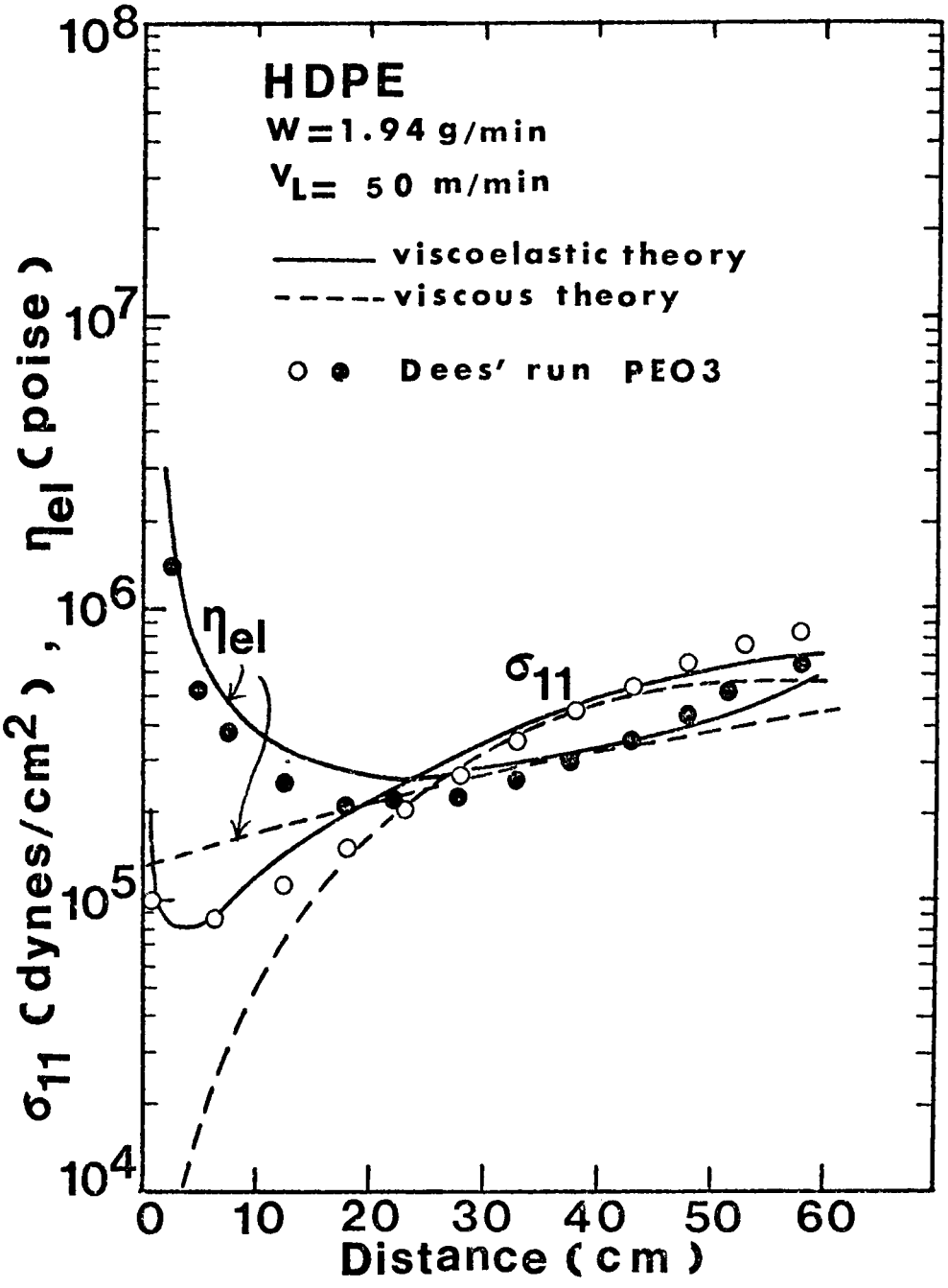

Figure 32. Tensile Stress and Apparent Elongational Viscosity in Melt Spinning for High Density Polyethylene for Dees' Run PE03.

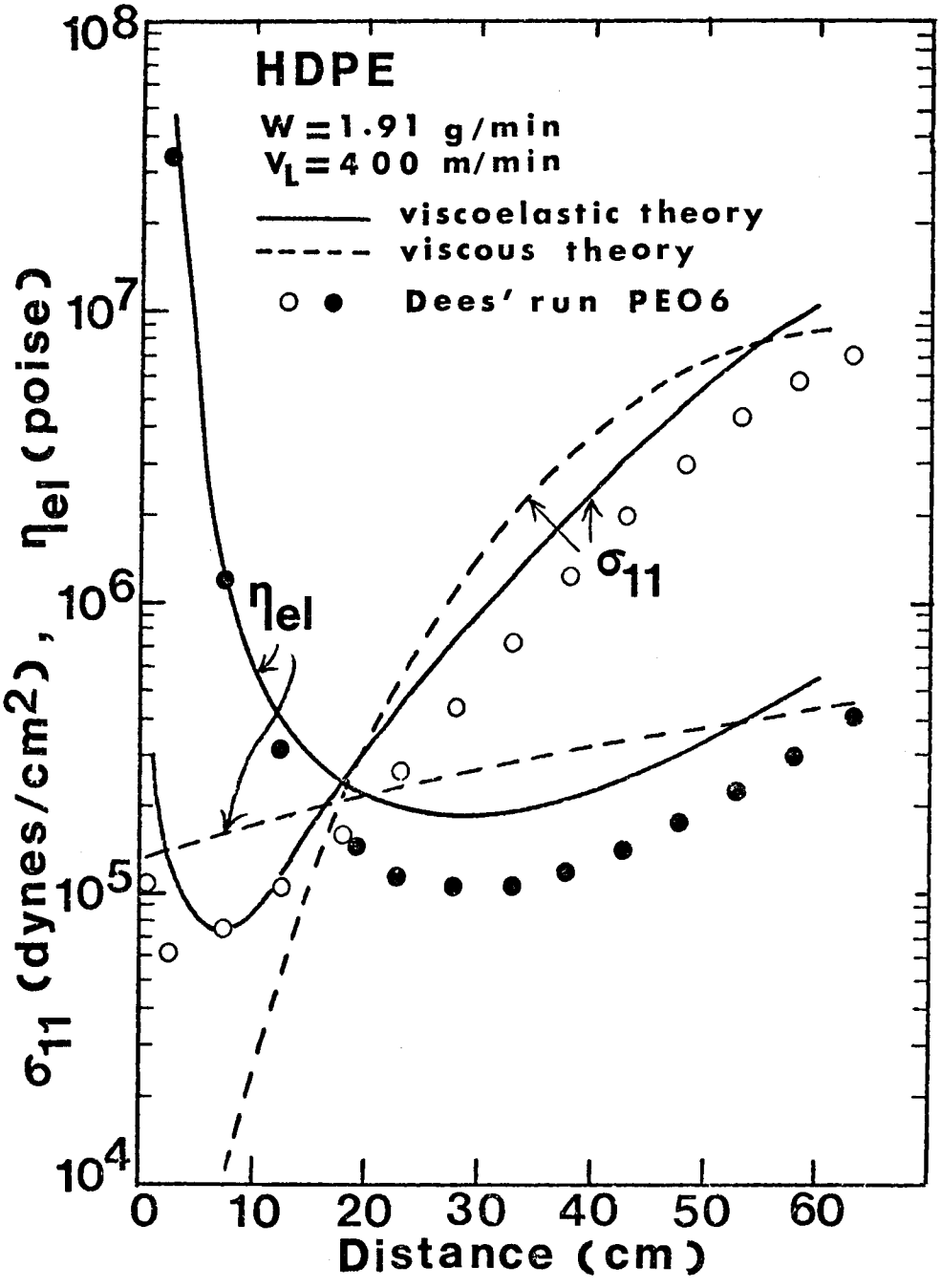

Figure 33. Tensile Stress and Apparent Elongational Viscosity in Melt Spinning for High Density Polyethylene for Dees' Run PE06.

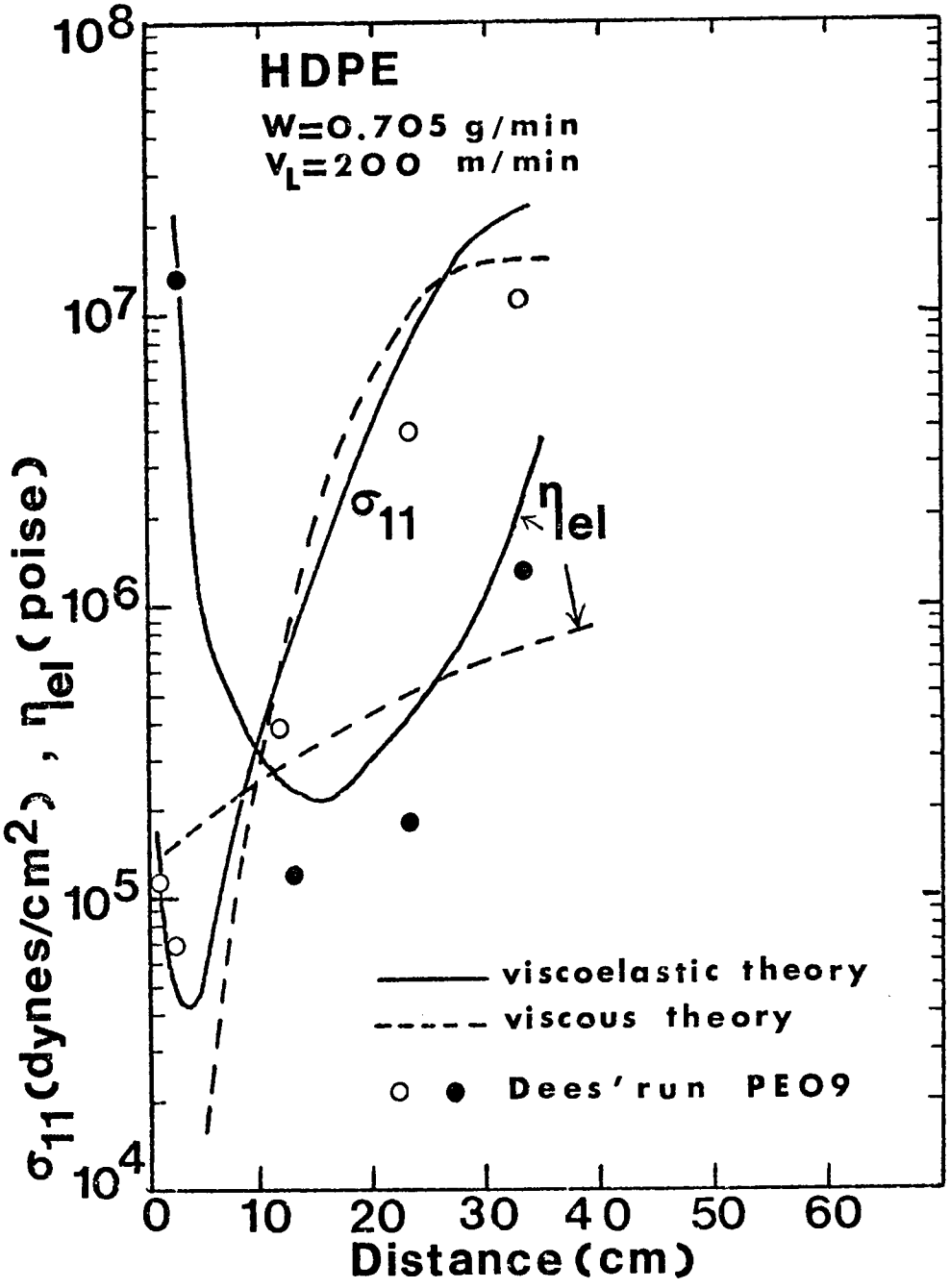

Figure 34. Tensile Stress and Apparent Elongational Viscosity in Melt Spinning for High Density Polyethylene for Dees' Run PE09.

spinneret up to the point at which crystallization occurs). Beyond the crystallization point, the present analysis cannot be applied because the heat of crystallization is involved and also the material properties vary with it.

In spite of these difficulties the prediction of Equation (V-19) shows remarkable agreement with Dees' data, perhaps fortuitously in view of the assumptions that have been made. The dotted lines in the figures show the Trouton (viscous) asymptote, calculated from a point elongation rate combined with an elongational viscosity taken simply as three times the zero shear viscosity at the point temperature in question. Differences between the two theoretical curves for the apparent elongational viscosity curve as one nears the spinneret, in which region the experimental elongational viscosity decreases while the filament temperature decreases and the rate of elongation increases. A peculiar shape of the kind has not been reported for easily spinnable polymers such as polyester and Nylon 6 although the tendency might have been there (32). It seems impossible to explain this part with any viscous theory because the observed elongational viscosities are much higher than three times the shear viscosities.

On the other hand, the nonisothermal viscoelastic theory (Equation (V-19)) gives a clear interpretation in terms of the normal stress effect due to the shear flow in the die; that is, near the die the effect of the normal stress is not relaxed and still dominates the tensile stress; but then the viscoelastic stress due to elongation takes over. In Figures 30, 31, and 32, the nonisothermal viscoelastic theory (solid lines) and the simple viscoelastic theory (dotted lines)

come together at a distance about 20 centimeters from the die. This coincidence is interesting but should be deemed rather incidental, because in other runs (Figures 33 and 34) where the elongation rates are higher than in runs 1, 2, and 3, there are significant differences in both the shapes and magnitudes of the two theoretical curves. The general discussion of the differences (or coincidences) is not straight forward because in melt spinning the elongation rate is not constant but increases first, reaches a maximum, and then falls off. To have a better understanding of this problem a more tractable theoretical analysis will be discussed in Chapter VI. From that analysis we learn that an apparent viscous flow can occur if the rate of change of temperature is large.

CHAPTER VI

THEORETICAL CONSIDERATION OF CONSTANT ELONGATIONAL FLOW WITH COOLING

A. THEORETICAL ANALYSIS

As mentioned in the previous section, elongational flows have recently been widely studied. One concludes that if the elongation rate is small enough (i.e., $\dot{E}\tau < 1/2$) a steady state is achieved (with the elongational viscosity approaching a steady value), but if the elongation rate is large (i.e., $\dot{E}\tau \geq 1/2$) a steady state cannot be achieved (with the elongational stress or viscosity ever increasing until failure occurs). This has been shown both experimentally and theoretically under isothermal conditions (17, 56). One may then associate elongational viscosities which are higher than three times the zero shear viscosity with a high elongation rate.

In melt spinning, however, the apparent elongational viscosity often seems to be close to three times the shear viscosity (as analyzed in the last section) even though the elongation rates were high (of order $10 \sim 10^2$ sec^{-1}); the maxumum relaxation times were of order $1 \sim 10$ sec. Also, no "blowing up" of the stress has been seen yet. This seems to be so because of nonisothermal effects; that is, one may imagine that the fast temperature changes overpower the effects of changing deformation history. One would like to find some mathematical basis for this rather intuitive argument.

A tractable problem of this kind can be stated by consideration of starting up a flow at a constant elongation rate, upon which is

imposed a constant rate of cooling. To make the problem simple a model of one relaxation time will be considered.

The Finger tensors are given by

$$C_{ij} = \begin{vmatrix} \exp(2\dot{E}s) & 0 & 0 \\ 0 & \exp(-\dot{E}s) & 0 \\ 0 & 0 & \exp(-\dot{E}s) \end{vmatrix} \quad (t' \geq 0) \qquad \text{(VI-1)}$$

$$C_{ij} = \begin{vmatrix} \exp(2\dot{E}t) & 0 & 0 \\ 0 & \exp(-\dot{E}t) & 0 \\ 0 & 0 & \exp(-\dot{E}t) \end{vmatrix} \quad (t' < 0) \qquad \text{(VI-2)}$$

where $s = t - t'$. The second invariant of the deformation rate tensor is calculated as

$$\Pi_d^{1/2} = \sqrt{3}\,\dot{E} \qquad \text{(VI-3)}$$

Substituting Equations (VI-1), (VI-2), and (VI-3) into Equations (II-17) and (II-18), one can obtain the tensile stress, considering the boundary condition $\sigma_{22} = 0$ as follows:

$$\sigma_{11} = G\dot{E} \int_0^t \exp\left[-\int_{t'}^{t} \frac{dt''}{\tau[T(t'')]}\right] \left\{ 2\exp[A\dot{E}(t-t')] + \exp[-B\dot{E}(t-t')] \right\} dt' \qquad \text{(VI-4)}$$

where $A = 2 - \sqrt{3}\,b$ and $B = 1 + \sqrt{3}\,b$.

The temperature change is described by

$$T(t) = T_i - R\,t \tag{VI-5}$$

where T_i and R denote the initial temperature and the cooling rate, respectively.

The shift factor of the relaxation time is assumed to be approximated by

$$\ln a_T[T(t)] = -\alpha[T(t) - T_0]. \tag{VI-6}$$

Equation (IV-6) should be described by the WLF equation, but the simpler assumption of Equation (VI-6) seems adequate for understanding the nonisothermal behavior.

Then one obtains the integral

$$\int_{t'}^{t} \frac{dt''}{\tau[T(t'')]} = \frac{1}{\tau_0} \int_{t'}^{t} \exp\,[\alpha(T_i - Rt'' - T_0)]\,dt''$$

$$= \frac{\exp(-\alpha Rt) - \exp[-\alpha R(t-s)]}{\alpha R\tau(0)} \tag{VI-7}$$

where $\tau(0) = \tau[T_i] = \tau[T(0)]$. The tensile stress may be rearranged to

$$\sigma_{11} = G\dot{E} \int_0^t \exp\left[\frac{\exp(-\alpha Rt) - \exp[-\alpha R(t-s)]}{\alpha R\tau(0)}\right] [2\exp(A\dot{E}s) + \exp(-B\dot{E}s)]ds. \tag{VI-8}$$

It is usually of interest to express the elongational viscosity η_{el} in

terms of the zero shear viscosity η^{o}_{sh}. This can be done by defining the transient elongational viscosity η_{el} and the corresponding zero shear viscosity at the point temperature as follows:

$$\eta_{el} = \frac{\sigma_{11}}{\dot{E}} \tag{VI-9}$$

$$\eta^{o}_{sh} = G\,\tau[T(t)] = G\,\tau(0)\,\exp(\alpha R t) \tag{VI-10}$$

Thus, the ratio of the elongational viscosity to the zero shear viscosity leads to

$$\frac{\eta_{el}}{\eta^{o}_{sh}} = \int_0^t \frac{\exp(-\alpha R t)}{\tau(0)} \exp\left[\frac{\exp(-\alpha R t)-\exp[-\alpha R(t-s)]}{\alpha R \tau(0)}\right] \left\{2\exp(A\dot{E}s) + \exp(-B\dot{E}s)\right\} ds \tag{VI-11}$$

The above equation is too complicated to integrate analytically. However, one can deduce significant results by bounding the complicated integrand with integretable functions.

Condition of Convergence

Because of the relationahip

$$\exp\left[\frac{\exp(-\alpha R t) - \exp[-\alpha R(t-s)]}{\alpha R \tau(0)}\right] < 1 \text{ (always)}, \tag{VI-12}$$

one obtains the inequality

$$\frac{\eta_{el}}{\eta^{o}_{sh}} < \int_0^t \frac{\exp(-\alpha R t)}{\tau(0)} \left\{ 2\exp(\dot{A}E s) + \exp(-\dot{B}E s) \right\} ds$$

$$= \frac{2}{\dot{A}E\tau(0)} \left\{ \exp(\dot{A}E - \alpha R)t - \exp(-\alpha R t) \right\} - \frac{\exp(-\alpha R t)}{\dot{B}E\tau(0)} [\exp(-\dot{B}E t) - 1]. \quad \text{(VI-12a)}$$

Provided that

$$\alpha R > \dot{A}E \text{ (i.e., rapid cooling)} \quad \text{(VI-13)}$$

one finds that η_{el}/η^{o}_{sh} converges to zero as time goes to infinity.

Condition of Divergence

Also one has the following inequality:

$$\exp\left[\frac{\exp(-\alpha R t) - \exp[-\alpha R(t-s)]}{\alpha R\tau(0)}\right] > \exp\left[\frac{\exp(-\alpha R t) - 1}{\alpha R\tau(0)}\right] \quad \text{(VI-14)}$$

The viscosity ratio obeys the inequality

$$\frac{\eta_{el}}{\eta^{o}_{sh}} > \int_0^t \frac{\exp(-\alpha R t)}{\tau(0)} \exp\left[\frac{\exp(-\alpha R T) - 1}{\alpha R\tau(0)}\right] [2\exp(\dot{A}E s) + \exp(-\dot{B}E s)] ds$$

$$= \exp\left[\frac{\exp(-\alpha R t) - 1}{\alpha R\tau(0)}\right] \left[\frac{2}{\dot{A}E\tau(0)} \left\{ \exp(\dot{A}E - \alpha R t) - \exp(-\alpha R t) \right\} \right.$$

$$\left. - \frac{1}{\dot{B}E\tau(0)} [\exp(-\dot{B}E t) - 1] \right] \quad \text{(VI-16)}$$

One then finds that, if

$$\alpha R < \dot{AE} \text{ (i.e., slow cooling)}, \qquad \text{(VI-16)}$$

n_{el}/n_{sh}^{o} goes to infinity with increasing time.

Critical Condition

The above analysis shows that the ratio $\alpha R/\dot{AE}$ determines whether n_{el}/n_{sh}^{o} converges or diverges. It is, therefore, of considerable interest to consider the critical case for which $\alpha R/\dot{AE}$ is equal to unity.

Equation (VI-11) can be integrated by parts as follows:

$$\frac{n_{el}}{n_{sh}^{o}} = 3 - \exp\left[\frac{\exp(-\alpha Rt)-1}{\alpha R\tau(0)}\right]\left\{2\exp[(\dot{AE}-\alpha R)t] + \exp[-(\dot{BE}+\alpha R)t]\right\}$$

$$+ \int_0^t \exp\left[\frac{\exp(-\alpha Rt)-\exp[-\alpha R(t-s)]}{\alpha R\tau(0)}\right]\left\{2(\dot{AE}-\alpha R)\exp[(\dot{AE}-\alpha R)s]\right.$$

$$\left. - (\dot{BE}+\alpha R)\exp[-(\dot{BE}+\alpha R)s]\right\} ds. \qquad \text{(VI-17)}$$

If $\alpha R = \dot{AE}$ one can reduce Equation (VI-17) to

$$\frac{n_{el}}{n_{sh}^{o}} = 3 - \exp\left[\frac{\exp(-\dot{AE}t) - 1}{\dot{AE}\tau(0)}\right]\left[2 + \exp(-3\dot{E}t)\right]$$

$$- 3\dot{E}\int_0^t \exp\left[\frac{\exp(-\dot{AE}t) - \exp[-\dot{AE}(t-s)]}{\dot{AE}\tau(0)}\right]\exp(-3\dot{E}s)\, ds. \qquad \text{(VI-18)}$$

Then one finds the critical asymptote as follows:

$$\lim_{t\to\infty} \left(\frac{\eta_{el}}{\eta^{o}_{sh}}\right) = 3 - 2 \exp\left(\frac{-1}{\dot{A}E_{\tau}(0)}\right) - 3\,\dot{E} \int_0^{\infty} \exp(-3\dot{E}s)\, ds$$

$$= 2\left(1 - \exp\left(\frac{-1}{\dot{A}E_{\tau}(0)}\right)\right) \qquad \text{(VI-19)}$$

These results may be summarized as follows:

$$\lim_{t\to\infty} \left(\frac{\eta_{el}}{\eta^{o}_{sh}}\right) = \begin{cases} \infty & (Q < 1, \text{ slow cooling}) \\ 2\left[1 - \exp\left(-1/\dot{A}E_{\tau}(0)\right)\right] & (Q = 1, \text{ critical}) \\ 0 & (Q > 1, \text{ rapid cooling}) \end{cases} \qquad \text{(VI-20)}$$

where $Q = \alpha R/\dot{A}E$ and $A = 2 - \sqrt{3}\, b$. This means that if the initial value of $\dot{E}_{\tau}(0)$ is much smaller than $1/A$, the ratio η_{el}/η^{o}_{sh} becomes two at the critical condition ($Q = 1$), but that if $\dot{E}_{\tau}(0)$ is larger than $1/A$, η_{el}/η^{o}_{sh} becomes lower than two at $Q = 1$.

The dimensionless number Q is the ruling parameter of the elongational flow under cooling, while $\dot{E}_{\tau}$ is that of the isothermal case. The above results are very interesting. If the cooling rate is large, one case seems, in fact, to approach something similar to a Trouton-like viscous response; however, for certain critical conditions one can see apparent viscosities lower than the Trouton viscosity, even at very high deformation rates. The value of this asymptote is expressed by

$$2\left[\,1 - \exp\left(-1/\dot{A}E_{\tau}(0)\right)\,\right].$$

B. RESULTS AND DISCUSSION

The numerical calculations are shown in detail in Figures 35 and 36, where the b value was set equal to zero (i.e., the linear viscoelastic case). Figure 35 shows the case $\dot{E}_\tau(0) < 1/2$. The arrows indicate the positions at which the point value of $\dot{E}_\tau[T(t)]$ exceeds 1/2. The time at these positions are expressed by the equation

$$t_b = \frac{1}{\alpha R} \ln \left[\frac{1}{A\dot{E}_\tau(0)}\right]. \qquad \text{(VI-21)}$$

For very slow cooling (number 2), the elongational viscosity first rises to the plateau (at which $\eta_{el}/\eta^o_{sh} = 3$), stays here for a while and then finally blows up because of the increase of $\tau[T(t)]$. If the cooling rate is increased (numbers 3 and 4), the positions of the blowing-up come earlier in time. If, however, the cooling becomes much higher (number 5) the elongational viscosity returns to the falling off type of behavior, although a final blowing up still can be seen. Also, it should be noted that it takes some while before the blowing up occurs. The time at which the elongational viscosity begins to blow up is nearly equal to the t_b of Equation (VI-21). When the cooling rate reaches the critical value (number 6), the elongatioal viscosity does not blow up but converges to the asymptotic value (1.99 in this case). If the cooling rate increases further (number 7), the elongational viscosity shows first a rise, followed by a sudden falling off.

Figure 36 shows the case $\dot{E}_\tau(0) > 1/2$. There is no steady state in the isothermal case as mentioned before. The behavior of the viscosity

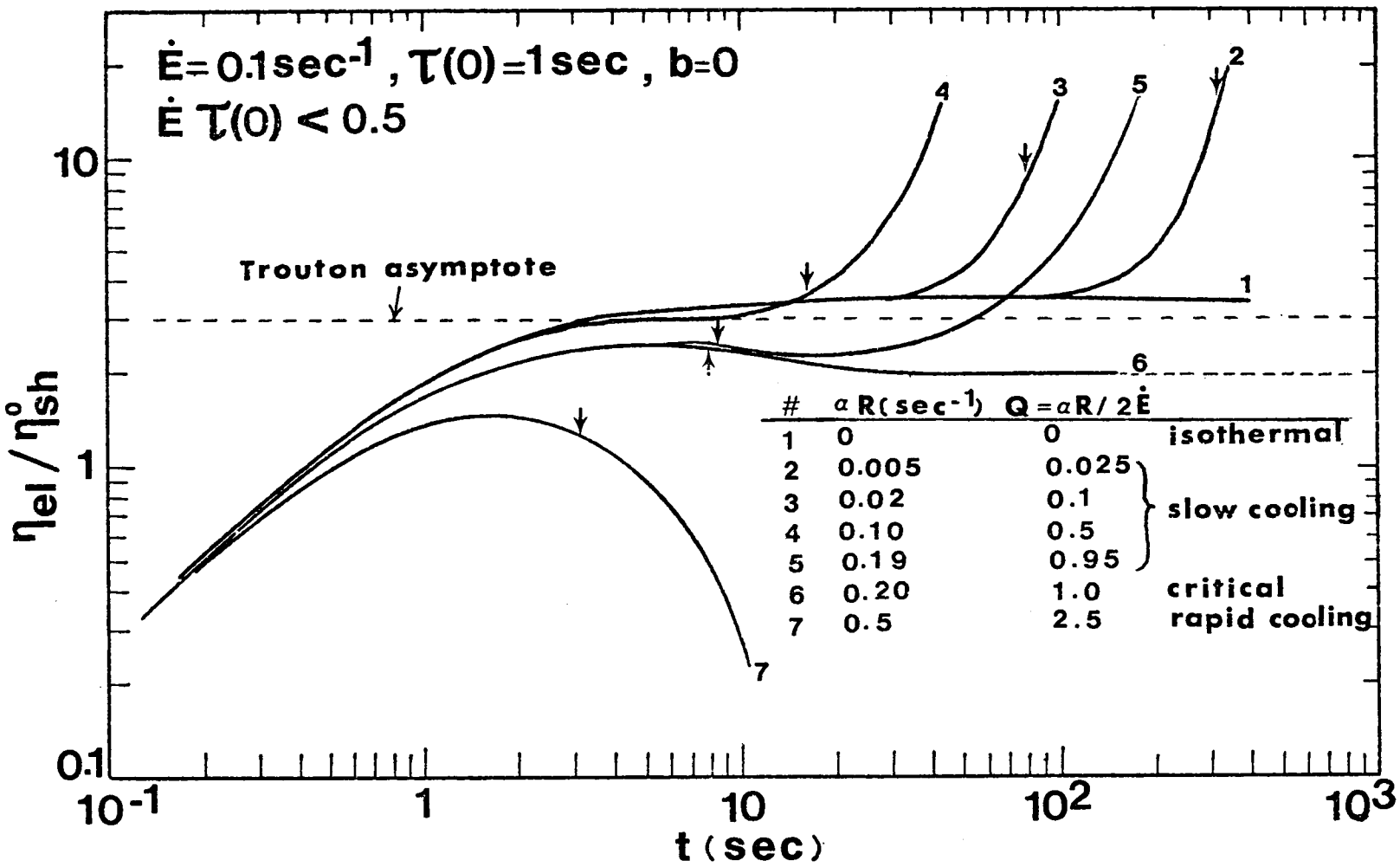

Figure 35. Theoretical Calculation of Transient Elongational Viscosity under Constant Rate of Cooling at $\dot{E}\tau(0) = 0.1$.

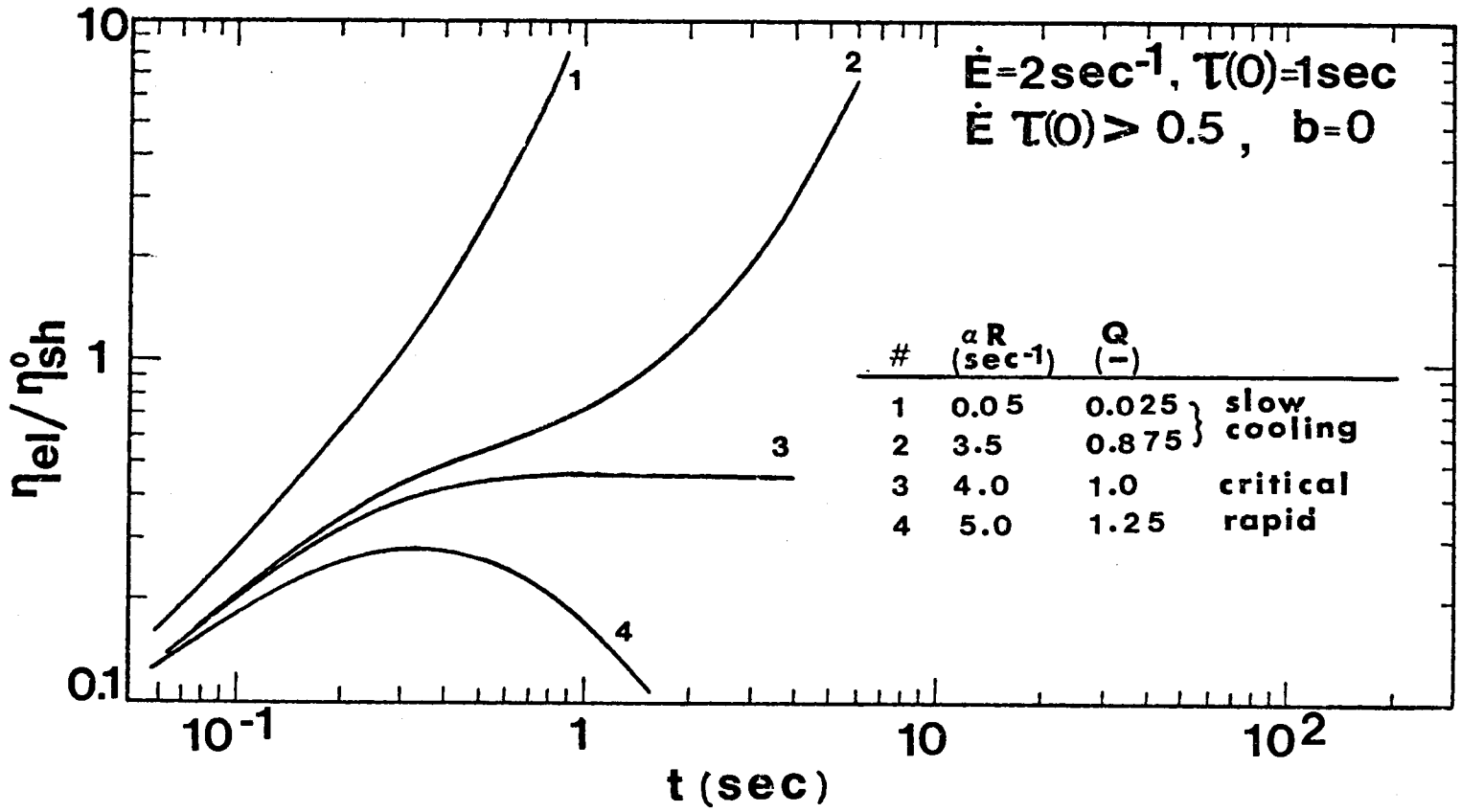

Figure 36. Theoretical Calculation of Transient Elongational Viscosity under Constant Rate of Cooling at $\dot{E}\tau(0) = 2.0$.

is simpler than the last case and essentially the same trend can be seen. The asymptotic value of the viscosity ratio for the critical cooling rate is 0.44. The case which involves a nonlinearity (for example, b = 0.5) was calculated, but the results were nearly the same as those shown in Figures 34 and 35. The above results clearly show that the high rate of cooling ($Q > 1$) overpowers the effect of a viscoelastic history. Also, it should be noted that even in the case of slow cooling (i.e., $Q < 1$) the ratio η_{el}/η^{o}_{sh} remains around three for a fairly long time before a blowing up appears. The smaller the initial $\dot{E}\tau(0)$ becomes, the later a blowing up occurs, as may be seen in Equation (VI-21).

This analysis cannot be directly applied to melt spinning because $\dot{E}$ and R vary and because materials have a distribution of relaxation times. However, it is interesting to obtain estimates of parameters such as $\dot{E}\tau(0)$ and Q to see their magnitudes. Dees' spinning data were taken as an example:

$\alpha = 0.016\ (\text{deg}^{-1})$

$A = 2-\sqrt{3}\ b = 1.13$

$\tau_{max}(0) = 1.35$ sec.

The point value of Q was calculated at a certain distance from the spinneret, as shown in Table IV.

The initial values of $\dot{E}\tau_{max}(0)$ are all very small (i.e., less than (1/A)). One may, therefore, roughly refer to Figure 35. In addition the initial maximum relaxation time is close to that in Figure 34.

TABLE IV

COOLING PARAMETERS IN MELT SPINNING DATA OF DEES

Run Number	Initial Value of $\dot{E}\tau_{max}(0)$	Distance (cm)	Q	Time of Transit (sec)
PE01	0.019	60	0.72	4.0
PE02	0.019	60	0.50	3.2
PE03	0.061	60	0.98	4.0
PE06	0.022	60	0.05	3.0
PE09	0.007	22	0.30	5.8

Judging from the Q values, all of these runs are in the range of slow cooling although run PE03 is nearly critical; run PE06 seems to show very, very slow cooling but the fact that it is far out of line with the other runs suggests some kind of calculational or measurement error. However, all of the transit times lie between three and six seconds. In other words, the elongational viscosities are thought to correspond to the plateau of Figure 34, at which η_{el}/η^{o}_{sh} is about three. The above analysis is not rigorous, but one may reasonably suppose that the point apparent elongational viscosity is not far from three times shear viscosity in Dees' melt spinning data. This result was already noted in Chapter V in which the complete melt spinning analysis compared reasonably well with an analysis based on a point Trouton viscosity.

CHAPTER VII

SUMMARY OF IMPORTANT RESULTS

The major results of the present work may be summarized as follows:

1. Existing viscoelastic constituitive theory can be generalized to nonisothermal histories by using the concept of a weighted time scale to account for the speeding up or slowing down of the relaxation processes.

2. Two kinds of nonisothermal experiments, involving changes of temperature during tensile pulling and after it, were carried out.

   a. In the latter (stress relaxation) experiments, the time scale of stress change due to the imposed temperature jump was well-explained by the weighted time history used in the theory.

   b. In the former (tensile pulling) experiments, the time scale of the accomodation to the new temperature was smaller than expected from theory; that is, the deformation seems to help the molecules accomodate themselves rapidly to the new temperature.

3. The melt spinning data of Dees (for high density polyethylene) were analyzed using the generalized theory. Some assumptions were necessary to evaluate the material parameters and to correct for experimental difficulties in the temperature measurements. However, certain conclusions were possible as follows:

   a. The predicted values for stress versus distance from the

spinneret were in reasonable agreement with the experimental data.

b. Despite the highly transient nature of the deformation, a theoretical curve based on three times the shear viscosity gives surprisingly close agreement with the complete viscoelastic theory.

4. To understand melt spinning flows better, a simpler but theoretically more tractable problem was considered: that of constant elongational flow with an imposed constant rate of cooling.

a. In slow cooling the transient elongational viscosity is similar to that of the isothermal case, although it will ultimately "blow up" at large times because of the ever-increasing relaxation time.

b. In fast cooling one can see a Trouton-like viscous response if a certain critical condition of temperature rate and deformation rate is achieved. The asymptotic viscosity becomes <u>two</u> times the shear viscosity if the deformation rate is small. For non-critical cooling conditions the asymptotic value is three times the shear viscosity if the deformation rate is small.

REFERENCES

REFERENCES

1. Abbott, L. E. and J. L. White, Appl. Poly. Symp., No. 20, 247 (1973).

2. Acierno, D., J. N. Dalton, J. M. Rodriguez, and J. L. White, J. Appl. Poly. Sci., 15, 2395 (1971).

3. Ballman, R. L., T. Shusman, and H. L. Toor, Ind. Eng. Chem., 51, 847 (1959); Modern Plastics, 37 (Sept), 105 (1959).

4. Berger, J. L. and C. G. Gogos, Poly. Eng. Sci., 13, 102 (1973).

5. Bernstsin, B., E. A. Kearsley, and L. J. Zapas, Trans. Soc. Rheology, 7, 391 (1963); J. Res. NBS, 68B, 103 (1964).

6. Bird, R. B., O. Hassager, and S. I. Abdel-Khalil, AIChE J., 20, 1041 (1974).

7. Bogue, D. C., Ind. Eng. Chem., 5, 253 (1966).

8. Bogue, D. C. and J. O. Doughty, Ind. Eng. Chem., 5, 243 (1966).

9. Bogue, D. C., T. Masuda, Y. Einaga, and S. Onogi, Polymer J., 1, 563 (1970).

10. Bogue, D. C. and J. L. White, "Engineering Analysis of Non-Newtonian Fluids," NATO Agardograph 144 (1970).

11. Broyer, E., Z. Tadmor, and C. Gutfinger, Israel J. Tech., 11, 189 (1973).

12. Carreau, P. J., Trans. Soc. Rheo., 16:1, 99 (1972).

13. Casey, J. O., Ph.D. dissertation, University of Tennessee, 1969.

14. Chang, H. and A. S. Lodge, Rheol. Acta, 11, 127 (1972).

15. Chen, I-J., Ph.D. dissertation, University of Tennessee (1971).

16. Chen, I-J. and D. C. Bogue, Trans. Soc. Rheo., 16, 59 (1972).

17. Chen, I-J., G. E. Hagler, L. E. Abbott, J. N. Dalton, D. C. Bogue, and J. L. White, Trans. Soc. Rheo., 16, 473 (1972).

18. Clark, E. S., "Structure of Crystalline Polymers," in "Polymeric Materials," American Soc. of Metals, Metals Park, Ohio, 1975.

19. Cogswell, F. N., Appl. Poly. Symp. No. 27, 1 (1975).

20. Coleman, B. D., and W. Noll, Arch. Rat. Mech. Anal., 3, 289 (1959); 6, 355 (1960); 9, 273 (1962).

21. Crochet, M. J., "Theoretical Rheology," Appl. Sci. Publ., 1975; see also M. J. Crochet and P. M. Naghdi, J. de Mecanique, 13, (1974).

22. Dealy, J. M., Poly. Eng. Sci., 11, 433 (1971).

23. Dees, J. R., Ph.D. dissertation, University of Tennessee, 1974.

24. Dees, J. R. and J. E. Spruiell, J. Appl. Poly. Sci., 18, 1053 (1974).

25. Denn, M. M. and G. Marrucci, AIChE J., 17, 101 (1971).

26. Eckert, E. R. G. and R. M. Drake, "Heat and Mass Transfer," 2nd edition, McGraw-Hill, 1959.

27. Ferry, J. D., J. Amer. Chem. Soc., 72, 3746 (1950).

28. Ferry, J. D., "Viscoelastic Properties of Polymers," 2nd edition, Wiley, New York, 1970.

29. Fisher, R. and M. M. Denn, Appl. Poly. Symp. No. 27, 103 (1975).

30. Graessley, W. W. in "Advances in Polymer Science," vol. 16, Springer Verlag, 1974.

31. Green, A. E. and R. S. RIvlin, Arch. Rat. Mech. Anal., 1, 1 (1957).

32. Hamana, I., M. Matsui, and S. Kato, Melliand Textiber., 50, 382 (1969).

33. Han, C. D., J. Appl. Poly. Sci., 18, 3581 (1974).

34. Han, C. D., K. U. Kin, N. Siskovic, and C. R. Huang, Rheol. Acta, 14, 533 (1975).

35. Han, C. D. and R. R. Lamonte, Trans. Soc. Rheo., 16, 447 (1972).

36. Han, C. D., R. R. Lamonte, and Y. T. Shah, J. Appl. Poly. Sci., 16, 3307 (1972).

37. Harry, D. H. and R. G. Parrott, Poly. Eng. Sci., 10, 209 (1970).

38. Huppler, J. D., I. F. McDonald, E. Ashare, T. W. Spriggs, R. B. Bird, and L. A. Holmes, Trans. Soc. Rheo., 11, 181 (1967).

39. Ide, Y., Ph.D. dissertation, University of Tennessee, in preparation.

40. Kamal, M. R. and S. Kenig, Poly. Eng. Sci., 12, 294 (1972).

41. Kamei, E. and S. Onogi, Proceedings of the 20th Meeting of Rheology, 149 (1972), Fukui, Japan.

42. Kase, S. and T. Matsuo, J. Poly. Sci., A3, 2541 (1966); J. Appl. Poly. Sci., 11, 251 (1967).

43. Kase, S., T. Matsuo, and Y. Yoshimoto, Seni Kikai Gakkaishi, 10, T63 (1966).

44. Katayama, K., T. Amano, and K. Nakamura, Kolloid Z.-Z. Polym., 226, 125 (1968).

45. Leaderman, H., Text. Res., 11, 171 (1941).

46. Leppard, W. R. and E. B. Christiansen, AIChE J., 21, 999 (1975).

47. Lodge, A. S., Trans. Far. Soc., 52, 120 (1956).

48. Lodge, A. S., "Elastic Liquids," Academic Press, New York, 1964.

49. Markovitz, H., J. Poly. Sci.: Polymer Symp. No. 50, 431 (1975).

50. Masuda, T., Ph.D. dissertation, Kyoto University, Japan (1973).

51. Meissner, J., Rheol. Acta, 8, 78 (1967); 10, 230 (1971).

52. Metzner, A. B. in "Advances in Heat Transfer," J. P. Hartnett and T. F. Irvine, Jr., eds., vol. 2, Academic Press, 1965.

53. Morland, L. W. and E. H. Lee, Trans. Soc. Rheo., 4, 233 (1960).

54. Nakamura, K., T. Watanabe, T. Amano, and K. Katayama, J. Appl. Poly. Sci., 17, 1031 (1973).

55. Oldroyd, J. G., Proc. Roy. Soc., A245, 278 (1958).

56. Onogi, S., and coworkers, Macromolecules, 3, Part I (S. Onogi, T. Masuda, and K. Kitagawa) 109 (1970); Part II (T. Masuda, K. Kitagawa, and S. Onogi) 116 (1970).

57. Onogi, S., T. Matsumoto, and E. Kamei, Polymer J., 3, 531 (1970).

58. Pearson, J. R. A., "Mechanical Principles of Polymer Melt Processing," Pergamon, London, 1966.

59. Pearson, J. R. A. and M. A. Matovich, IEC Fund., 8, 605 (1969).

60. Richardson, S., J. Fluid Mech., 56, 609 (1972).

61. Shah, M. J. and J. R. A. Pearson, IEC Fund., 11, 145, 150 (1972); Trans. Soc. Rheo., 16, 519 (1972).

62. Spriggs, T. W., J. D. Huppler, and R. B. Bird, Trans. Soc. Rheo., 10, 191 (1966).

63. Spruiell, J. E. and J. L. White, Poly. Eng. Sci., 15, 660 (1975).

64. Spruiell, J. E. and J. L. White, Appl. Poly. Symp. No. 27, 121 (1975).

65. Takahashi, M., T. Masuda, and So Onogi, J. Soc. Rheo. Japan, 1, 16 (1973).

66. Takahashi, M., T. Masuda, and S. Onogi, "New Integral Constitutive Equations for Polymer Solutions," submitted for publication, 1975.

67. Takaki, T., M. S. Thesis, University of Tennessee (1973).

68. Takaki, T. and D. C. Bogue, J. Appl. Poly. Sci., 19, 419 (1975).

69. Tanner, R. I., Trans. Soc. Rheo., 12:1, 15 (1968); AIChE J., 15, 177 (1969).

70. Uhlmann, D. R. and A. G. Kolbeck, Sci. Amer., 233, 96, December 1975.

71. White, J. L., Poly. Eng. Sci., 15, 44 (1975).

72. White, J. L. and H. B. Dee, Poly. Eng. Sci., 14, 212 (1974).

73. White, J. L., K. C. Dharod, and E. S. Clark, J. Appl. Poly. Sci., 18, 2539 (1974).

74. White, J. L. and Y. Ide, Appl. Poly. Symp. No. 27, 61 (1975).

75. White, J. L. and A. B. Metzner, AIChE J., 11, 324 (1965).

76. White, J. L., J. E. Spruiell, and D. C. Bogue, "Fundamental Study of the Rheological and Morphological Aspects of Synthetic Fiber Processing," NSF proposal, 1972.

77. White, J. L. and J. F. Roman, J. App. Poly. Sci., in press.

78. Williams, M. L., R. F. Landel, and J. D. Ferry, J. Am. Chem. Soc., 77, 3701 (1955).

79. Yamamoto, M., "Buttai no Henkei Gaku," Seibundō Shinkosha, Tokyo, 1972.

80. Ziabicki, A. in "Man-Made Fibers," H. Mark, S. Atlas, and E. Cernia, eds., Wiley, New York, 1967.

81. Ziabicki, A., "Fizyka Procesow Formowania Wlokien," Wydawnictwa Naukowo-Techniczne, Warsaw, 1970.

82. Ziabicki, A. and K. Kedzierska, Kolloid Z., 171, 51, 111 (1960); 175, 14 (1961).

APPENDIX

APPENDIX

HEAT TRANSFER BETWEEN SAMPLE AND AMBIENT AIR

In order to estimate the time lag in heating the sample, a theoretical estimate was made. If the heating was completely due to radiant heating, no external heat transfer resistance need be included. However, to understand the effect of heating in air, the following analysis was done.

The problem is that of a temperature T_a imposed on the surface of a cylinder which is initially at a uniform temperature T_o. The solution is given by

$$\frac{T - T_a}{T_o - T_a} = \sum_{n=1}^{\infty} \frac{4J_1^2(\lambda_n)\ \exp(-\lambda_n^2 \alpha t/R^2)}{\lambda_n^2[J_o^2(\lambda_n) + J_1^2(\lambda_n)]} \qquad \text{(A-1)}$$

where λ_n is the n th root of the following equation involving Bessel functions (80):

$$\xi J_1(\xi) = (hR/K_p)\ J_o(\xi) \qquad \text{(A-2)}$$

and T is the average temperature of the sample; α, the thermal diffusivity; R, the radius; K_p, the thermal conductivity; h, the heat transfer coefficient at the boundary. Usually h is expressed in terms of the Nusselt number Nu ($=2Rh/K_a$)

$$\frac{hR}{K_p} = 0.5\ \frac{K_a}{K_p}\ Nu \qquad \text{(A-3)}$$

where K_a is the thermal conductivity of air. Nu is empirically expressed as a function of Reynolds number Re (= $2RU/\upsilon_a$), with U and υ_a being the air velocity and kinematic viscosity of air, respectively. There are many empirical equations for Nu. Some of them are summarized by Ziabicki (80). As it was difficult to analyze the air flow pattern in the present heater, Nu was estimated as about three from prior results (80). The values of the physical properties were taken as follows:

density (ρ)	1.1 g/cm^3
specific heat (c_p)	0.3 cal/g-deg
thermal conductivity (K_p)	3×10^{-3} cal/cm-sec-deg
thermal diffusivity ($\alpha=K_p/\rho c_p$)	$\simeq 10^{-3}$ cm^2/sec
ratio of K_a/K_p	$\simeq 0.1$
thermal expansion	7 to 10×10^{-5} cm/deg

The radius of the sample was about 0.5 mm. Then λ_1 was calculated from Equation (A-2), neglecting λ_2, λ_3, etc.

$$\lambda_1 \simeq 0.55$$

From Equation (A-1) the time scale of the temperature change (i.e., for about 63 percent completion) is equal to about

$$\left(\frac{R^2}{\lambda_n^2 \alpha}\right) = 9 \text{ (sec)}$$

of the temperature jump.

VITA

Michikage Matsui was born in Hyogo Prefecture, Japan on July 14, 1941. He grew up there and attended Kaibara High School. In 1964 he graduated from Kyoto University with a Bachelor of Science degree in physics. He accpeted a job with Teijin Limited in Osaka, Japan. From 1964 to 1974 he worked on fiber and textile research in the company.

He married Aiko Kadama in 1965. They have three children: Takafumi (son), Yakari (daughter), and Koji (son).

In 1974 he met Professor D. C. Bogue in Kyoto University, who was a Visiting Professor in the university at that time. With kind advice of Dr. Bogue, he entered the University of Tennessee in September, 1974. His family joined him in this country. This was the first trip abroad for them.

He received a Masters Degree in Chemical Engineering in March, 1976. He will return to Japan in March, 1976 with his family and will rejoin the Fiber and Textile Research Institute of Teijin Limited.